# NOVEL POSITIONING ALGORITHMS AND NODE CONFIGURATION OPTIMISATION FOR NON-GPS WIRELESS SYSTEMS

by

Kewei Clare Xu Guo


Dissertation submitted in fulfillment of the requirements

for the degree of

DOCTOR OF PHILOSOPHY

Department of Engineering
Faculty of Science
Macquarie University
Sydney, Australia

August 2013

## ABSTRACT

This thesis presents a system study on the theory, methodology, and architecture for non-GPS based wireless positioning systems. In particular, the focus is to devise new algorithms and methodologies to improve the positioning accuracy of existing methods, and to develop the theoretical framework for node configuration optimisation.

Node configuration is one of the main subjects studied in this thesis. To understand the effect of node configuration on positioning accuracy, we first examine the challenging scenario of tracking swimmers in a swimming pool using a two dimensional (2D) and a three dimensional (3D) distributed sensor network, respectively. By employing the spherical interpolation approach (SIA) as the positioning algorithm and the cumulative distribution function (CDF) as the objective function, a methodology for optimising the configuration of the positioning network for tracking swimmers is proposed. Secondly, we propose a hybrid optimisation algorithm combining the particle swarm optimisation (PSO) and the classical sequential quadratic programming (SQP) method for node placement optimisation using the geometric dilution of precision (GDoP) as the objective function. It is observed that the result of such an optimisation strategy is different from that obtained from the CDF method. This seemingly contradictory finding could potentially be beneficial in practical network deployment: Given a coverage area, the optimal positions of the node obtained from GDoP optimisation would result in the lowest Cramér-Rao lower bound, but such a configuration would require the use of an optimum positioning algorithm. If one doesn't have the option of choosing the

algorithm, as in the case when the positioning algorithm is embedded in the device at hand, the CDF based method would result in a positioning network with greater achievable accuracy.

Triangulation based positioning methodology employing direction-of-arrival (DoA) estimation suffers from a deficit in the antenna radiation pattern when the impinging signal is close to the antenna plane. To overcome this difficulty, we propose a weighted least squares method (WLSM) with the weighting matrix derived from the angle of incidence of each array for wireless positioning using multi-angulation. The algorithm is suited for both 2D and 3D positioning when a number of sensor arrays are employed, and it is proven to be far superior to the conventional least squares method (LSM).

To take advantage of the proliferation of low cost wireless ranging devices, such as wireless LAN and ultra wideband (UWB), a new positioning method employing ranging based sensor arrays is presented and the associated location estimator is developed. Such an array is of low cost and is easy to maintain. The Cramér-Rao lower bound of the proposed location estimator is derived. A closed form expression of the standard deviation is given and proved to reach the Cramér-Rao lower bound.

Finally, a co-operative positioning system based on the co-operation between adjacent sensor arrays is proposed. The Cramér-Rao lower bounds for two arrays and three arrays for 2D and 3D cases, respectively, are derived. It is shown that the co-operation between arrays lead to much improved positioning accuracy compared with the employment of a stand-alone array and non-co-operative arrays, thus reaching the Cramér-Rao lower bound.

## STATEMENT OF CANDIDATE

I certify that the work in this thesis has not previously been submitted for a degree nor has it been submitted as part of the requirements for a degree to any other university or institution other than Macquarie University.

I also certify that the thesis is an original piece of research and has been written by me.

In addition, I certify that all information sources and literature used are indicated in the thesis.

. . . . . .

Kewei Clare Xu Guo

## ACKNOWLEDGMENTS

I would like to acknowledge my supervisors Prof. Eryk Dutkiewicz (Macquarie University, Australia) and Dr Xiaojing Huang (ICT Centre, CSIRO, Australia) for their support, advice and encouragement throughout this work.

Furthermore, I would like to thank the Australian Institute of Sport (AIS) and Swimming Australia (SAL) for their generous financial support.

Finally, I owe my sincere thanks to Dr Keith Imrie for proofreading this thesis.

"*Not only God does play dice, but he sometimes confuses us by throwing them where they can't be seen.*"

Stephen William Hawking

# List of Figures

# List of Tables

# Contents

# Chapter 1

# Introduction

## 1.1 Background

Position information is of great importance to numerous commercial, public safety, and defense applications. It is probably fair to say that any spatial information without the corresponding position information is of only limited value [1]. The ever increasing mobility of our society and industry renders that most positioning applications and services require a wireless solution. The most commercially successful and widely used wireless positioning system is the global positioning system (GPS). GPS provides three dimensional (3D) positioning information at any time, with almost any device and anywhere outdoors. Unfortunately, GPS fails to locate in harsh radio environments such as inside buildings, underground, in mines, under forest canopies, and in certain urban settings [2], [3]. Furthermore, a GPS chip is power hungry and can be too expensive for certain low cost applications such as wireless sensor networks (WSN) [4]. Thus, in the last decade, a significant amount of research has been focused on localised positioning systems employing other wireless technologies. The majority of local wireless positioning systems are range based and the distance can be

estimated using the delay in the transmitted signal or its attenuation. Delay based systems, which include time-of-arrival (ToA) based systems and time-difference of arrival (TDoA) systems, have the potential of delivering high positioning accuracy, but they require accurate clocks and relatively complicated signal processing which increases the complexity of the system. On the other hand, attenuation based systems, known as received signal strength (RSS) based systems, bypass the requirement of additional hardware and are hence ideal for low complexity networks such as wireless sensor networks (WSN). Unfortunately, the RSS based positioning systems do have the disadvantage of relatively lower positioning accuracy [5]. Other positioning techniques include direction-of-arrival (DoA) based and inertia sensor based ones [6], [7], [8]. The former requires an antenna array with relatively sophisticated signal processing and the accuracy is quite often inadequate, whilst the latter tends to suffer from the problem of drifting and is therefore typically used as a complementary means to enhance the accuracy of a primary positioning technique.

Currently there is no solution which can perform high accuracy positioning seamlessly indoors and outdoors at a commercially acceptable cost. In the short to medium term, new application-specific solutions will be developed to strike a balance between benefit and cost. In the long run, the integration of global positioning system (GPS) and inertia sensors into cellular phones, in conjunction with WiFi localisation, will provide ubiquitous location-awareness, meeting most civil and industrial requirements [3]. In the coming years, we will also expect to see the emergence of high-definition situation aware (HDSA) systems which can operate in both benign and harsh propagation environments where GPS typically fails. Such applications would require localisation systems with submeter accuracy. Reliable localisation in such conditions is a key enabler for a diverse set of applications including logistics, security, medical services, search and rescue operations, control of home appliances,

industrial safety, defense systems, and a large set of emerging wireless sensor network (WSN) applications. Other applications include networking protocols taking advantage of the position information to improve the performance of routing algorithms (geo-routing), as well as interference avoidance techniques in future cognitive radios [9].

## 1.2 Research Objectives

This thesis is aimed at solving some key problems in wireless positioning to achieve high accuracy in GPS-denial scenarios. In particular, we are interested in self-contained areas, such as warehouses, museums, or sports fields and swimming pools. It is focused on the positioning algorithms and methodologies, system architecture, node placement optimisation and hybrid techniques to deliver superior performance. Moreover, we aim to develop solutions to scenarios where there are no pre-installed reference nodes in order to meet such needs as emergency rescue, rural fire-fighting, worksite management and open mine management.

Using a set of known location arrays, a target position can be estimated by using the geometric relations between the incoming signal directions to each array and the arrays' locations. Due to the element radiation pattern, the accuracy of DoA estimation decreases when the signal direction approaches alignment with the array plane. To this end, a further objective of the research is to develop weighted least squares solutions to overcome the difficulty, thus enhancing the DoA based wireless positioning systems.

Finally, the research is intended to take advantage of the proliferation of low cost ranging based sensors to develop new array based positioning systems and to investigate possible ways to improve the positioning performance by virtue of co-

operation between arrays.

## 1.3 Thesis Organisation

This thesis consists of eight chapters as follows:

1. Chapter 1 presents an overview of the overall background, the research project and the research objectives. It outlines the thesis structure, our own research contributions to the field, and lists our publications.

2. The purpose of positioning is to obtain the unknown positions of targets based on a set of measurements. Positioning is normally conducted in two main steps:

   (i) parameter estimation where the estimates of the parameters required for position calculation between the wireless positioning nodes are obtained;

   (ii) position update or localisation where these estimates are processed to determine the positions of target nodes.

   In a two-step positioning system, the positioning accuracy increases as the position-related parameters in the first step are estimated more precisely. As a foundation to later chapters, Chapter 2 describes various commonly used parameter estimation techniques for wireless positioning. These include the time-of-arrival (ToA) based ranging, the radio signal strength (RSS) based ranging, direction-of-arrival (DoA) estimation, and the inertial sensor based positioning. Then it discusses a number of popular positioning update/localisation schemes. Finally, the advantages and disadvantages of a number of existing wireless positioning systems are discussed.

3. Node configuration in positioning networks is of great importance for practical network deployment, as it has significant impact on the positioning accuracy in

the coverage area and the number of nodes required. Chapter 3 is concerned with the problem of node configuration or node placement using trilateration. We consider the scenario where there is the freedom to choose the locations of the reference nodes and we aim to optimise these locations in order to minimise the position estimation errors. A scenario we have studied is the monitoring of elite swimmers in a swimming pool. To ease the analysis, we assume certain statistics regarding the range measurements without specifying the techniques used for measuring the ranges. In this chapter, we first introduce the spherical interpolation approach (SIA) as the chosen positioning algorithm. Then, the configuration of the network, namely, the arrangement of sensor nodes in the swimming pool, is optimised to achieve the highest accuracy with the minimum number of nodes and therefore the lowest cost. The objective function used for the node configuration optimisation is the cumulative distribution function (CDF). The study includes both two dimensional (2D) and three dimensional (3D) cases to understand the variation of the positioning estimation accuracy in the horizontal and vertical planes.

4. The positioning accuracy of ranging based methods is determined by three main factors, namely, the ranging accuracy, the localisation algorithm and the configuration of the sensor nodes. The geometric configuration of the reference sensors or anchor nodes in relation to the area in which the target nodes are to be located is critically important, sometimes even dominant. The geometric dilution of precision (GDoP) is commonly used to describe how the positioning accuracy is related to such geometric factors. To certain extent, without doing any detailed analysis of the positional errors, GDoP can be used to assess the "fitness" of given sensor placement and optimise it accordingly. It provides an approximation to the Cramér-Rao lower bound. In Chapter 4, we first present the

theory of GDoP. Then, a hybrid optimisation algorithm combining the particle swarm optimisation (PSO) method and the sequential quadratic programming (SQP) method is proposed. Using the average GDoP as the objective function, the hybrid optimisation algorithm is used to optimise the locations of the reference sensor nodes. The effectiveness of the hybrid optimisation method is demonstrated by simulations.

5. Triangulation is another positioning method which uses more than one direction-of-arrival (DoA) estimate at spatially separated arrays. By using a number of arrays whose positions are known, one can locate the position of the target using simple geometrical equations. A critical problem associated with DoA estimation is that the accuracy of the estimation falls rapidly when the signal direction is close to the plane on which the array is placed. This is due to the physical property of the array element which radiates or receives energy as a function of the direction of the signal. As a result, the signal-to-noise ratio deteriorates significantly as the DoA moves away from the normal direction. In Chapter 5, we propose a weighted least squares method (WLSM) with the weighting matrix derived from the angle of incidence of each array. Since the weight applied to each array is a function of the DoA seen by the array, the variances of the DoA estimation at each array is taken automatically when conducting positioning. We start from 2D scenarios, and then extend the WLSM to 3D cases. Simulation results show that the new method outperforms the conventional LSM significantly.

6. Chapter 6 presents a novel wireless positioning system which employs an array of sensors to estimate the position of a mobile target without using fixed reference nodes. In contrast to the traditional array based method, every sensor

in the positioning array is capable of doing ranging measurements individually by communicating with the target, but no phase measurement is required. These range measurements lead to a bearing estimate as well as a high accuracy ranging estimate via averaging. In this chapter, the new location estimator is presented, and the Cramér-Rao lower bound of the proposed location estimator is derived. We also present a closed form expression of the standard deviation and prove that the estimator can reach the Cramér-Rao lower bound. Theoretical results are validated by simulations.

7. All bearing or DoA based methods suffer from a main limitation: the positioning error caused by the DoA estimation error increases with the distance from the target to the array used for DoA estimation. To solve the problem, Chapter 7 introduces the use of co-operation between adjacent sensor arrays for wireless positioning. The Cramér-Rao lower bounds for two arrays and three arrays for 2D and 3D cases, respectively, are derived. It is shown that co-operation between arrays leads to much improved positioning accuracy compared with the employment of a stand-alone array and non-co-operative arrays, thus reaching the Cramér-Rao lower bound.

8. Chapter 8 concludes the thesis and presents some research directions.

## 1.4 Contributions

This thesis presents a system study on the algorithms, methodology and node configuration optimisation of non-GPS based wireless positioning systems. In particular, the focus is to devise new algorithms and methodologies to improve the positioning accuracy of existing methods, and to develop the theoretical frameworks to support

the proposed algorithms. Key contributions of the thesis can be summarised as follows:

- By using the spherical interpolation approach (SIA) as the positioning algorithm and the cumulative distribution function (CDF) as the objective function, a methodology for optimising the configuration of the positioning network for tracking swimmers is proposed. The study includes both two dimensional (2D) and three dimensional (3D) cases to understand the variation of the positioning estimation accuracy in the horizontal and vertical planes (Chapter 3).

- A hybrid optimisation algorithm combining the particle swarm optimisation (PSO) and the classical sequential quadratic programming (SQP) method is proposed for node placement optimisation using the geometric dilution of precision (GDoP) as the objective function. The optimal positions of the node would result in the lowest Cramér-Rao lower bound (Chapter 4). The effectiveness of the proposed scheme is verified by simulations.

- A weighted least squares method (WLSM) with the weighting matrix derived from the angle of incidence of each array is proposed for wireless positioning using triangulation. The algorithm is suited for both 2D and 3D positioning when a number of sensor arrays are employed, and is proven to be much superior to the conventional least squares method (LSM) (Chapter 5).

- A new positioning method employing ranging based sensor arrays is presented and the associated location estimator is developed. The Cramér-Rao lower bound of the proposed location estimator is derived. A closed form expression of the standard deviation is given and proven to reach the Cramér-Rao lower bound (Chapter 6).

- A co-operative positioning method based on the co-operation between adjacent sensor arrays is proposed. The Cramér-Rao lower bounds for two arrays and three arrays for 2D and 3D cases, respectively, are derived. It is shown that the co-operation between arrays lead to much improved positioning accuracy compared with the employment of a stand-alone array and non-co-operative arrays, thus reaching the Cramér-Rao lower bound (Chapter 7).

## 1.5 Publications

As part of the outcomes of the research, the following papers have been published:

[1] K. Clare Xu, E.Dutkiewicz, Xiaojing. Huang, Y.J. Guo, "Ranging based positioning employing co-operative Arrays,"International Symposium on Communications and Information Technologies (ISCIT), Gold Coast, Oct., 2012.

[2] K. Clare Xu, Y. J. Guo, Xiaojing. Huang, E. Dutkiewicz, "A hybrid wireless positioning system," IEEE International Symposium on Antennas and Propagation and USNC/URSI National Radio Science Meeting, Chicago, July 2012.

[3] K. Clare Xu, Y.J. Guo, Xiaojing Huang E. Dutkiewicz, "DoA based positioning employing uniform circular arrays," International Symposium on Communications and Information Technologies (ISCIT), Hangzhou, October 2011.

[4] K. Clare Xu, Y. Jay Guo, Xiaojing Huang, Eryk Dutkiewicz, "3D wireless positioning using uniform circular arrays," IEEE International Symposium on Antennas and Propagation and USNC/URSI National Radio Science Meeting, Spokane, July 2011.

[5] K. Clare Xu, Y. Jay Guo, Xiaojing Huang, Eryk Dutkiewicz, "Weighted least squares method for wireless positioning using multiple linear antenna arrays," IEEE International Symposium on Antennas and Propagation and USNC/URSI National

Radio Science Meeting, Spokane, July 2011.

[6] K. Clare Xu, Y.J. Guo, E. Dutkiewicz, "Swimmer tracking with underwater acoustic networks,"International Symposium on Communications and Information Technologies (ISCIT), Tokyo, October 2010.

# Chapter 2

# Literature Review

## 2.1 Introduction

The purpose of positioning is to obtain the unknown positions of target nodes based on a set of measurements. Positioning is normally conducted in two main steps: (i) Parameter estimation where the measurements of the parameters required for position calculation are performed and the parameter estimates are conducted; (ii) localisation where these estimates are processed to determine the position of target nodes. In a two-step positioning system, the positioning accuracy increases when the position-related parameters in the first step are estimated more precisely. In this chapter, various commonly used parameter estimation techniques for wireless positioning are described in Section 2.2. Section 2.3 discusses some key issues related to localisation including node configuration, distributed positioning networks and co-operative localisation. A number of current wireless positioning systems are presented in Section 2.4. Section 2.5 concludes the chapter.

## 2.2 Parameter Estimation Techniques

A. Time-of-Arrival (ToA) Estimation

Wireless positioning can be conducted based on many properties of radio, optical or acoustic waves, but most commonly used systems are based on the determination of the time-of-flight (ToF) which is the time taken for a signal to travel from the transmitter to the receiver, or a similar concept, the time-of-arrival (ToA) [10], [11]. In principle, if the time of the start of a transmission and the time of reception are both known, the ToF can be used to determine the range from the transmitting node to the receiving node. As radio waves propagate at about $0.3m$ per nanosecond, assuming the accuracy of an indoor positioning system is, say, less than a metre, timing measurements must be made to the order of one nanosecond. This precision of time measurement is very challenging, particularly when using cheap devices [12].

In a single-path propagation environment with no interfering signals and no obstructions between the nodes, extremely accurate ToF estimation can be performed. However, in practical environments, signals arrive at a receiver via multiple signal paths, and there are interfering signals and obstructions as well. Those error sources make it difficult to achieve high accuracy ToF estimation in practice, which are explained in details in the following.

1) Multipath Propagation: In a multipath environment, a transmitted signal arrives at the receiver via multiple paths. Owing to the high resolution of wideband signals, the pulses received via multiple paths are usually resolvable at the receiver. For narrow-band systems, however, pulses received via multiple paths overlap with each other as the pulse duration tends to be considerably larger than the relative time delays between the multipath components. This causes a shift in the delay corresponding to the correlation peak and can result in erroneous ToA estimation.

In order to mitigate those errors, super resolution time-delay estimation algorithms, such as that described in [13], [14], have been proposed for narrow-band systems. However, the high resolution of wideband signals in the time domain facilitates accurate correlation-based ToA estimation without the use of such complex algorithms. A number of first path detection algorithms have been proposed for ultra wideband (UWB) systems to accurately estimate ToA by determining the delay of the first incoming signal path [15], [16]. The effects of multipath propagation on ToA estimation can be analysed by employing accurate characterisation of wideband channels.

2) Non-line-of-sight (NLoS) Propagation: When the direct line-of-sight (LoS) between two nodes is obstructed, the direct signal component is attenuated significantly so it becomes considerably weaker than some other multipath components, or it cannot even be detected by the receiver. For the former case, first-path detection algorithms may still be utilised to estimate the ToA accurately. In the latter case, however, the delay of the first detectable signal path does not represent the true ToA, as it includes a positive bias, called NLoS error [17], [18]. Mitigation of NLoS errors is one of the most challenging tasks in accurate ToA estimation [19], [20], [21]. In the presence of statistical information about NLoS errors, various NLoS identification and mitigation algorithms can be employed. For example, in [22], the fact that the variance of ToA measurements in the NLoS case is usually considerably larger than that in the LOS case is used in order to identify NLoS situations, and then a simple LOS reconstruction algorithm is employed to reduce the positioning error. In addition, statistical techniques are studied in [23] and [24] in order to classify a set of measurements as LOS or NLoS. Finally, based on various scattering models for a given environment, the statistics of ToA measurements can be obtained, and then well-known techniques, such as maximum a priori (MAP) and maximum likelihood (ML), can be employed to mitigate the effects of NLoS errors [25], [26], [27].

3) Multiple-Access Interference: In the presence of multiple users in a given environment, signals can interfere with each other, and the accuracy of ToA estimation can degrade significantly [28], [29], [30]. A common approach to mitigate the effects of multiple access interference (MAI) is to assign different time slots or frequency bands to different users in a network [31]. However, there can still be interference among different networks that operate at the same time intervals and/or in the same frequency bands [32]. Therefore, various MAI mitigation techniques, such as non-linear filtering [33] and training sequence design [34], are commonly employed. For high end applications where the size and the cost of the nodes are less constrained, one can employ smart antennas to minimise the MAI effect [35].

B. Radio Signal Strength (RSS) Based Ranging

The simplest method to estimate the radio propagation range is to measure the signal strength and then exploit the relationship between the power loss and the distance between the transmitter and receiver. Such methods can be implemented, for instance, using commercial of the shelf (COS) ZigBee or WLAN hardware. Whilst signal strength measurements are available in even the simplest of single-chip radios, the accuracy of such measurements is limited mostly due to the complexity of propagation environment caused by shadowing and multipath, and the interaction with the human body when worn by a person [36], [37]. Generally speaking, signal strength varies in a complex fashion as a function of the position, so that a simple loss versus range function doe not exist. The changes in the transmission path loss are characterised primarily by shadowing, multipath fading and the distance between the transmitter and the receiver [38]. Shadowing is characterised by long-term fading or lognormal fading and its variations are due to terrain contour between the transmitter and receiver. It represents a slow variation in the mean envelope over a distance. The multipath fading is caused by NLoS propagation. The multipath fading or short-term

fading is characterised by the fast variation of received signal strength over a short distance on the order of a few wavelengths or over short time durations on the order of seconds [39], [40]. As a result, the path loss, which is the signal power attenuation with the increasing distance between the transmitter and the receiver, can fluctuate as much as $30-40dB$, thus degrading the ranging estimation accuracy [41], [42], [43].

One method to improve the RSS based ranging accuracy is to generate a path-loss map of the area concerned, which allows a database matching algorithm to improve the accuracy of the position fix [5], [44], [45], [46]. However, even with such a technique, and particularly when using cheap body-worn mobile units, the positional accuracy is likely to be of the order of a few metres. Thus signal strength methods are likely to be limited to applications where only crude positional accuracy, such as in wireless sensor network applications, is sufficient. A typical example is to locate the patients in a hospital, in which case a few metres of accuracy is adequate.

C. Direction-of-Arrival (DoA) Estimation

The direction of an incoming signal can be estimated by using an array. If one can measure the distance between the target and the array, the position of the target can be easily obtained. This is the basic principle of radar. One problem with this approach is that it demands a high accuracy of DoA estimation. Given an DoA estimation error, the associated position error increases as the target moves away from the array.

An improved method of using DoA estimation for positing is to employ more than one array. Given a set of arrays each of which are placed at a known position, there exists a simple geometric relationship between the array positions and the signal directions of arrival (DoA) estimated by each array. Using this geometrical relationship, the target which sends the signal can be located and tracked. The advantages of this approach are that the synchronisation between the target and the arrays is

not necessary; the signal format can be very simple; and the system can be operated in a very narrow band. This kind of positioning systems is more suited for scenarios where there are lines-of-sight (LoS) between the target and the super-nodes equipped with arrays. Such systems can be employed in applications like warfare, sport and underwater tracking of submarines. The key to this approach is also high accuracy and low complexity DoA estimation [47].

There are a number of techniques to estimate DoAs [48], and the most fundamental one is the conventional beamformer, also known as Bartlett beamformer [49]. For a signal coming from a given direction, the algorithm of the conventional beamformer maximises the power of the array output by weighting the signals at each array element. The optimum weighting vector obtained contains the DoA information. A study on the incoherent wideband MUSIC (IWM) and coherent wideband MUSIC (CWM) algorithms is presented with experimental analysis in [50]. It is shown that, given adequate SNR, the IWM performs well and yields sharp and distinct peaks in the beam pattern. However, frequency selective fading may be an issue here, as the inclusion of low SNR frequency bins tends to degrade the resulting beampattern, thus reducing height of peaks and introducing spurious peaks. In contrast, the coherent MUSIC approach is much more statistically stable, with a beampattern that generally improves with the addition of lower SNR bins. However, the inclusion of more frequency bins can introduce bias errors. The coherent approach outperforms the incoherent in terms of DoA accuracy with sources that have relatively flat spectra. Conversely, for sources with highly peaked spectra the incoherent approach yields better DoA results. In general, the coherent focused wideband methods are much more statistically stable than any of the incoherent wideband methods but at higher computational cost [51]. It is noted that coherent processing has great practical importance because it can handle fully correlated signals (e.g., multipath).

A critical problem associated with DoA estimations is that the accuracy of the estimation falls rapidly when the signal direction is close to the plane on which the array is placed. This is due to the physical property of the array element which radiates or receives energy as a function of the direction [52]. As a result, the signal-to-noise ratio deteriorates significantly as the DoA moves away from the normal direction. In other words, the variance of the DoA estimation changes according to DoA itself. This issue will be addressed in Chapter 5.

## 2.3 Localisation

Given an underlying transmission technology, the positioning performance is largely dependent on the specific algorithm used in the position update phase. In fact, although the parameter estimation accuracy provides the inherent limit on positioning accuracy, the positioning accuracy actually achieved in a system is determined by a number of other major factors and architecture decisions. For instance, in systems where anchor or reference nodes are employed, the number of reference nodes and the configuration of the reference nodes, referred to as node placement, play an import role in determining the system accuracy.

Traditionally, the architecture of a positioning system is based on the concept of reference nodes and target nodes whose position is required. In GPS, satellites can be considered as reference nodes, even though the satellites are moving relative to the earth, their positions at any time are accurately known [2], [53], [54], [55]. For indoor applications, a logical development would be to enhance the existing wireless local area network (WLAN) to incorporate positioning capability [9], [56]. For outdoor applications, base stations of cellular networks may serve as the positioning network infrastructure [57], [58], [59]. For specialist applications, an optimal node configura-

tion can be deployed to achieve the required accuracy with the minimum number of nodes [60].

An interesting area of research is distributed ad hoc wireless positioning networks. In such a network, small and low cost nodes are organised in an ad hoc manner. Nodes communicate among themselves for both data communications and position determination [61], [62]. Distributed positioning schemes are particularly suited to situations where a positioning infrastructure is not available. In a distributed positioning network, nodes are able to communicate directly only with their neighbours and compute the distances to their neighbours [63], [64]. Multilateration techniques, which encompass collaborative and iterative position determination based on distance estimates, are then used in a distributed manner to estimate the location of each sensor node. Distributed positioning algorithms generally have three positioning phases: the distance estimation phase where nodes estimate the distances to their neighbours, the position estimation phase where a system of linear equations is generally solved using a least squares approach to estimate the position of the node, and finally a refinement phase where the accuracy of the algorithm is improved by using an iterative algorithm.

An emerging paradigm is co-operative localisation, in which nodes help each other to determine their locations [65]. Co-operative localisation has received extensive interest from the robotics, optimisation, and wireless communications communities. The premise of co-operative positioning is this: while each mobile node cannot independently determine its own position based on distance estimates with respect to the anchor or reference nodes, they can co-operatively find their positions. In general, co-operative localisation can dramatically increase localisation performance in terms of both accuracy and coverage. Apparently, there is a blurred distinction between distributed and co-operative positioning networks as the latter are necessarily

distributed. A common view is that the latter is more focused on the co-operation between adjacent nodes to extend the coverage of positioning network and increase accuracy.

All the positioning techniques described above need an infrastructure. In contrast, the inertia sensor base positioning is infrastructure-free [3]. The concept is biologically inspired; a hummingbird obtains the relevant information on spatial position from its sophisticated equilibrium organs. By means of inertial sensor systems, the motion of an object, animal, or person can be continuously measured. The current position is calculated on the basis of the distance that was covered within a certain time interval and the direction of the motion with reference to the last known position. The basic idea behind an inertial navigation system (INS) is to measure the acceleration and angular rate in order to calculate the position. In principle, three angular rate or rotation sensors (gyroscopes) and three acceleration or motion sensors (accelerometers) which are orthogonally positioned to each other are required to continuously track the position, orientation, and velocity of a moving object without the need for external references. The update or tracking is done via dead reckoning, a method to predict a future position by the course and speed from a known present position. Dead-reckoning is simple, inexpensive, and easy to accomplish in real-time. But the disadvantage of dead-reckoning is its unbounded accumulation of errors [66]. Typical dead-reckoning errors are so large that the position estimate may become unacceptably wrong after as little as ten metres of travel.

INS is used on vehicles such as ships, aircraft, submarines, guided missiles, and spacecraft. For military and other mission critical applications where cost is not a major objective, high-end INS serves as a superb positioning technology. With the current state of the art of sensor technologies, however, it is found that low-cost and low form factor inertial sensors suffer from a phenomenon known as drift, so the

position values need to be calibrated after, say, a few metres for a walking person with an external reference. Therefore, for handheld devices, the INS as a positioning system may remain as a complementary technology for some years [4], [8] to come.

## 2.4 Current Wireless Positioning Systems

1. Wireless Positioning in Cellular Networks: At the onset of 3G standardisation in the late 1990s, it was predicted that location based services (LBS) such as localised advertising, clubbing and workforce and fleet management would become pervasive. Consequently, four positioning schemes were introduced to third generation partnership project (3GPP) standards including Cell ID, assisted GPS (A-GPS), observed time-difference of arrival (OTDOA) and uplink time-difference of arrival (UTDOA) [67]. The Cell ID method locates a mobile terminal according to the radio cell, typically a sector, to which it is connected. A-GPS is a version of the GPS which employs the cellular system to aid the acquisition process. OTDOA is basically a time difference measurement technique (TDoA) to locate a mobile terminal by trilateration. Each OTDOA measurement for a pair of downlink transmissions from two adjacent base stations describes a line of constant difference along which the mobile terminal may be located. The mobile terminal position is determined by the intersection of these lines for at least two pairs of base stations. UTDOA is the uplink version of OTDOA, in which the time-of-flight measurements are done by the network instead of the mobile terminal using the uplink signals from a mobile to a number of adjacent base stations.

The latest 3GPP long term evolution (LTE) standards support assisted-global navigation satellite system (A-GNSS), which is similar to A-GPS but supports other satellite systems, as well as OTDOA in Release 9. The UTDOA was standardised in

Release 11 [68], [69], [70]. Field trials by Nokia Siemens Network demonstrated that A-GNSS is the most accurate for outdoor applications with two metres accuracy at the best, and OTDOA is the second most accurate reaching fifty metres at the best.

2. Wireless Local Area Networks (WLAN): The WLAN technology currently is based on the IEEE 802.11 specifications, which define a number of different physical layers for data transmission operating in the $2.4GHz$ ISM band and at $5.2GHz$. Positioning capability is not part of the normal operation, but the functionality could be added. The simplest implementation is based on signal strength measurements, but techniques using ToA also could be implemented. The range of the current WLAN is typically limited to about fifty metres indoors, and a similar range could be expected for a positioning application.

There are three types of positioning systems based on the WLAN platform. The first is RSS based, the second is to introduce a tag such as CISCO's choke point which is effectively a proximity detector and the third one is based on database to do localisation. The U.S. Wireless Corporation's fingerprinting scheme falls under the third category. Instead of exploiting signal timing or signal strength, this scheme relies on the received signal structure characteristics to do localisation. By combining the multi-path pattern with other signal characteristics, the algorithm creates a signature unique for every given location in the area. This can be achieved by carrying the target node through the area and acquiring the signal characteristic information. By comparing the received signal characteristic to all the fingerprints in the database, a node's location can be determined. The major drawback of this technique is the substantial effort needed for generating the signal signature database. Hence, it is not suited for the ad hoc deployment scenarios where the radio environment is not known in advance. Besides, the positioning accuracy is also limited.

3. Radio Frequency Identification (RFID): RFID is a simple radio technology

mainly aiming at providing identification of objects based on a unique multi-digit identifier, usually associated with inventory control applications. RFID tags are small and very cheap, but their range is limited to about one metre. Normally a special tag reader, often hand held, is used to identify the tag. Such technology is not particularly aimed at position determination, but a simple adaptation would allow its use for position determination to a limited extent. For example, tag readers at a strategic locations such at doorways can be used to identify people moving through a building. In an office building, one reader located at the entrance of each floor would provide the information needed for emergency evacuation. The positional accuracy would be typically few metres (the size of a room) at the best.

4. Ultra-Wideband (UWB): UWB uses a very wide bandwidth (greater than $500MHz$ [71]), but is restricted to a very low transmitter power density to minimise the interference to other existing radio systems which use part of the same frequency band ($3GHz$ to $10.7GHz$). UWB technology is mainly aimed at short-range (typically ten metres) and high data rates links. However, the large bandwidths are ideal for indoor positioning systems, as the large bandwidth can bed used to mitigate the effects of multipath propagation by allowing very fine (sub-nanosecond) time resolutions, thus resulting in an accuracy of the order of twenty cetimetres. The short range nature of UWB means that the number of base stations required to cover an area can be very large.

5. IEEE 802.15.8: The IEEE is currently in the process of developing a peer aware communications (PAC) system for wireless personal area networks. The communications range is from two hundred metres to five hundred metres. It shall operate in the ISM bands and the UWB bands. An interesting fact is that it shall support peer to peer ranging. In fact, one of the companies participating in the standardisation process, Nanotron, has already developed a ranging chipset based on chirp spread

spectrum across a bandwidth of $80MHz$. As far as positioning is concerned, IEEE 802.15.8 is the most interesting standard to watch.

6. Underwater Sensing and Positioning Networks: Although underwater sensor networks share some common properties with ground based wireless sensor networks, such as the large number of nodes and limited energy available to each node, they possess some unique characteristics [72], [73]. First, radio communications do not work well under the water due to the absorption of radio waves by water, especially the sea water, so they must be replaced by acoustic communications. Second, the propagation of acoustic waves in water has very different characteristics. With the speed of $1500m/s$, underwater acoustics waves are five orders of magnitude slower than radio, thus leading to large latency [74]. Further, the available bandwidth of underwater acoustic channels is drastically limited due to water absorption at high frequencies. Most acoustic systems operate below $30kHz$, and rarely above $1MHz$. It is reported that no research or commercial system can exceed $40km \times kb/s$ as the product of *maximum available range* $\times$ *rate*. This means that the bandwidth of underwater acoustic channels operating over several kilometres is about several tens of kilobits per second, while short-range systems over several tens of metres can reach hundreds of kilobits per second. Fifth, whilst most ground based sensors are static, underwater sensor nodes may move with water currents and other underwater activities. Some empirical study showed that underwater objects may move at the speeds of $3 - 6km/h$ under a typical condition.

The mobility of the anchor nodes poses a great challenge to the localisation of a mobile sensor. By utilising the predictable mobility patterns of underwater objects, [75] proposed scalable localisation scheme with mobility prediction (SLMP), which divides under water localisation into two parts: anchor node localisation and ordinary node localisation. Anchor nodes, of which positions are known, will control

the whole localisation process, and every ordinary node predicts its future mobility pattern according to its past known location information. [75] introduced the three dimensional underwater localisation (3DUL) algorithm that seeks to achieve 3D localisation in large-scale underwater acoustic sensor networks in a dynamic, energy efficient, simple and accurate way. This process dynamically iterates along all directions in 3D topology to localise as many nodes as possible. In [76], the localisation problem in sparse 3D underwater sensor networks is transformed into its two dimensional counterpart via a projection technique. Other papers examined the 3D localisation problem from a different angle, such as the difficulties of precise deployment of underwater sensor networks [77], [78], [79], the limitation of bandwidth and battery power in underwater environment [80], [81], distance measurements underwater suffer from large errors due to the fact that the speed of sound is affected by water temperature, pressure, and salinity [82]. [83] proposed a 3D localisation scheme using directional beacons (LDB) for under water sensor networks. LDB employs an acoustic directional transducer which acoustic beam under the AUV to aid localisation underwater.

## 2.5 Conclusion

In this chapter, we have reviewed various parameter estimation techniques for wireless positioning and their latest development, including multipath, NLoS and multiple access interference mitigation techniques. The latest research in localisation such as co-operative and distributed ad hoc positioning networks are discussed. We complete the literature review by outlining a number of existing systems employed by industry and the research community, namely, cellular systems, WLAN, RFID, ultra-wideband (UWB), IEEE 802.15.8 peer aware communications (PAC) and underwater

positioning networks.

GPS denial wireless positioning is currently an area of active research aiming to achieve a number of major objectives: 1) higher accuracy; 2) lower overall system cost; 3) less dependency on the infrastructure; 4) seamless positioning. The following chapters detail our achievements in addressing the first three issues.

# Chapter 3

# Node Configuration in Positioning Networks

## 3.1 Introduction

Node configuration in positioning networks is of great importance for practical network deployment, as it has significant impact on the positioning accuracy in the coverage area and the number of nodes required. The latter can be translated into network capital and maintenance cost, and it also affect the network capacity and therefore the maximum update frequency. Recently, in a paper entitled "Sensor placement for triangulation-based localisation" by Tekdas and Isler [84], the authors studied the problem of finding the minimum number, and placement of sensors in such a way that the uncertainty in localisation is bounded at every point in a given space. The method Tekdas and Isler employed to determine the location of an object is triangulation, in which two bearing measurements at two sensors are made. Given the positions of the two sensors and the two bearing measurements, the location of an unknown target can be obtained.

The relative positions between target node and sensors nodes play a significant role in the accuracy of an estimation obtained via triangulation. If the target and the two sensors are collinear, the sensors cannot localise the target. In general, the uncertainty in bearing-only triangulation is proportional to the product of target-sensor distances and inversely proportional to the sine of the angle between the target and the sensors [85]. The environment also plays a role in localisation with triangulation. For example, occlusions caused by the environment may prevent a sensor from participating in the triangulation process.

The most well-known node placement problem is perhaps the Art Gallery Problem that involves cameras [86] where a minimum number of omnidirectional cameras is sought to guard every point in a gallery represented by a polygon. Art gallery problems emphasise visibility/occlusion issues and there is no explicit representation of the quality of guarding. The problem of relocating sensors to improve coverage has been studied in [87]. In the formulation, It is assumed that the sensors can individually estimate the positions of the targets, but the quality of coverage decreases with increasing distance. The problem of choosing the best subset of cameras for a given placement has been studied recently in [88]. In this work, the focus is on selecting a small subset of cameras to minimise a joint uncertainty measure.

This chapter is concerned with the problem of node placement or node configuration using trilateration. Similar to triangulation, two range measurements instead of bearing measurement from two sensor nodes are required to locate an unknown target. Naturally, the quality of the localisation is a function of relative position between the target node and reference nodes. We consider the scenario where there is the freedom to choose the locations of the reference nodes and we aim to optimise those locations in order to minimise the position estimation errors. The scenario we presented is the monitoring of elite swimmers in a swimming pool. As is known in the sport commu-

nity, a monitoring system which can provide timely feedback to the swimmer, coach and sport scientists regarding the performance and physiological capabilities of an athlete is critical for the development of optimal personal training plans that could ensure a swimmer's continued improvement and enhance their ability to win medals in major competitions such as the Olympics Game [89]. To ease the analysis, we assume certain statistics regarding the range measurements without specifying the techniques used for measuring the ranges [90]. Given the fact that radio waves do not travel far underwater, the most practical underwater ranging technique may be via acoustics or optics for short ranging applications, but these details are beyond the scope of the thesis.

The chapter is organised as follows. Following Section 3.1, in Section 3.2, we introduce the spherical interpolation approach as the chosen positioning algorithm [91]. In Section 3.3, the configuration of the network, namely, the arrangement of sensor nodes in the swimming pool, is optimised to achieve the highest accuracy with the minimum number of nodes and therefore the lowest cost. The objective function used for the node configuration optimisation is the cumulative distribution function (CDF). The study includes both two dimensional (2D) and three dimensional (3D) cases to understand the variation of the positioning estimation accuracy in the horizontal and vertical planes. Finally, the conclusions are presented in Section 3.4.

## 3.2 Spherical Interpolation Approach

Using the trilateration approach, the determination of the position of a target node is based on the distance or range measurements between the target node and the sensor nodes. Two types of ranging methods are commonly used, the time-of-flight (ToF) and the time-difference-of-arrival (TDoA). The TDoA method has the

advantage that no synchronisation between the target nodes and the sensor nodes is required, and therefore it is much easier for implementation and has been more widely employed. For this reason, the TDoA method is employed in the study. Furthermore, we assume that the target nodes are for transmission only, and all the sensor nodes placed in a swimming pool are for receiving only, and they are all connected to a central signal processing unit. When a signal is sent from a swimmer, all the sensor nodes will receive the signal with a time delay determined by the distances from the target to each sensor node. Different delays are then used to determine the position of the target.

The TDoA measurements lead to a set of non-linear equations whose solution yields the position of the target node. One way to solve the non-linear equations is to use a linear approximation based on Taylor series expansion and find the position iteratively [92]. This method has the advantage of low computational complexity and is therefore suited for the implementation in a real-time system. A more elegant way to solve the non-linear equation is to employ the spherical interpolation approach (SIA) [93]. A salient advantage of SIA is that the position estimate is expressed in a closed form so it is easier to ensure the accuracy. The disadvantage of SIA is that it doesn't have the lowest complexity. Since the positioning calculation is done in the network but not in the target node, the complexity of the algorithm is not really an issue for our study. Furthermore, an instantaneous report on the positions of targets is not required for the application concerned and it is acceptable for the position data to be obtained after the completion of the measurements (training session or competition). For these reasons, the SIA is used in our study.

Given the position estimates across the node covering area, i.e., the swimming pool, one can calculate the cumulative distribution function (CDF) of positioning. It is shown in the following that different node configurations result in different CDF.

Mathematically, the SIA scheme is shown in Fig. 3.1. The target is assumed to be at position $(x, y, z,)$ at a given instant, the distance from the target to node $i$ is denoted as $d_i$, the distance from the origin of the Cartesian coordinate to node $i$ is denoted as $R_i$, and $d_j$ represents the distance from the target to node $j$. Assuming that node $i$ receives the signal from the target node at time $t_i$ and node $j$ receives the signal at time $t_j$, one has

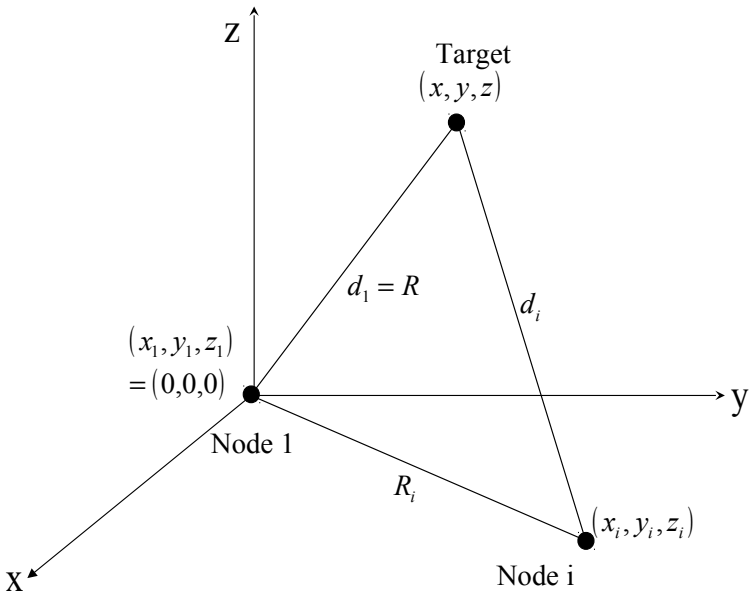


**Figure 3.1:** Co-ordinate used for spherical interpolation approach

$$R_i = \sqrt{{x_i}^2 + {y_i}^2 + {z_i}^2}, \tag{3.1}$$

$$\mathbf{p} = \begin{bmatrix} x, & y, & z \end{bmatrix}^T, \tag{3.2}$$

$$d_{ij} = d_i - d_j = v(t_i - t_j), \tag{3.3}$$

where $d_{ij}$ is the TDoA measurement from node $i$ and node $j$, and $v$ is the speed of sound in water. It is assumed that the target node and the sensor nodes are all immersed in water. Denoting the measurement error for $d_{ij}$ as $\varepsilon_{ij}$ , and the measured distance of TDoA as $\hat{d}_{ij}$ , one has

$$\hat{d}_{ij} = d_{ij} + \varepsilon_{ij}. \tag{3.4}$$

The position of the target is given by [47] as

$$\hat{\mathbf{p}} = \frac{1}{2}\left(\mathbf{A}^T\mathbf{W}\mathbf{A}\right)^{-1}\mathbf{A}^{\mathbf{T}}\mathbf{W}\left(\mathbf{I} - \frac{\hat{\mathbf{d}}\hat{\mathbf{d}}^T\mathbf{B}\mathbf{V}\mathbf{B}}{\hat{\mathbf{d}}^T\mathbf{B}\mathbf{V}\mathbf{B}\hat{\mathbf{d}}}\right)\boldsymbol{\delta}, \tag{3.5}$$

where

$$\boldsymbol{\delta} = \begin{bmatrix} {R_2}^2 - \hat{d}_{21}^2, & {R_3}^2 - \hat{d}_{31}^2, & \cdots, & {R_N}^2 - \hat{d}_{N1}^2 \end{bmatrix}^T, \tag{3.6}$$

$$\hat{\mathbf{d}} = \begin{bmatrix} \hat{d}_{21}, & \hat{d}_{31}, & \cdots, & \hat{d}_{N1} \end{bmatrix}^T, \tag{3.7}$$

$$\mathbf{A} = \begin{bmatrix} x_{21} & y_{21} & z_{21} \\ x_{31} & y_{31} & z_{31} \\ \vdots & \vdots & \vdots \\ x_{N1} & y_{N1} & z_{N1} \end{bmatrix}, \tag{3.8}$$

$$\mathbf{B} = \mathbf{I} - \mathbf{A}\left(\mathbf{A}^T\mathbf{W}\mathbf{A}\right)^{-1}\mathbf{A}^T\mathbf{W}. \tag{3.9}$$

The weighting matrices $\mathbf{V}$ and $\mathbf{W}$ are employed for emphasising the contributions of the measurements that are more reliable. If the quality of the ranging measurements is known, the weighting matrices should be chosen accordingly to achieve good accuracy. In this study we consider homogenous transmission, so $\mathbf{V}$ and $\mathbf{W}$ are chosen as unit matrix.

From (3.8) one can see that, in general, to avoid $\mathbf{A}$ being singular, the minimum number of reference node is 4.

## 3.3 Optimisation by Using a Cumulative Distribution Function

A simulation study has been conducted to investigate the effect of the network configuration on the accuracy of localisation using the following methodology. The TDoA measurement is modeled by a range measurement with errors following a Gaussian distribution with a standard deviation $\sigma$ given by

$$pdf\,(x) = \frac{1}{\sqrt{2\pi}\sigma} \exp\left(-\frac{(x-\mu)^2}{2\sigma^2}\right), \tag{3.10}$$

where $\mu$ is the true value of the range. A standard size training pool as that used at the Australian Institute of Sports (AIS), which is $50m$ long, $25m$ wide and $3m$ deep, is assumed. A simulation run is conducted for each given configuration. For each simulation run, 1000 random locations are chosen for 2D cases and 10000 for 3D cases, and 100 positioning estimates using SIA is performed for each given location. The cumulative distribution function (CDF) of estimation errors are produced for each given configuration.

The study starts with 2D cases first. Fig. 3.2 shows different configurations and their CDFs. The nodes number are chosen to be four, six and eight, and all the nodes are placed in the same horizontal plane as the target node. The standard deviation, $\sigma$, is chosen to be $0.1m$ to meet the measurement accuracy of the most common devices. It is seen that, for a given network size, there is an optimum network configuration which produces the highest positioning accuracy. The smaller the number of the sensor nodes, the more sensitive the CDFs are to the network configuration. When the node number or the network size increases, the effect of the network configuration decreases.

The greater the number of the sensor nodes, the higher the positioning accuracy.

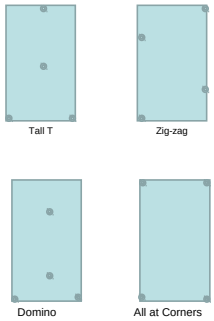


(a) Configurations of four nodes

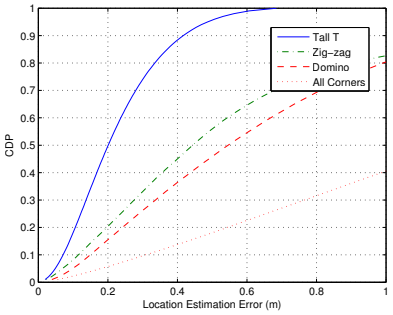


(b) CDFs of 4-node configuration

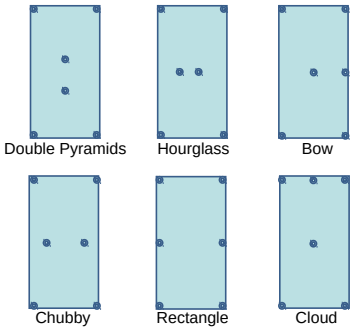


(c) Configurations of six nodes

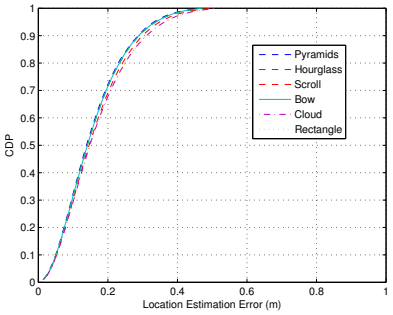


(d) CDFs of 6-node configuration

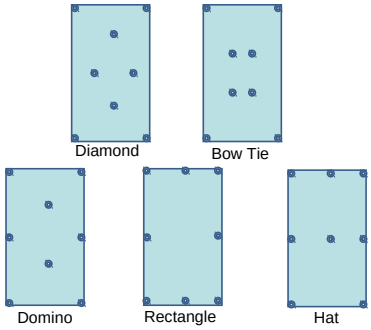


(e) Configurations of eight nodes

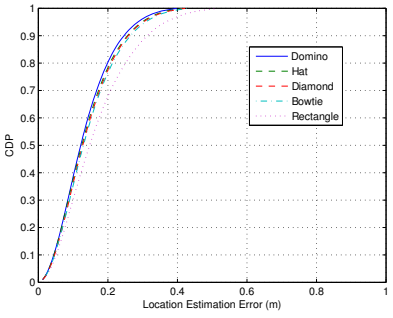


(f) CDFs of 8-node configuration

**Figure 3.2:** Different configurations and their CDFs, the STD of measurement is $0.1m$

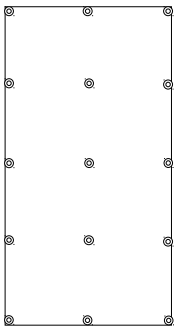

(a) Configuration of fifteen nodes

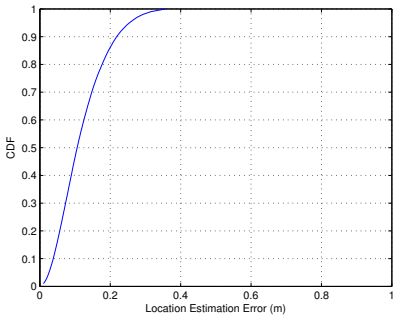


(b) CDF of 15-node configuration

**Figure 3.3:** Configurations of fifteen nodes and its CDF, the STD of measurement is $0.1m$

It is found that when the number of sensor nodes is further increased, the network size becomes the dominating factor. Fig. 3.3 shows the CDF using the network configuration with 15 sensor nodes.

Next we move to the 3D case. Since the depth of the swimming pool is much smaller than the width and the length, the positioning accuracy in the vertical direction is expected to be lower than that in the horizontal plane. This is a general problem in 3D positioning for both wireless and underwater networks as one always has limited flexibility in placing sensor nodes vertically [94]. Fig. 3.4 shows an underwater acoustic network configuration with three tiers of sensor nodes placed on three horizontal planes at $z = 0$ (bottom), $z = 1.5m$ (middle) and $z = 3m$ (just beneath the water surface), each tier contains fifteen sensor nodes and its CDFs, one for the overall 3D position estimation, one for horizontal plan position estimation and the other for the position estimation in the vertical direction.

It is seen, in Fig. 3.4, that positioning accuracy is slightly better in the horizontal plane by comparing with single layer of fifteen nodes, as shown in Fig. 3.3. However, the overall estimation accuracy is reduced significantly due to the lower accuracy

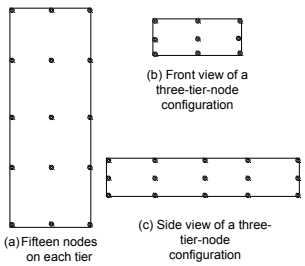


(a) Configuration of 3 tiers

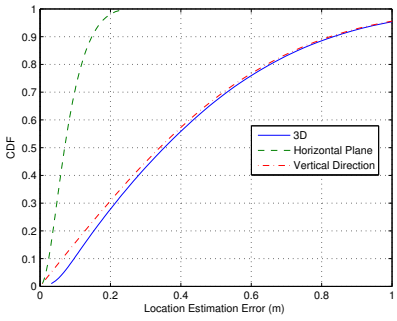


(b) CDFs of 3 tier Configuration

**Figure 3.4:** Configuration of 3 tiers with 15 nodes on each layer and CDF, the STD of measurement is $0.1m$

in the vertical direction. An improvement in the accuracy can be made by either increasing the ranging accuracy from $0.1m$ to a few millimetres or by placing more sensor nodes in the middle of the pool. The former would demand for more delicate and more expensive sensor nodes or hydrophones, whereas the latter may cause certain inconvenience which is not ideal but can be acceptable in practice. A practical problem associated with the latter is the difficulty in keeping positions of the sensor nodes in the middle of the space or swimming pool fixed.

Fig. 3.5 shows for a network configuration with three tiers each contains forty-five sensor nodes placed on planes and the CDF.

With three tiers and each tier contains forty-five nodes,the 3D positioning accuracy can reach 95 per cent within $1m$ when the standard deviation is $0.1m$. To reach positioning accuracy within $0.1m$, the standard deviation needs to be narrowed down to $0.01m$; and to reach positioning accuracy within $2-3cm$, the standard deviation needs to be further reduced down to $5mm$, as shows in Fig. 3.6.

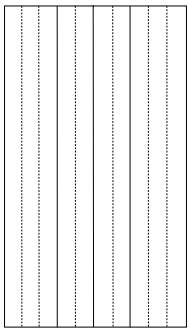

(a) A horizontal plane of 45 sensor nodes placed on the solid dividing lines.

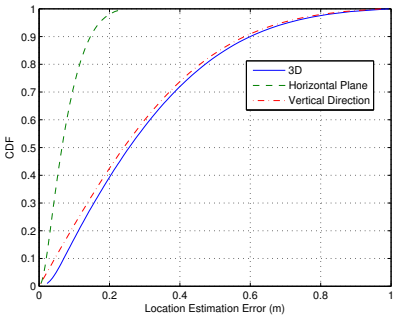


(b) CDFs for configuration of 3 tiers each with 45 nodes. The STD of measurement is $0.1m$.

**Figure 3.5:** A network configuration with three tiers each contains forty-five sensor nodes and the CDFs.

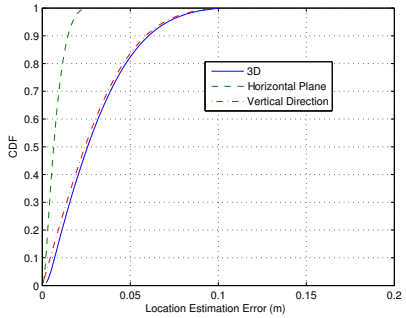


(a) When STD of measurement is $1cm$.

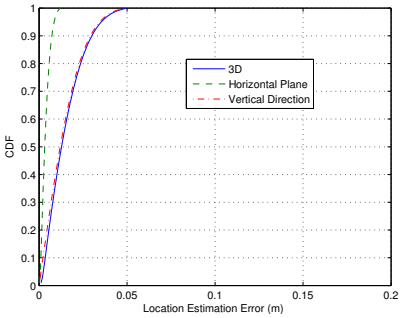


(b) When STD of measurement is $5mm$.

**Figure 3.6:** CDFs for a network configuration with three tiers each contains forty-five sensor nodes.

## 3.4 Conclusion

The sensor configuration using TDoA has been investigated in this chapter. The spherical interpolation approach is used as the positioning algorithm. The evaluation of different configurations is to achieve the maximum CDF using the minimum number of sensor nodes. A parametric study on the configuration of the network and the size of the network is presented to understand their effect on the positioning accuracy. It is found that the configuration of the network, i.e., the arrangement of the sensor nodes, has a strong effect on the positioning accuracy. The smaller the number of the sensor nodes, the more sensitive the CDFs are to the network configuration. When the sensor node number increases, the effect of network configuration decreases. The greater the number of the sensor nodes, the higher the positioning accuracy. When the number of sensor nodes is large, say more than ten, it becomes the dominating factor. With $1cm$ standard deviation for ranging, a $2cm$ positioning accuracy in the horizontal plane can be achieved by employing three tiers with fifteen sensor nodes on each, which is adequate for monitoring the speed of targets. Owing to the limited depth of a swimming pool, however, it is shown that monitoring the 3D movement of targets proved to be very challenging, demanding a ranging accuracy of at least a few millimetres.

It should be pointed out that the dependance of the positioning accuracy, CDF in the current context, on the node configuration is also a function of the positioning algorithm used. The fact that one node configuration is better than another for a given positioning algorithm may not hold for a different positioning algorithm [92]. A more general approach to optimising the node configuration for a given coverage scenario is to use the geometric dilution of precision (GDoP) as the fitness function, as GDoP provides a good approximation to the Cramér-Rao lower bound (CRLB) [95]

which is algorithm independent. This is the topic for the next chapter.

# Chapter 4

# A Hybrid Node Configuration Optimisation Scheme Using GDoP

## 4.1 Introduction

The accuracy of ranging based positioning methods is determined by three main factors, namely, the ranging accuracy, the positioning algorithm and the configuration of the reference nodes. The geometric configuration of the reference nodes or anchor nodes in relation to the area in which the target nodes are to be located is critically important, sometimes even dominant. The geometric dilution of precision (GDoP) is used to describe how the positioning accuracy is related to such geometric factors [96]. To certain extent, without doing any detailed analysis of the positional errors, GDoP can be used to assess the "fitness" of given reference node placement and optimise it accordingly [97], [98]. A further advantage of employing GDoP as the fitness function is that GDoP provides a good approximation to the Cramér-Rao lower bound (CRLB) [95] and, therefore, the optimised node configuration is independent of the positioning algorithm used.

This chapter is organised as follows. Following Section 4.1, we first present the theory of GDoP in Section 4.2. In Section 4.3 we introduce particle swarm optimisation (PSO) method. Then, in Section 4.4, a hybrid optimisation algorithm combining the particle swarm optimisation (PSO) method and the sequential quadratic programming (SQP), using the average GDoP as the objective function is proposed. In this section, the hybrid optimisation algorithm is used to optimise the locations of the reference nodes. The effectiveness of the hybrid optimisation method is demonstrated by simulation results. Finally, Section 4.5 concludes the chapter.

## 4.2 Geometric Dilution of Precision of Positioning System

We assume a positioning system based on ranging measurement. Every range estimate would incur certain errors which contribute to the positional inaccuracy. For simplicity, a 2D geometric model of the reference node $i$, the target and the estimated position is shown as Fig. 4.1. Its extension to 3D is straightforward.

Assume that the $i^{th}$ reference node is located at $(x_i, y_i, z_i)$, and the true position of the target is $(x, y, z)$, the distance between the $i^{th}$ sensor node and the target, $d_i$ , is given by $d_i = \sqrt{(x - x_i)^2 + (y - y_i)^2 + (z - z_i)^2}$ , $i = 1, \cdots, N$. Denoting $c$ as the propagation speed, if all the sensors are time synchronised, $r_i$ is expressed as the sum of propagation distance between the target and the sensor node, $d_i$, and an unknown error caused by a time offset which is expressed as $c\phi$, i.e.

$$r_i = d_i + c\phi. \tag{4.1}$$

If the position coordinate estimation errors $\Delta x$, $\Delta y$ and $\Delta z$ are small, and the time estimation error, $\Delta\phi$, is also small, the corresponding ranging error associated

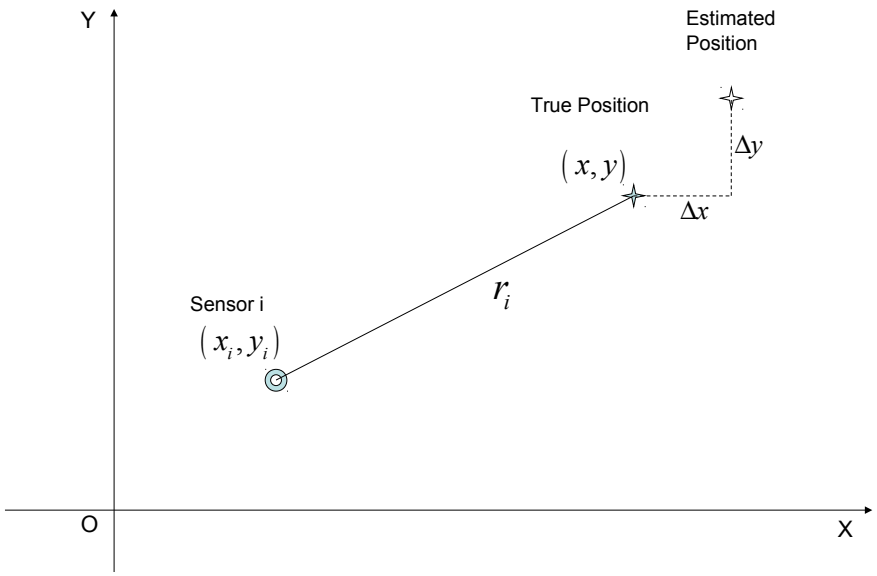


**Figure 4.1:** Distance and its measurement error

with the $i^{th}$ sensor can be expressed as

$$\Delta r_i \approx \frac{\partial r_i}{\partial x}\Delta x + \frac{\partial r_i}{\partial y}\Delta y + \frac{\partial r_i}{\partial z}\Delta z + \frac{\partial r_i}{\partial \phi}\Delta \phi. \tag{4.2}$$

To emphasis the nodes configuration effect, we assume that the clocks are perfectly synchronised so $\frac{\partial r_i}{\partial \phi} = 0$. Denote $\alpha_i$ the derivative of the range of $i^{th}$ sensor with respect to the target Cartesian coordinate $x$, and $\beta_i$ the derivative of the range with respect to the target coordinate $y$, $\gamma_i$ the derivative of the range with respect to the target coordinate $z$, i.e.,

$$\begin{aligned} \alpha_i &= \frac{\partial r_i}{\partial x} = \frac{x - x_i}{r_i}, \\ \beta_i &= \frac{\partial r_i}{\partial y} = \frac{y - y_i}{r_i}, \\ \gamma_i &= \frac{\partial r_i}{\partial z} = \frac{z - z_i}{r_i}. \end{aligned} \tag{4.3}$$

From (4.3), the $N$ range errors $\Delta r_i$, $i = 1, 2, \cdots, N$, can be used to estimate the

positioning errors by performing least squares fitting. Denote

$$\mathbf{A} = \begin{bmatrix} \alpha_1 & \beta_1 & \gamma_1 \\ \alpha_2 & \beta_2 & \gamma_2 \\ \vdots & \vdots & \vdots \\ \alpha_N & \beta_N & \gamma_N \end{bmatrix}, \quad \boldsymbol{\delta} = \begin{bmatrix} \Delta x \\ \Delta y \\ \Delta z \end{bmatrix}, \quad \mathbf{h} = \begin{bmatrix} \Delta r_1 \\ \Delta r_2 \\ \vdots \\ \Delta r_N \end{bmatrix}. \tag{4.4}$$

Equation (4.1) can be re-written as

$$\mathbf{A}\boldsymbol{\delta} \approx \mathbf{h}. \tag{4.5}$$

The least squares solution of (4.5) is given by

$$\boldsymbol{\delta} = \left(\mathbf{A}^T\mathbf{A}\right)^{-1}\mathbf{A}^T\mathbf{h}. \tag{4.6}$$

Denote

$$\mathbf{Z} = \left(\mathbf{A}^T\mathbf{A}\right)^{-1}, \tag{4.7}$$

the elements in (4.4) can be expressed as

$$\begin{aligned} \Delta x &= Z_{1,1}\sum_{i=1}^{N}\alpha_i\Delta r_i + Z_{1,2}\sum_{i=1}^{N}\beta_i\Delta r_i + Z_{1,3}\sum_{i=1}^{N}\gamma_i\Delta r_i \\ &= \sum_{i=1}^{N}\rho_i\Delta r_i, \\ \Delta y &= Z_{2,1}\sum_{i=1}^{N}\alpha_i\Delta r_i + Z_{2,2}\sum_{i=1}^{N}\beta_i\Delta r_i + Z_{2,3}\sum_{i=1}^{N}\gamma_i\Delta r_i \\ &= \sum_{i=1}^{N}\kappa_i\Delta r_i, \\ \Delta z &= Z_{3,1}\sum_{i=1}^{N}\alpha_i\Delta r_i + Z_{3,2}\sum_{i=1}^{N}\beta_i\Delta r_i + Z_{3,3}\sum_{i=1}^{N}\gamma_i\Delta r_i \\ &= \sum_{i=1}^{N}\chi_i\Delta r_i. \end{aligned} \tag{4.8}$$

where $Z_{i,j}$ represents the element in $i^{th}$ row and $j^{th}$ column in matrix $\mathbf{Z}$, and

$$\begin{aligned} \rho_i &= Z_{1,1}\alpha_i + Z_{1,2}\beta_i + Z_{1,3}\gamma_i, \\ \kappa_i &= Z_{2,1}\alpha_i + Z_{2,2}\beta_i + Z_{2,3}\gamma_i, \\ \chi_i &= Z_{3,1}\alpha_i + Z_{3,2}\beta_i + Z_{3,3}\gamma_i. \end{aligned} \tag{4.9}$$

The mean and variance of the positioning errors $\Delta x$ are given by

$$\begin{aligned} E\left[\Delta x\right] &= E\left[\sum_{i=1}^{N} \rho_i \Delta r_i\right] = \sum_{i=1}^{N} \rho_i E\left[\Delta r_i\right] = 0, \\ {\sigma_x}^2 &= E\left[(\Delta x)^2\right] = E\left[\left(\sum_{i=1}^{N} \rho_i \Delta r_i\right)^2\right] = \sum_{i=1}^{N} {\rho_i}^2 E\left[(\Delta r_i)^2\right] = {\sigma_r}^2 \sum_{i=1}^{N} {\rho_i}^2, \end{aligned} \tag{4.10}$$

and similarly, the means and variances of the positioning errors $\Delta y$ and $\Delta z$ are given by

$$\begin{aligned} E\left[\Delta y\right] &= E\left[\sum_{i=1}^{N} \kappa_i \Delta r_i\right] = 0, \\ {\sigma_y}^2 &= E\left[(\Delta y)^2\right] = E\left[\left(\sum_{i=1}^{N} \kappa_i \Delta r_i\right)^2\right] = {\sigma_r}^2 \sum_{i=1}^{N} {\kappa_i}^2, \end{aligned} \tag{4.11}$$

and

$$\begin{aligned} E\left[\Delta z\right] &= E\left[\sum_{i=1}^{N} \chi_i \Delta r_i\right] = 0, \\ {\sigma_z}^2 &= E\left[(\Delta z)^2\right] = E\left[\left(\sum_{i=1}^{N} \chi_i \Delta r_i\right)^2\right] = {\sigma_r}^2 \sum_{i=1}^{N} {\chi_i}^2. \end{aligned} \tag{4.12}$$

The GDoP is defined as [92]

$$GDoP = \sqrt{\frac{\sigma_x^2 + \sigma_y^2 + \sigma_z^2}{\sigma_r^2}}. \tag{4.13}$$

Substituting (4.10), (4.11) and (4.12) in (4.13) results in

$$GDoP = \sqrt{\sum_{i=1}^{N} \rho_i^2 + \sum_{i=1}^{N} \kappa_i^2 + \sum_{i=1}^{N} \chi_i^2}. \tag{4.14}$$

Since $\rho_i$, $\kappa_i$ and $\chi_i$ in (4.14) are related to the coordinates of sensor node $i$ and the target, GDoP reflects how the node configuration affects the positioning accuracy. The lower the GDoP level, the more accuracy positioning a system can provide. Since our aim is to achieve the highest positioning accuracy at most places, we choose the average GDoP as the objective function for an optimisation process. Bearing in mind that the GDoP theory assumes that the ranging errors are much smaller than the ranges themselves, circular areas with a predetermined radius around every sensor node are excluded in the calculation of GDoP. This is different from the CDF analysis in the previous chapter.

## 4.3 Particle Swarm Optimisation

Given the number of sensor nodes and the area within which they can be placed, the average GDoP across a given area can be minimised by finding the optimum sensor locations. Such an optimisation process is unfortunately complicated. There exists a vast number of optimisation algorithms in the open literature. Different optimisation algorithms are classified based on the type of the search space and the objective (cost) function. The simplest technique is linear programming (LP) which concerns the case where the objective function is linear and the set is specified using only linear equality and inequality constraints. In our case, however, the objective function and the constraints are both non-linear. In theory, one can resort to non-linear programming (NLP), but such a strategy proves ineffective due to the complexity of the objective function.

Computational intelligence-based techniques, such as the genetic algorithm (GA) and particle swarm optimisation (PSO), can be applied to tackle the problem at hand. GA is a search technique used in computer science and engineering to find the approximate solutions to optimisation problems [99], [100], [101]. GA represents a particular class of evolutionary algorithms that uses techniques inspired by evolutionary biology such as inheritance, mutation, natural selection, and recombination (or crossover). While it can rapidly locate good solutions even for difficult search spaces, it has some disadvantages as follows:

i) Unless the fitness function is defined properly which is a very difficult task itself in practice, GA has a tendency to converge towards local optima rather than the global optimum of the problem.

ii) For specific optimisation problems and given the same amount of computation time, simpler optimisation algorithms which employ PSO may find better solu-

tions than employ GAs [102], [103].

In the study, we have used GA to optimise the locations of reference nodes to achieve minimum average GDoP. Unfortunately, an exhaustive investigation proved that in most cases the algorithm would converge to a local optima. Therefore, we moved our attention to the particle swarm optimisation (PSO) algorithm instead.

Similar to GA, PSO is another evolutionary computation technique that mimicks what happens in nature. Inspired by the social behavior of bird flocking and fish schooling, the algorithm was developed by Eberhart and Kennedy [104] in 1995. It utilises a population of particles that fly through the problem hyperspace with given velocities. At each iteration, the velocities of the individual particles are stochastically adjusted according to the historical best position for the particle itself and the neighbourhood best position. Both the particle best and the neighbourhood best are derived according to a user defined fitness/objective function. The movement of each particle naturally evolves to an optimal or near-optimal solution. The word swarm comes from the irregular movements of the particles in the problem space, more similar to a swarm of mosquitoes rather than a flock of birds or a school of fish which, to some extent, ensures that the algorithm would converge to a global optima. PSO is largely not affected by the size and nonlinearity of the problem, and can converge to the optimal solution in many problems where most analytical methods fail to converge. Moreover, in comparison to GA, PSO has the following advantages:

i) PSO is easier to implement and there are fewer parameters to adjust.

ii) In PSO, every particle remembers its own previous best value as well as the neighbourhood best. Therefore, it has a more effective memory capability than the GA which helps avoid wasteful random iterations.

iii) PSO is more efficient in maintaining the diversity of the population since all the

particles use the information related to the most successful particle in order to improve themselves. In contrast, the worse solutions are discarded in GA and only the fit ones are kept, which contributes to its suboptimum nature.

In PSO, the term particles refers to population members which are mass-less and volume-less and are subject to velocities and accelerations towards a better mode of behavior. In addition, PSO uses the swarm intelligence concept, which is the property of a system, whereby the collective behaviors of unsophisticated agents that interact locally with their environment create coherent global functional patterns. Therefore, the cornerstones of PSO can be described as swarm intelligence principles: swarm intelligence can be described by considering five fundamental principles:

a. Proximity Principle: the population should be able to carry out simple space and time computations.

b. Quality Principle: the population should be able to respond to quality factors in the environment.

c. Diverse Response Principle: the population should not commit its activity along excessively narrow channels.

d. Stability Principle: the population should not change its mode of behavior every time the environment changes.

e. Adaptability Principle: the population should be able to change its behavior when it is worth the price.

In the real number space, each individual possible solution can be modeled as a particle that moves through the problem hyperspace. The position of each particle is determined by the position vector and its movement which is determined by the

velocity of the particle [105]:

$$\mathbf{x}_i(t) = \mathbf{x}_i(t-1) + \mathbf{v}_i(t). \tag{4.15}$$

The information available for each individual is based on its own experience, i.e., the decisions that it has made so far and the success of each decision, and the knowledge of the performance of other individuals in its neighbourhood. Since the relative importance of these two factors can vary from one decision to another, it is reasonable to apply random weights to each part, and therefore the velocity can be determined by

$$\mathbf{v}_i(t) = \mathbf{v}_i(t-1) + \varphi_1 \cdot rand_1 \cdot (\mathbf{p}_i - \mathbf{x}_i(t-1)) + \varphi_2 \cdot rand_2 \cdot (\mathbf{p}_g - \mathbf{x}_i(t-1)), \tag{4.16}$$

where $\varphi_1$ and $\varphi_2$ are two positive numbers and , $rand_1$ and $rand_2$ are two random numbers with uniform distribution in the range of [0.0, 1.0]. The velocity update equation in (4.16) has three major components:

- The first component is sometimes referred to as inertia, momentum, or habit. It models the tendency of the particle to continue in the same direction it has been traveling.

- The second component is a linear attraction towards the best position ever found by the given particle whose corresponding fitness value is called the particle's best, scaled by a random weight $\varphi_1$. This component is referred to as memory, self-knowledge, nostalgia, or remembrance.

- The third component of the velocity update equation is a linear attraction towards the best position found by any particle whose corresponding fitness value is called global best, scaled by another random weight $\varphi_2$. This component is referred to as co-operation, social knowledge,group knowledge, or shared information.

According to the formulation above, the following procedure can be used for implementing the PSO algorithm.

1. Initialise the swarm by assigning a random position in the problem hyperspace to each particle.

2. Evaluate the fitness function for each particle.

3. For each individual particle, compare the particle's fitness value with its $p_{best}$. If the current value is better than the value $p_{best}$, then set this value as the $p_{best}$ and the current particle's position $\mathbf{x}_i$, as $\mathbf{p}_i$.

4. Identify the particle that has the best fitness value. The value of its fitness function is identified as $g_{best}$ and its position as $\mathbf{p}_g$.

5. Update the velocities and positions of all the particles using (4.15) and (4.16).

6. Repeat steps 2 to 5 until a stopping criterion is met. This could be the maximum number of iterations or a sufficiently good fitness value. In our study, he former criterion is adopted.

## 4.4 GDoP Based Node Configuration Optimisation Using a Hybrid Algorithm

Using the PSO algorithm, it is possible to optimise the average GDoP to obtain the optimum locations of the reference nodes. However, it is found that the PSO algorithm tends to produce near-optimum answers but stop or slows down the search significantly before the optimum solution is obtained. To overcome the problem, we propose a hybrid two-step optimisation algorithm as follows. First, the PSO algorithm

is used to find the near-optimum solution. Then, using the near optimum solution as the initial value, we conduct the final search using the classical optimisation algorithm. In particular, we employ the sequential quadratic programming (SQP) algorithm in our study. It is found that such a hybrid algorithm can produce the optimum solution in most cases.

A number of scenarios have been used to verify the effectiveness of the proposed hybrid optimisation scheme. In the simulations, we assume that the mobile target nodes is within the radio range of all the reference nodes. To verify the algorithm, we consider the scenario of a circular area to which the optimum solution is to distribute the nodes uniformly along the perimeter. Three different number of nodes, four, six and eight are used, respectively. The simulation results are presented in the way that red dots illustrate the locations of the reference nodes as a result of the first optimisation step, PSO, and the blue dots illustrate the locations of the reference nodes after the second optimisation step. It is seen in Fig. 4.2 that all the results agree with expectations, that the reference nodes are uniformly distributed along the perimeter. A special phenomenon is observed for the scenario when six reference nodes are deployed in a circular area: the PSO optimisation can reach the best result due to the highly symmetrical property, as seen in Fig. 4.2(c), therefore, the blue dots are co-located with the red dots.

The second scenario we considered is an elliptical area of which the ratio of the major axis to the minor axis is $2:1$. As shown in Fig. 4.3, four, six and eight nodes are used again, respectively. The results show that all the reference nodes should be optimally place along the major axis direction.

The third scenario we considered is a square area. As shown in Fig. 4.4, four, six and eight nodes are used, respectively. It is seen that, as expected, all the reference nodes are uniformly distributed along the perimeter, being similar to the circular

case. The six node case is probably the most interesting one as it may not be obvious where the optimal node locations should be. The fourth scenario we considered is a rectangular area with a ratio of length to width is 2 : 1. As shown in Fig. 4.5, the optimisation results are very similar to the elliptical case.

The final scenario we considered are two types of right-angled triangle areas, one being a right-angle isosceles triangle, as shown in Fig. 4.6, and the other being a right-angle triangle of which the ratio of the two catheti is 2 : 1, as shown in Fig. 4.7. Only eight nodes are used for both triangles. The results are intuitively instructive: the nodes are more sparsely placed in the narrow section of the triangle and more densely placed in the wide section.

It may be noted that the optimal node configurations shown in this chapter are different from those shown in the previous chapter. This is due to the fact GDoP optimisation leads to the configuration which corresponds to the Cramér-Rao lower bound but may not be optimal for a given algorithm, such as the spherical interpolation approach (SIA).

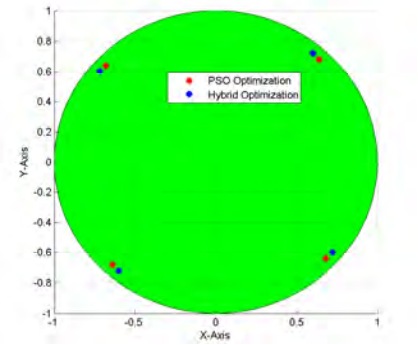


(a) Optimised four-node configuration

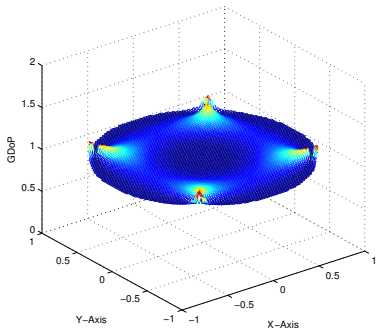


(b) GDoP of optimised configuration of four nodes

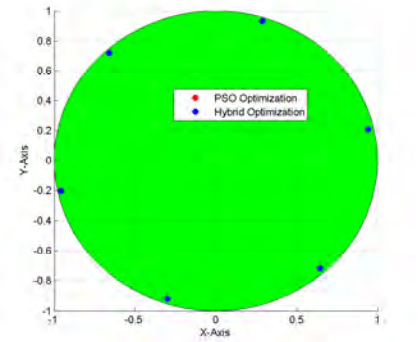


(c) Optimised six-node configuration

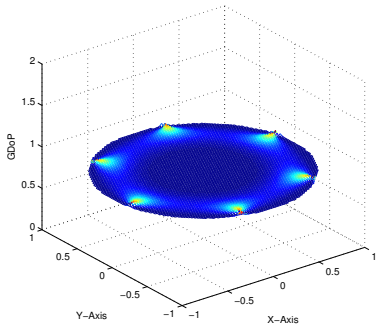


(d) GDoP of optimised configuration of six nodes

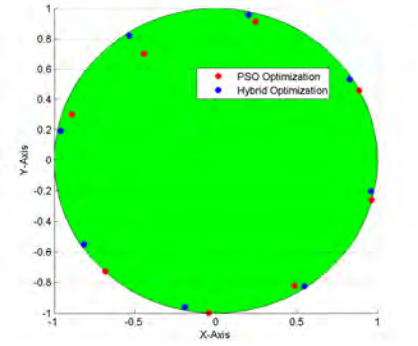


(e) Optimised eight-node configuration

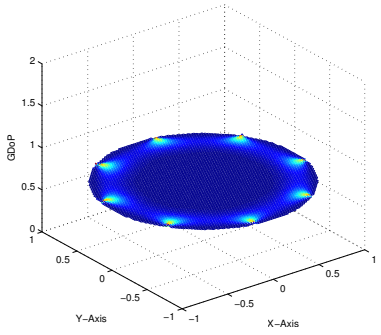


(f) GDoP of optimised configuration of eight nodes

**Figure 4.2:** Optimised node configurations for a unit circle area

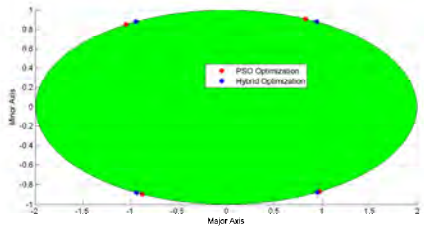


(a) Optimised four-node configuration

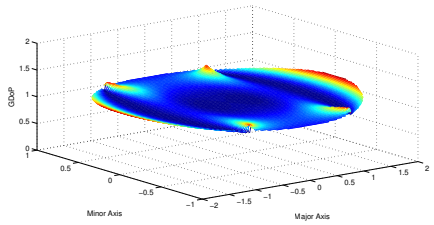


(b) GDoP of optimised configuration of four nodes

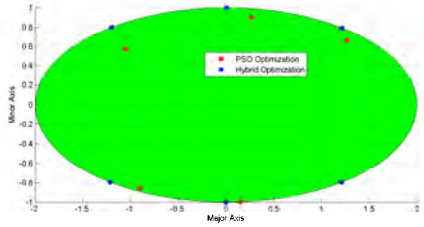


(c) Optimised six-node configuration

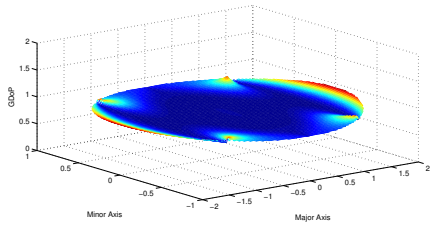


(d) GDoP of optimised configuration of six nodes

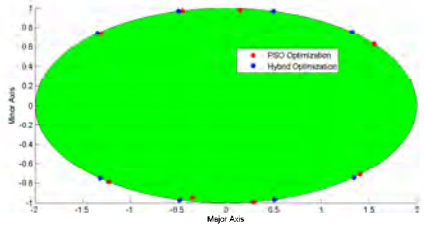


(e) Optimised eight-node configuration

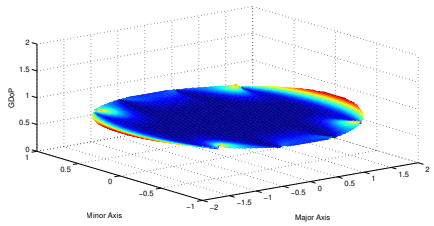


(f) GDoP of optimised configuration of eight nodes

**Figure 4.3:** Optimised node configurations for an elliptic area of which the ratio of the major axis to the minor axis is 2 : 1

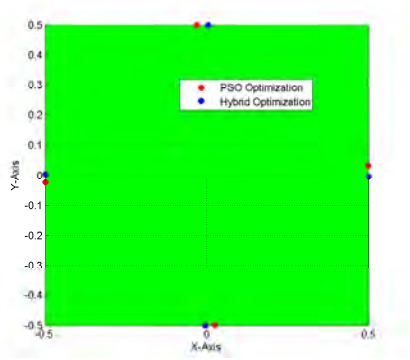


(a) Optimised four-node configuration

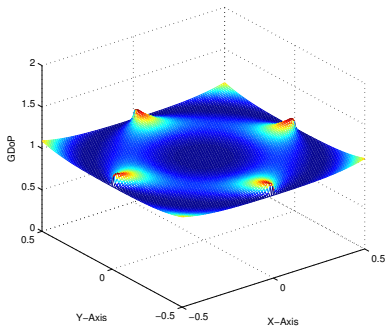


(b) GDoP of optimised configuration of four nodes

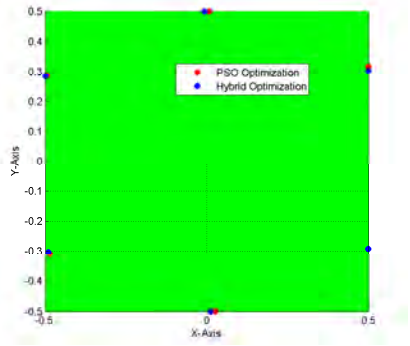


(c) Optimised six-node configuration

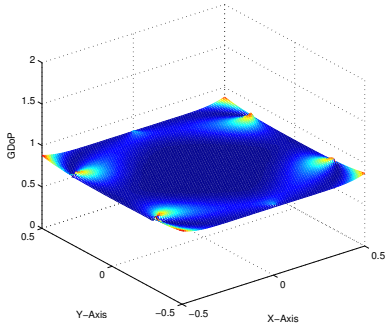


(d) GDoP of optimised configuration of six nodes

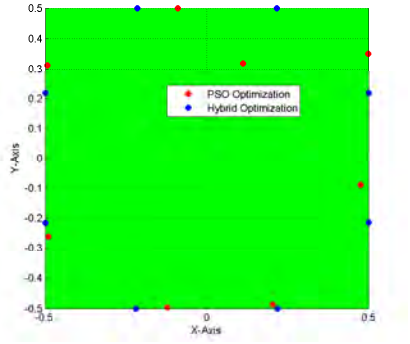


(e) Optimised eight-node configuration

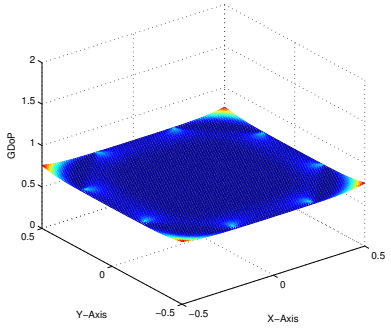


(f) GDoP of optimised configuration of eight nodes

**Figure 4.4:** Optimised node configurations for a unit square area

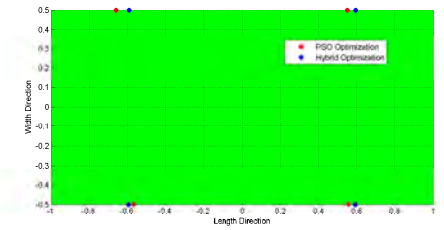


(a) Optimised four-node configuration

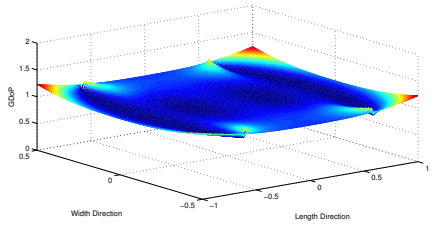


(b) GDoP of optimised configuration of four nodes

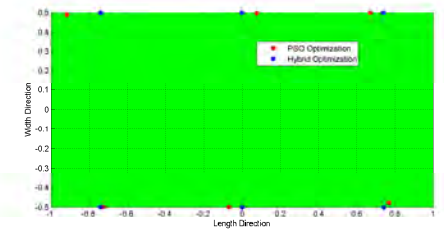


(c) Optimised six-node configuration

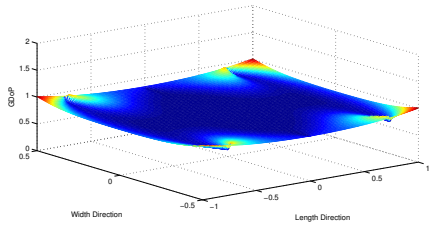


(d) GDoP of optimised configuration six nodes

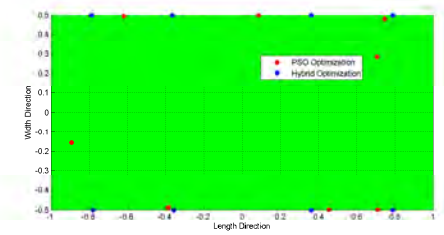


(e) Optimised eight-node configuration

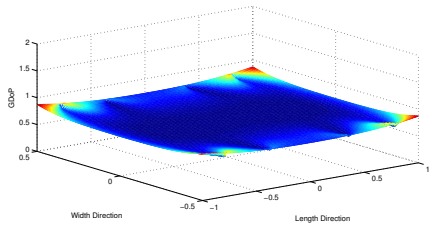


(f) GDoP of optimised configuration of eight nodes

**Figure 4.5:** Optimised node configurations for a rectangle of which the ratio of the length to the width is 2 : 1

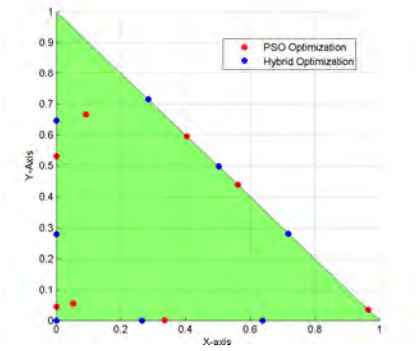


(a) Optimised eight-node configuration

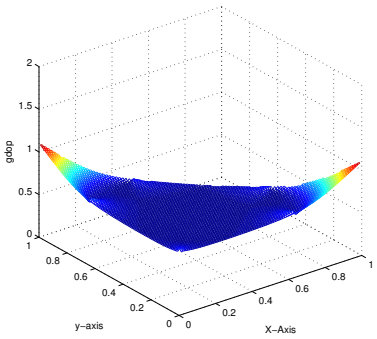


(b) GDoP of optimised configuration of eight nodes

**Figure 4.6:** Optimised node configurations for a right-angled isosceles triangle area for which the length of cathetus is a unit

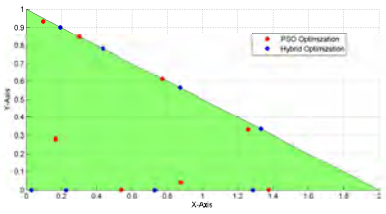


(a) Optimised eight-node configuration

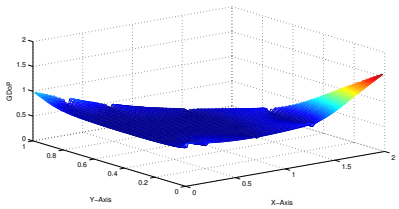


(b) GDoP of optimised configuration of eight nodes

**Figure 4.7:** Optimised node configurations for a right-angled triangle area for which the ratio of the two catheti is 2 : 1

## 4.5 Conclusion

In this chapter, a study of the node configuration optimisation is presented. A new hybrid optimisation algorithm combining the particle swarm optimisation and the classical sequential quadratic programming (SQP) method is proposed. The optimisation is carried for positioning a target in a restricted area with the average GDoP as the objective function. Simulation results for a variety of scenarios demonstrate the effectiveness of the proposed scheme.

As pointed out in the previous chapter, the actual positioning accuracy obtained with a given positioning algorithm for a given coverage scenario is largely dependent on the node configuration. The optimal node configuration for the given positioning algorithm may not hold for a different positioning algorithm. For instance, ToA algorithm and TDoA algorithm provide different optimal configuration. The algorithm of GDoP is based on the distance measurement, related to ToA technique, while spherical interpolation approach (SIA), which is used in previous chapter, is based on the TDoA measurement. The advantage of optimisation of GDoP leads to the lowest Cramér-Rao lower bound (CRLB) [95] but the optimal node configuration may not be optimal for other given positioning algorithm, for instance SIA, which employs TDoA technique avoiding synchronisation of target clock. For a practical application, therefore, one can take two different approaches. The first is to use the GDoP-optimised node configuration to deploy the reference nodes and to employ a positioning algorithm which can reach or approach CRLB; this would be the optimal approach. The second is to optimise the node configuration based on the positioning algorithm implemented in the mobile and reference nodes. In the latter scenario, the hybrid optimisation algorithm presented in this chapter is equally applicable.

# Chapter 5

# Weighted Least Squares Method for DoA Based Positioning

## 5.1 Introduction

The majority of known positioning methods are based on trilateration using the measurements of the time-of-arrival (ToA) or the time-difference of arrival (TDoA) [92]. In the former, the time-of-flight (ToF) taken for the signal from each transmitter to reach the receiver is obtained, whereas in the latter only the differences between the times of flight are obtained. The accuracy of such systems depends largely on the accuracy of the timing measurements, which is the detection of the moment when the signal from the transmitter is received by a receiver. In order to obtain a high accuracy of timing measurements, one needs to have a wide bandwidth to achieve a sharp pulse at the output of the receiver [90]. Therefore, these systems are usually referred to as wideband positioning systems.

An alternative approach to wireless positioning is based on the triangulation using more than one direction-of-arrival (DoA) estimate at spatially separated arrays [106].

By using multiple arrays whose positions are known, one can locate the position of the target using simple geometrical equations (see Fig. 5.1). There is a number of advantages in adopting this approach: the synchronisation between the target and the arrays is not necessary; the signal format can be very simple; and the system can be operated in a very narrow band. These kind of positioning systems are more suited to situations where there are lines-of-sight (LoS) between the target and some anchor nodes where the employment of arrays is practical. Such systems can be employed in such applications as warfare, sport and underwater tracking of submarines. The key to this approach is the high accuracy and low complexity DoA estimation [107].

There are a number of techniques to estimate DoAs [51], and the most fundamental one is the conventional beamformer also known as Bartlett beamformer. For a signal coming from a given direction, the algorithm of the conventional beamformer maximises the power of the array output by weighting the signals at each array element. The optimum weighting vector obtained at the beamformer contains the DoA information. A critical problem associated with DoA estimation is that the accuracy of the estimation falls rapidly when the signal direction is close to the plane on which the array is placed. This is due to the physical property of the array element which radiates or receives energy as a function of the direction [108]. As a result, the signal-to-noise ratio deteriorates significantly as the DoA moves away from the normal direction. In other words, the variance of the DoA estimation changes according to DoA itself.

Owing to the inherent nature of DoA estimation, when a number of arrays are employed to estimate the direction of a signal, each of the arrays estimates their own DoAs with the associated variances. Therefore, for a given signal, the DoA estimations made by a set of the arrays may have different variances. From statistics point of view, the conventional least squares method (LSM) may be inaccurate for

locating the target by using these DoAs. To solve the problem, a weighting matrix should be introduced to take into the account of the unequal variances. This technique is known as generalized least squares method (GLSM) in the literature [109], [110]. To our knowledge, however, we are the first to apply the GLSM concept to solve DoA problems.

In this chapter, we propose a weighted least squares method (WLSM) with the weighting matrix derived from the angle of incidence of each array [111], [112], [113]. Since the weight applied to each array is a function of the DoA observed by the array, the variances of the DoA estimation at each array is taken automatically when conducting positioning. We start from 2D scenarios, and then extend the WLSM technique to 3D cases. Simulations results show that the new method outperforms the conventional LSM significantly. Without loss of generality, the conventional beamformer is used in this chapter as the method to estimate the DoA of the incoming signal at the individual arrays.

The chapter is organised as follows. Following Section 5.1, the 2D positioning using DoAs and WLSM is studied in Section 5.2. We first present the method of 2D positioning method using multiple arrays. Then, the derivation of WLSM is presented. The DoA estimation error distribution is discussed, and the performance of WLSM is simulated using a standard swimming pool, and evaluated by comparing with the conventional LSM. In Section 5.3, the WLSM method is extended to 3D cases using uniform circular arrays. The theoretical framework is presented first. It is then applied to the case of tracking swimmers in a swimming pool. It is demonstrated that the weighted least squares method (WLSM) outperform the conventional least squares method (LSM) significantly. Section 5.4 concludes the chapter.

## 5.2 2D Positioning Using Multiple Linear Uniform Arrays

### 5.2.1 Positioning Using Multiple Arrays

Given a 2D area in which a mobile target is contained, one can employ a number of arrays at known positions to track the target, as shown in Fig. 5.1.

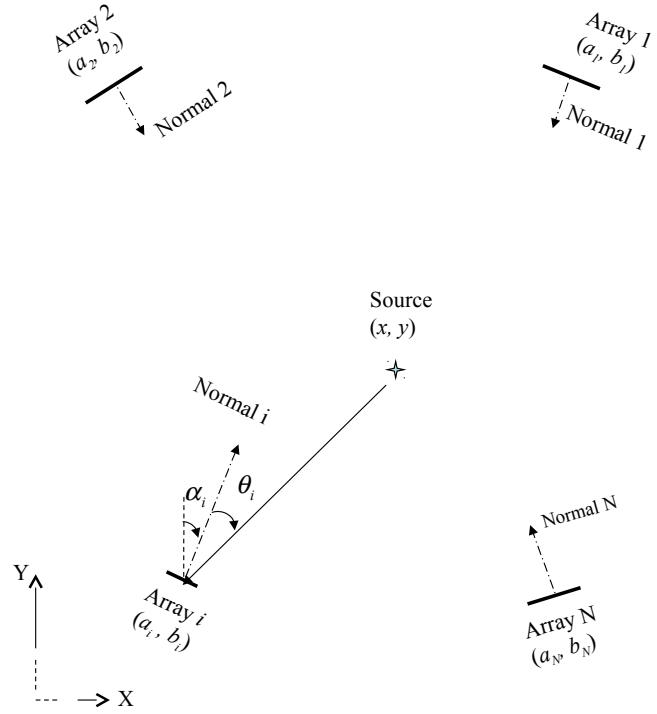


**Figure 5.1:** Positioning using $N$ arrays in 2D

Assume that the target is located at $(x, y)$. Denote $(a_i, b_i)$ as the coordinates of the center of the array $i$ , and $\alpha_i$ the bearing of the array $i$. The signal incident angle

estimated by the array $i$ is $\theta_i$. Then, one has the following geometric equation:

$$\frac{x - a_i}{y - b_i} = \frac{\sin(\alpha_i + \theta_i)}{\cos(\alpha_i + \theta_i)}. \tag{5.1}$$

For simplicity, denote

$$\begin{cases} q_{i1}(\theta) = \cos(\alpha_i + \theta_i), \\ q_{i2}(\theta) = -\sin(\alpha_i + \theta_i), \end{cases} \tag{5.2}$$

and

$$p_i(\theta_i) = \cos(\alpha_i + \theta_i) a_i - \sin(\alpha_i + \theta_i) b_i. \tag{5.3}$$

Then, (5.1) can also be written as

$$q_{i1}(\theta_i) x + q_{i2}(\theta_i) y = p_i(\theta_i). \tag{5.4}$$

Since $a_i$, $b_i$ and $\alpha_i$ are known, (5.4) describes the relationship between the DoA estimation $\theta_i$ and the target position $(x, y)$.

When $N$ $(N > 1)$ arrays are employed, $N$-DoA estimations can be obtained as $\theta_1, \theta_2, \cdots$, and $\theta_N$. From the geometric point of view, only two of the $N$ parameters are necessary to find a position. However, the participation of more arrays would lead to a more robust solution. From the $N$-DoA estimations, one has a set of $N$ straight line equations given by

$$\begin{cases} q_{11}(\theta_1) x + q_{12}(\theta_1) y - p_1(\theta_1) = 0, \\ q_{21}(\theta_2) x + q_{22}(\theta_2) y - p_2(\theta_2) = 0, \\ \vdots \\ q_{N1}(\theta_N) x + q_{N2}(\theta_N) y - p_N(\theta_N) = 0. \end{cases} \tag{5.5}$$

The signal position $(\tilde{x}, \tilde{y})$ can be determined by using the least squares method (LSM), which finds $(\tilde{x}, \tilde{y})$ by minimising the sum of squared residuals, $\sum_{i=1}^{N} {\varepsilon_i}^2$, where $\varepsilon_i$, for

$i = 1, \cdots, N$ satisfy

$$\begin{cases} q_{11}(\theta_1)\,\tilde{x} + q_{12}(\theta_1)\,\tilde{y} - p_1(\theta_1) = \varepsilon_1, \\ q_{21}(\theta_2)\,\tilde{x} + q_{22}(\theta_2)\,\tilde{y} - p_2(\theta_2) = \varepsilon_2, \\ \vdots \\ q_{N1}(\theta_N)\,\tilde{x} + q_{N2}(\theta_N)\,\tilde{y} - p_N(\theta_N) = \varepsilon_N. \end{cases} \tag{5.6}$$

Defining the residual vector $\varepsilon$ as

$$\varepsilon = \begin{bmatrix} \varepsilon_1, & \varepsilon_2, & \cdots, & \varepsilon_N \end{bmatrix}^T. \tag{5.7}$$

and denoting the superscript $T$ as the transpose operator to a matrix or a vector, the sum of square residuals can be expressed as

$$\sum_{i=1}^{N} {\varepsilon_i}^2 = \varepsilon^T \varepsilon. \tag{5.8}$$

$(\tilde{x}, \tilde{y})$ can be obtained by minimising (5.8) using the least squares method (LSM).

Denoting

$$\mathbf{Q} = \begin{bmatrix} q_{11}(\theta_1) & q_{12}(\theta_1) \\ q_{21}(\theta_2) & q_{22}(\theta_2) \\ \vdots & \vdots \\ q_{N1}(\theta_N) & q_{N2}(\theta_N) \end{bmatrix}, \tag{5.9}$$

and

$$\mathbf{p} = \begin{bmatrix} p_1(\theta_1) \\ p_2(\theta_2) \\ \vdots \\ p_N(\theta_N) \end{bmatrix}, \tag{5.10}$$

equation (5.6) can be re-written as

$$\mathbf{Q} \begin{bmatrix} \tilde{x} \\ \tilde{y} \end{bmatrix} - \mathbf{p} = \varepsilon, \tag{5.11}$$

and the LSM solution of (5.5) can be expressed as

$$\begin{bmatrix} \tilde{x} \\ \tilde{y} \end{bmatrix} = \left(\mathbf{Q}^T\mathbf{Q}\right)^{-1}\mathbf{Q}^T\mathbf{p}. \tag{5.12}$$

### 5.2.2 Weighted Least Squares Method

Owing to the physical characteristics of array elements, the received power of an array decreases sharply when the signal direction moves away from the array normal direction. As a result, the signal-to-noise ratio deteriorates as the signal direction moves towards the array plane, thus increasing the variances of the measurement. Fig. 5.2 shows the root-mean-square error (RMSE) of DoA estimation for the array used for the simulation later this chapter. Since the RMSE is over one thousand iterations, one can treat it as the square root of the variances.It is seen that the lower the SNR, the worse the DoA estimate towards $\pm 90°$. In the following, we propose a weighted least squares method (WLSM). By employing weights applied to different arrays as functions of the DoA observed by each array, the accuracy of the DoA estimation of each array can be taken into account automatically when conducting positioning. This could improve the positioning accuracy significantly.

When a number of arrays are employed to conduct positioning, each array estimates their DoAs of the signal sent from position $(x, y)$ relative to the orientation of different arrays, so each DoA is related with different variances of measurement error. From statistics point of view, the conventional least squares method (LSM) is inaccurate for locating the target position by taking residuals in (5.6) equally. Instead, a weighting matrix should be introduced to weigh down the residuals according to the variances. This is known as the generalized least squares method (GLSM) [109].

GLSM is suited for applications when the variances of the observations are unequal, or when there is a correlation between the observations. In the application of

GLSM, every squared residuals $\varepsilon_i^2$, for $i = 1, 2, \cdots, N$, is weighted by the inverse of the covariances of residual terms, $E\left[(\varepsilon_i)(\varepsilon_j)\right]$, (for $i = 1, 2, \cdots, N$, and $j = 1, 2, \cdots, N$ ) if there are correlations; or weighted by the inverse of the variances of residual terms (for $j = i$, and $i = 1, 2, \cdots, N$ ) when there is no correlations. Denote the bold Greek letter $\mathbf{\Omega}$ as the covariance matrix of residual terms, i.e.

$$\mathbf{\Omega} = E\left[\varepsilon\varepsilon^T\right]. \tag{5.13}$$

GLSM aims to find the solution to a over-determined system by minimising *the sum of weighted squared residuals*, $\varepsilon^T\mathbf{\Omega}^{-1}\varepsilon$, instead of minimising the sum of squared residuals shown as (5.8). *The sum of weighted squared residuals* is known as the squared Mahalanobis length [110]. Denote $D$ as Mahalanobis length,

$$D^2 = \varepsilon^T\mathbf{\Omega}^{-1}\varepsilon. \tag{5.14}$$

Assuming that each DoA estimation $\theta_i$, $i = 1, 2, \cdots, N$ contains measurement errors $\Delta\theta_i$, $i = 1, 2, \cdots, N$ with respect to their true value $\theta_{i0}$, $i = 1, 2, \cdots, N$, one can re-write (5.11) as

$$\begin{bmatrix} q_{11}(\theta_{10}+\Delta\theta_1) & q_{12}(\theta_{10}+\Delta\theta_1) \\ q_{21}(\theta_{20}+\Delta\theta_2) & q_{22}(\theta_{20}+\Delta\theta_2) \\ \vdots & \vdots \\ q_{N1}(\theta_{N0}+\Delta\theta_N) & q_{N2}(\theta_{N0}+\Delta\theta_N) \end{bmatrix} \begin{bmatrix} \tilde{x} \\ \tilde{y} \end{bmatrix} - \begin{bmatrix} p_1(\theta_{10}+\Delta\theta_1) \\ p_2(\theta_{20}+\Delta\theta_2) \\ \vdots \\ p_N(\theta_{N0}+\Delta\theta_N) \end{bmatrix} = \begin{bmatrix} \varepsilon_1 \\ \varepsilon_2 \\ \vdots \\ \varepsilon_N \end{bmatrix}. \tag{5.15}$$

Assume that $\Delta\theta_i$, $i = 1, 2, \cdots, N$ cause small changes of $\Delta q_{ik}$, $i = 1, 2, \cdots, N, k = 1, 2.$ and $\Delta p_i$, $i = 1, 2, \cdots, N$, one has

$$\begin{aligned} & q_{ik}(\theta_{i0}+\Delta\theta_i) = q_{ik}(\theta_{i0}) + \frac{\partial q_{ik}(\theta_i)}{\partial\theta_i}\Delta\theta_i, \\ & i = 1, 2, \cdots, N, \\ & k = 1, 2. \end{aligned} \tag{5.16}$$

and

$$\begin{aligned} & p_i\left(\theta_{i0}+\Delta\theta_i\right)=p_i\left(\theta_{i0}\right)+\frac{\partial p_i\left(\theta_i\right)}{\partial\theta_i}\Delta\theta_i, \\ & i=1,2,\cdots,N. \end{aligned} \tag{5.17}$$

Since $\theta_{i0}$, $i=1,2,\cdots,N$, represent the true DoA values, $\tilde{x}=x$, and $\tilde{y}=y$, the straight lines of signal directions satisfy

$$\begin{bmatrix} q_{11}\left(\theta_{10}\right) & q_{12}\left(\theta_{10}\right) \\ q_{21}\left(\theta_{20}\right) & q_{22}\left(\theta_{20}\right) \\ \vdots & \vdots \\ q_{N1}\left(\theta_{N0}\right) & q_{N2}\left(\theta_{N0}\right) \end{bmatrix} \begin{bmatrix} \tilde{x} \\ \tilde{y} \end{bmatrix} - \begin{bmatrix} p_1\left(\theta_{10}\right) \\ p_2\left(\theta_{20}\right) \\ \vdots \\ p_N\left(\theta_{N0}\right) \end{bmatrix} = \mathbf{0}, \tag{5.18}$$

which leads to

$$\varepsilon = \begin{bmatrix} \varepsilon_1 \\ \varepsilon_2 \\ \vdots \\ \varepsilon_N \end{bmatrix} = \begin{bmatrix} \left(\dfrac{\partial q_{11}\left(\theta_1\right)}{\partial\theta_1}\tilde{x}+\dfrac{\partial q_{12}\left(\theta_1\right)}{\partial\theta_1}\tilde{y}-\dfrac{\partial p_1\left(\theta_1\right)}{\partial\theta_1}\right)\Delta\theta_1 \\ \left(\dfrac{\partial q_{21}\left(\theta_2\right)}{\partial\theta_2}\tilde{x}+\dfrac{\partial q_{22}\left(\theta_2\right)}{\partial\theta_2}\tilde{y}-\dfrac{\partial p_2\left(\theta_2\right)}{\partial\theta_2}\right)\Delta\theta_2 \\ \vdots \\ \left(\dfrac{\partial q_{N1}\left(\theta_N\right)}{\partial\theta_N}\tilde{x}+\dfrac{\partial q_{N2}\left(\theta_N\right)}{\partial\theta_N}\tilde{y}-\dfrac{\partial p_N\left(\theta_N\right)}{\partial\theta_N}\right)\Delta\theta_N \end{bmatrix}. \tag{5.19}$$

Applying (5.19) to (5.13), the residual covariance matrix can be obtained.

Assuming that each array estimates their DoAs independently, the covariance matrix $\mathbf{\Omega}$ becomes diagonal. This leads to the weighted least squares method (WLSM). By denoting $diag\left[\cdot\right]$ as a diagonal matrix, $\mathbf{\Omega}$ is obtained as

$$\begin{aligned} & \mathbf{\Omega}=diag\left[\left(\frac{\partial q_{i1}\left(\theta_i\right)}{\partial\theta_i}\tilde{x}+\frac{\partial q_{i2}\left(\theta_i\right)}{\partial\theta_i}\tilde{y}-\frac{\partial p_i\left(\theta_i\right)}{\partial\theta_i}\right)^2 E\left[\left|\Delta\theta_i\right|^2\right]\right]_{N\times N}, \\ & i=1,2,\cdots,N. \end{aligned} \tag{5.20}$$

The coordinates of estimated signal position $(\tilde{x},\tilde{y})$ can be obtained by the least squares estimation from (5.12), and $E\left[\left|\Delta\theta_i\right|^2\right]$ can be obtained from the RMSE of DoA estimation. Thus matrix $\mathbf{\Omega}$ can be obtained by (5.20).

By applying (5.11), Squared Mahalanobis Length is expressed as

$$\varepsilon^T \mathbf{\Omega}^{-1} \varepsilon = \left( \mathbf{Q} \begin{bmatrix} \tilde{x} \\ \tilde{y} \end{bmatrix} - \mathbf{p} \right)^T \mathbf{\Omega}^{-1} \left( \mathbf{Q} \begin{bmatrix} \tilde{x} \\ \tilde{y} \end{bmatrix} - \mathbf{p} \right). \tag{5.21}$$

Finding the minimum of (5.21) leads to

$$\begin{bmatrix} \tilde{x} \\ \tilde{y} \end{bmatrix} = \left( \mathbf{Q}^T \mathbf{\Omega}^{-1} \mathbf{Q} \right)^{-1} \mathbf{Q}^T \mathbf{\Omega}^{-1} \mathbf{p}. \tag{5.22}$$

### 5.2.3 DoA Estimation Error Distribution

To obtain the weighting matrix $\mathbf{\Omega}^{-1}$ requires the information of the DoA estimation error for each array as a function of the observation angle, which can be represented by the root-mean-squares error (RMSE). The RMSE as a function of the observation angle depends on the beamformer type, the physical parameters of the array, and the elements used. Without loss of generality, we employ the conventional beamformer to illustrate the effectiveness of WLSM in this chapter. A beamformer searches for an optimal weighting vector to find the direction of the incoming signal [49]. For the conventional beamformer, the weighting vector takes the form of the steering vector, which has the observation angle as the only variable. The observation angle which produces the maximum power value in the spatial spectrum gives the estimated DoA of the incoming signal [51]. The details of the method is presented below for two-dimensional (2D) positioning.

Assume that the array elements are arranged in one dimension with equal distances between the sensor elements. This kind of arrays are known as uniform linear arrays (ULA).

Let $M$ denote the number of the sensor elements in the array, $d$ the inter-element spacing, and $\lambda$ the wavelength corresponding to the carrier frequency. Without loss

of generality, we assume that $M$ is an odd number and the middle sensor is chosen as the reference one. Then, the steering vector is written as

$$\mathbf{a}(\theta) = \left[ \; e^{j\frac{M-1}{2}\frac{2\pi}{\lambda}d\sin(\theta)}, \;\; \cdots, \;\; 1, \;\; \cdots, \;\; e^{-j\frac{M-1}{2}\frac{2\pi}{\lambda}d\sin(\theta)} \; \right]^T. \tag{5.23}$$

In this 2D case, each element is assumed to be a linear source, $l$ is the length of the element and $\theta$ is the signal observation angle. The relative distribution of radiated power as a function of direction in space, known as the element radiation pattern, is given by [114], [115], [116]

$$g(\theta) = \frac{\sin\left(\frac{2\pi}{\lambda}\frac{l}{2}\sin(\theta)\right)}{\frac{2\pi}{\lambda}\frac{l}{2}\sin(\theta)}. \tag{5.24}$$

Denote $\mathbf{R}$ the covariance matrix of the received data, the superscript $H$ the Hermitian transpose operator (i.e. the conjugate transpose to a matrix or a vector) [51]. For a given DoA $\theta_0$ , the following spatial spectrum reaches maximum in an additive white Gaussian noise (AWGN) channel when $\theta = \theta_0$ in (5.23):

$$P(\theta) = \frac{\mathbf{a}^H(\theta)\mathbf{R}\mathbf{a}(\theta)}{\mathbf{a}^H(\theta)\mathbf{a}(\theta)}. \tag{5.25}$$

### 5.2.4 Simulation Using Uniform Linear Arrays for 2D

In this section, we present simulation results to demonstrate the effectiveness the proposed WLSM method. In the simulation study, we assume $M = 9$ , and $l$ in (5.24) is chosen to be $\lambda/2$ in order to avoid sidelobes [115], [116]. The direction-of-arrival is varied from $-85°$ to $85°$ with an increment of $15'$ . The scanning range for the conventional beamformer is from $-90°$ to $90°$ for every direction-of-arrival. It is assumed that the signal output is corrupted by additive white Gaussian noise. The root-mean-square of the DoA estimation error distributions are obtained for three different signal-to-noise ratios (SNR), namely, $5dB$, $0dB$, and $-5dB$, as shown in

Fig. 5.2. It is observed that the lower the SNR, the greater the DoA estimation error especially when the DOAs approach $\pm 90°$ . For SNR$= -5dB$, for instance, the DoA estimation error becomes too large beyond $\pm 80°$.

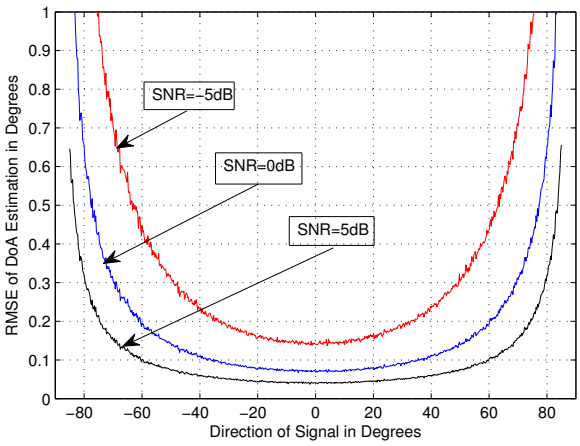


**Figure 5.2:** RMSE distribution of DoA estimation of a 9-element ULA.

The positioning simulation is carried out for a standard size Olympic swimming pool, which is $50m$ long and $25m$ wide, shown as Fig. 5.3(a). In this rectangular area, four identical uniform linear arrays (ULA) are employed, each of which is placed at the centre on one side of the swimming pool. For most positions in the pool, the distance from the target to any ULA is far great than the size of the ULA, so the positions of the ULAs can be represented by their centre coordinates .

The global coordinates are shown in Fig. 5.3(b), with the origin chosen at the centre of the swimming pool, the $X$-axis along the width of the pool, and the $Y$-axis along the length of the pool. The labels of these arrays are arranged anti-clock wise.

Given a signal emitted from within the swimming pool, one has four DoAs observed at the four ULAs, $\theta_1$, $\theta_2$, $\theta_3$ and $\theta_4$. A geometrical analysis produces the

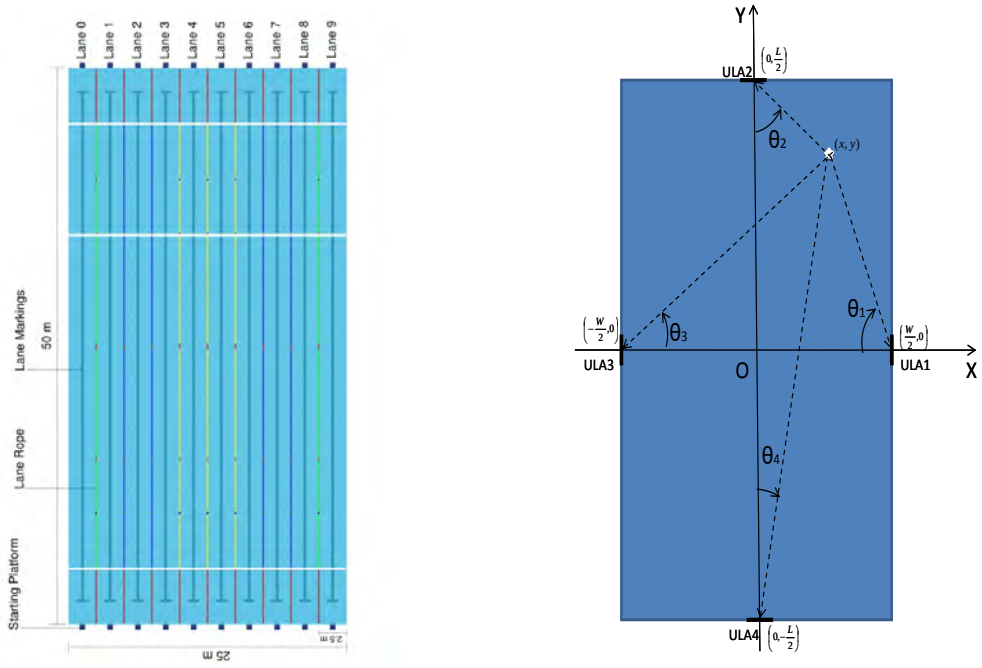


(a) Layout of standard swimming pool (b) 2D coordinates and ULA positioning

**Figure 5.3:** Standard swimming pool layout and coordinates

following set of equations:

$$\begin{cases} \sin(\theta_1)\, x + \cos(\theta_1)\, y = \dfrac{W}{2} \sin(\theta_1)\,, \\ \cos(\theta_2)\, x - \sin(\theta_2)\, y = -\dfrac{L}{2} \sin(\theta_2)\,, \\ \sin(\theta_3)\, x + \cos(\theta_3)\, y = -\dfrac{W}{2} \sin(\theta_3)\,, \\ \cos(\theta_4)\, x - \sin(\theta_4)\, y = \dfrac{L}{2} \sin(\theta_4)\,. \end{cases} \tag{5.26}$$

Applying (5.9) and (5.10) to (5.26) results in

$$\mathbf{Q} = \begin{bmatrix} \sin(\theta_1) & \cos(\theta_1) \\ \cos(\theta_2) & -\sin(\theta_2) \\ \sin(\theta_3) & \cos(\theta_3) \\ \cos(\theta_4) & -\sin(\theta_4) \end{bmatrix}, \tag{5.27}$$

$$\mathbf{p} = \begin{bmatrix} \frac{W}{2}\sin(\theta_1) \\ -\frac{L}{2}\sin(\theta_2) \\ -\frac{W}{2}\sin(\theta_3) \\ \frac{L}{2}\sin(\theta_4) \end{bmatrix}. \tag{5.28}$$

Substituting (5.27) and (5.28) into (5.12), the source position, $(\tilde{x}, \tilde{y})$ which is estimated by the LSM can be obtained. Applying (5.27), (5.28) and $(\tilde{x}, \tilde{y})$ to (5.20), the matrix $\mathbf{\Omega}$ can be obtained as

$$\mathbf{\Omega} = \begin{bmatrix} \Omega_{11} & & & 0 \\ & \Omega_{22} & & \\ & & \Omega_{33} & \\ 0 & & & \Omega_{44} \end{bmatrix}, \tag{5.29}$$

where

$$\begin{aligned} \Omega_{11} &= \left[\cos(\theta_1)\,\tilde{x} - \sin(\theta_1)\,\tilde{y} - \frac{W}{2}\cos(\theta_1)\right]^2 E\left[|\Delta\theta_1|^2\right], \\ \Omega_{22} &= \left[\sin(\theta_2)\,\tilde{x} + \cos(\theta_2)\,\tilde{y} - \frac{L}{2}\cos(\theta_2)\right]^2 E\left[|\Delta\theta_2|^2\right], \\ \Omega_{33} &= \left[\cos(\theta_3)\,\tilde{x} - \sin(\theta_3)\,\tilde{y} + \frac{W}{2}\cos(\theta_3)\right]^2 E\left[|\Delta\theta_3|^2\right], \\ \Omega_{44} &= \left[\sin(\theta_4)\,\tilde{x} + \cos(\theta_4)\,\tilde{y} + \frac{L}{2}\cos(\theta_4)\right]^2 E\left[|\Delta\theta_4|^2\right]. \end{aligned} \tag{5.30}$$

Finally, applying the weighting matrix $\mathbf{\Omega}^{-1}$, (5.27) and (5.28) into (5.22), the source position estimated by the weighted least squares method (WLSM) is obtained. It is noted that, based on the estimates obtained using LSM, the WLSM provides a means of improving the positioning estimation accuracy by introducing an extra step. In theory, one could use the previous WLSM position estimates to perform one or more WLSM operations, but simulation results showed that only one WLSM operation is sufficient and the improvement achieved using further iterations is negligible. For

comparison, the root-mean-square errors have been measured for the source positions estimated by both methods.

Simulations have been carried out for two different lanes, lane 6 and lane 8 (note that the lanes of the standard swimming pool are labeled from 0 - 9, see Fig. 5.3(a)), under the signal-to-noise ratio $5dB$ and $-5dB$. Fig. 5.4 shows the RMSE along lane 6 and lane 8.

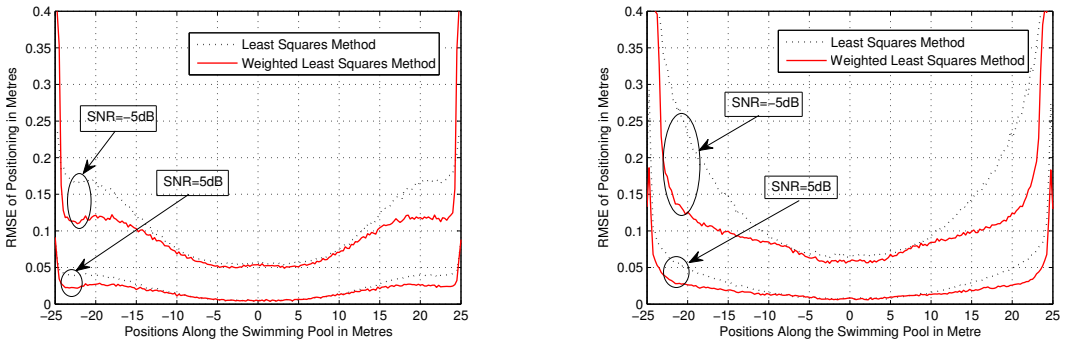


(a) Lane 6

(b) Lane 8

**Figure 5.4:** RMSE distribution and WLSM improvement.

From Fig. 5.4, it can be seen that the accuracy of positioning using WLSM outperforms that of the conventional LSM significantly, particularly when the swimmer is close to both ends of the pool. The overall conclusion is that the lower the signal-to-noise ratio, the better the improvement achieved by the WLSM. The improvements become quite significant when the positions are less than $10m$ towards either end of the swimming pool. The WLSM pushes the points where the positioning accuracy falls sharply much closer to the ends of the pool, at least within $2m$ of the end of the pool. It should be pointed out that some applications including the one presented in the chapter demand a positioning accuracy of millimetres. Therefore, the improvement achieved using WLSM even in centimetres is of practical importance.

## 5.3 3D DoA Positioning

### 5.3.1 Methodology and Theoretical Framework for 3D

For 3D DoA estimation using a planar array, one needs to measure both the elevation angle with respect to the array plane and azimuth angle. Without loss of generality, the uniform circular array (UCA) is employed for the study. A uniform circular array, as shown in Fig. 5.5, consists of $N$ elements located evenly on a circle with radius $R$.


(a) Birdeye view of uniform circular array and sensor coordinates

(b) Front view of uniform circular array and wave vector

**Figure 5.5:** Illustration of an uniform circular array with $N$ sensors

Using a spherical coordinate system, the position of each element is represented by

$$\begin{aligned} \mathbf{r}_n &= R \left[ \cos(n-1)\frac{2\pi}{N}, \quad \sin(n-1)\frac{2\pi}{N}, \quad 0 \right]^T, \\ n &= 1, 2, \cdots, N. \end{aligned} \tag{5.31}$$

where the superscript $T$ denotes the transpose operation. To avoid grating lobes, the distance between two adjacent elements is chosen as a half of the wavelength

$\lambda$ [115], [108], thus resulting in

$$R = \frac{\lambda}{4} \frac{1}{\sin(\pi/N)}. \tag{5.32}$$

When a plane wave impinges on the array, every element receives the same directional signal with different phase delays due to the position difference. We assume that the elevation angle, $\theta$, is measured to the opposite direction of the wave vector, i.e., $-\mathbf{k}$ direction. For the problem concerned, the range of the elevation angle is limited from 0 to $\frac{\pi}{2}$. The azimuth angle $\varphi$ is measured from $X$-axis to the projection of $-\mathbf{k}$ on the array plane. The range of the azimuth angle is from $-\pi$ to $\pi$.

The wave vector is expressed as

$$\mathbf{k} = -\frac{\lambda}{2\pi} \left[ \begin{array}{ccc} \sin(\theta)\cos(\varphi), & \sin(\theta)\sin(\varphi), & \cos(\theta) \end{array} \right]^T, \tag{5.33}$$

and the phase factor of each element in the UCA is expressed as

$$\begin{aligned} &-j\mathbf{k}^T\mathbf{r}_n = j\frac{\lambda}{2\pi} R\sin(\theta)\cos\left(\varphi - (n-1)\frac{2\pi}{N}\right), \\ &n = 1, 2, \cdots, N. \end{aligned} \tag{5.34}$$

For simplicity, denote

$$\begin{aligned} &\psi_n = \frac{\lambda}{2\pi} R\sin(\theta)\cos\left(\varphi - (n-1)\frac{2\pi}{N}\right), \\ &n = 1, 2, \cdots, N. \end{aligned} \tag{5.35}$$

The signal replica vector is given by [51]

$$\mathbf{a}(\theta, \varphi) = \mathsf{g}(\theta, \varphi)\, \mathbf{a}_s(\theta, \varphi), \tag{5.36}$$

where $\mathsf{g}(\theta, \varphi)$ is the common element pattern which depends on the specific element used. For an element with a circular aperture and radius $a$, $\mathsf{g}(\theta, \varphi)$ is given by

$$\mathsf{g}(\theta, \varphi) = \frac{J_1\left(\frac{\lambda}{2\pi} a\sin(\theta)\right)}{\frac{\lambda}{2\pi} a\sin(\theta)}, \tag{5.37}$$

where $J_1\left(\frac{\lambda}{2\pi}a\sin(\theta)\right)$ is Bessel function of the first kind and order one. The steering vector $\mathbf{a}_s(\theta,\varphi)$ is given by [51]

$$\mathbf{a}_s(\theta,\varphi) = \left[\begin{array}{cccc} e^{j\psi_1}, & e^{j\psi_2}, & \cdots, & e^{j\psi_N} \end{array}\right]^T. \tag{5.38}$$

Assume that the target to be positioned is contained in an enclosure with a rectangular floor area and height $C$ . The rectangular floor is defined by length $L$ and width $W$ , as shown in Fig. 5.6(a). The $XOY$ plane is chosen on the floor, with $X$-axis along the width, $Y$-axis along the length, and the origin at the centre of the area and $Z$-axis along the height.

Four uniform circular arrays (UCAs) are employed to locate a target in the enclosure as shown in Fig. 5.6(a). The four UCAs are all placed at a height of $h(h < C)$ above the floor. On each wall, the UCA is placed at the middle point along the wall. It should be noted that the walls are used to define the enclosure and they can be virtual ones as long as the UCAs can be somehow fixed on them. Table 5.1 lists the coordinates and the normal directions of each UCA, as shown in Fig. 5.6(b) - Fig. 5.6(e).

Assume that the target is located at $(x, y, z)$ and in the far field of all the UCAs. Each array estimates the signal direction from its own position. The elevation angle is measured from the normal direction of each array and the azimuth angle is measured from $Z$-axis. The sign of the azimuth angle is determined by the right-hand rule from the normal direction of the array to $Z$-axis.

Using $\theta_i$, $i = 1, 2, 3, 4$, to describe the elevation angle that is measured by each array, and $\varphi_i$, $i = 1, 2, 3, 4$, the azimuth angle is measured by each array, the geometrical relationship can be found as described by (5.39)

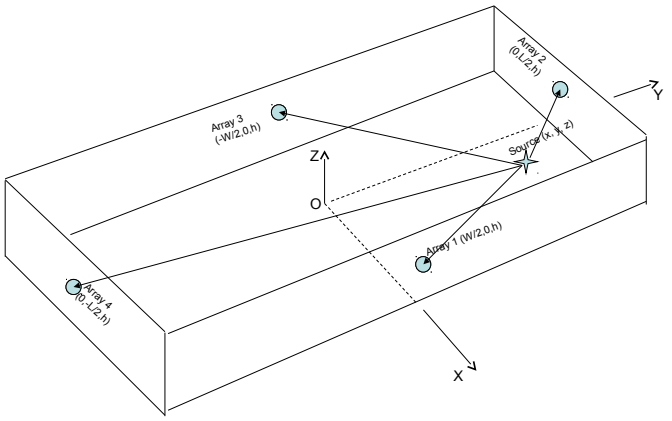


(a) An enclosure and uniform circular arrays

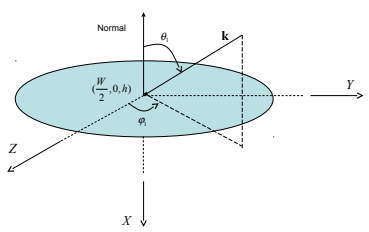


(b) Array 1

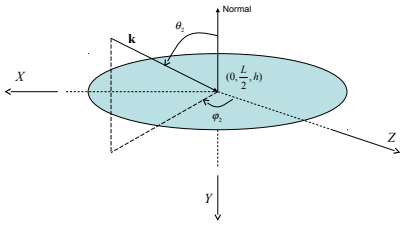


(c) Array 2

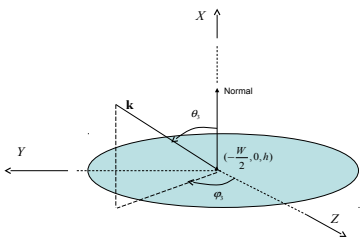


(d) Array 3

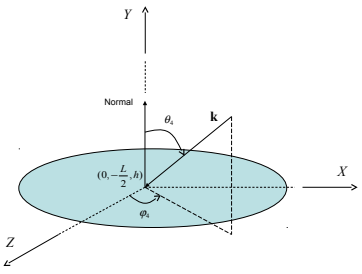


(e) Array 4

**Figure 5.6:** Centre coordinates and normal directions of uniform circular arrays and the enclosure

**Table 5.1:** Centre coordinates and normal direction of arrays

| Array order | Centre coordinates | Normal direction |
|---|---|---|
| Array 1 | $\left(\frac{W}{2}, 0, h\right)$ | Opposite to $X$-axis |
| Array 2 | $\left(0, \frac{L}{2}, h\right)$ | Opposite to $Y$-axis |
| Array 3 | $\left(-\frac{W}{2}, 0, h\right)$ | $X$-axis |
| Array 4 | $\left(0, -\frac{L}{2}, h\right)$ | $Y$-axis |

$$
\begin{cases}
\begin{cases}
\sin(\theta_1)\sin(\varphi_1)\,x + \cos(\theta_1)\,y - \dfrac{W}{2}\sin(\theta_1)\sin(\varphi_1) = 0, \\
\cos(\varphi_1)\,y - \sin(\varphi_1)\,z + h\sin(\varphi_1) = 0.
\end{cases} \\
\begin{cases}
\cos(\theta_2)\,x - \sin(\theta_2)\sin(\varphi_2)\,y + \dfrac{L}{2}\sin(\theta_2)\sin(\varphi_2) = 0, \\
\cos(\varphi_2)\,x + \sin(\varphi_2)\,z - h\sin(\varphi_2) = 0.
\end{cases} \\
\begin{cases}
\sin(\theta_3)\sin(\varphi_3)\,x + \cos(\theta_3)\,y + \dfrac{W}{2}\sin(\theta_3)\sin(\varphi_3) = 0, \\
\cos(\varphi_3)\,y + \sin(\varphi_3)\,z - h\sin(\varphi_3) = 0.
\end{cases} \\
\begin{cases}
\cos(\theta_4)\,x - \sin(\theta_4)\sin(\varphi_4)\,y - \dfrac{L}{2}\sin(\theta_4)\sin(\varphi_4) = 0, \\
\cos(\varphi_4)\,x - \sin(\varphi_4)\,z + h\sin(\varphi_4) = 0.
\end{cases}
\end{cases}
\tag{5.39}
$$

In a matrix-vector form, (5.39) can be written as

$$\mathbf{A}\begin{bmatrix} x \\ y \\ z \end{bmatrix} - \mathbf{b} = 0, \tag{5.40}$$

where

$$\mathbf{A} = \begin{bmatrix} \sin(\theta_1)\sin(\varphi_1) & \cos(\theta_1) & 0 \\ 0 & \cos(\varphi_1) & -\sin(\varphi_1) \\ \cos(\theta_2) & -\sin(\theta_2)\sin(\varphi_2) & 0 \\ \cos(\varphi_2) & 0 & \sin(\varphi_2) \\ \sin(\theta_3)\sin(\varphi_3) & \cos(\theta_3) & 0 \\ 0 & \cos(\varphi_3) & \sin(\varphi_3) \\ \cos(\theta_4) & -\sin(\theta_4)\sin(\varphi_4) & 0 \\ \cos(\varphi_4) & 0 & -\sin(\varphi_4) \end{bmatrix}, \tag{5.41}$$

and

$$\mathbf{b} = \begin{bmatrix} \frac{W}{2}\sin(\theta_1)\sin(\varphi_1) \\ -h\sin(\varphi_1) \\ -\frac{L}{2}\sin(\theta_2)\sin(\varphi_2) \\ h\sin(\varphi_2) \\ -\frac{W}{2}\sin(\theta_3)\sin(\varphi_3) \\ h\sin(\varphi_3) \\ \frac{L}{2}\sin(\theta_4)\sin(\varphi_4) \\ -h\sin(\varphi_4) \end{bmatrix}. \tag{5.42}$$

The LSM solution of (5.40) is obtained as

$$\begin{bmatrix} \tilde{x} \\ \tilde{y} \\ \tilde{z} \end{bmatrix} = \left(\mathbf{A}^H\mathbf{A}\right)^{-1}\mathbf{A}^H\mathbf{b}. \tag{5.43}$$

Next, we develop the weighted least square method (WLSM) for 3D. We assume that all the measurements are independent of each other, so there is no correlations between the arrays, nor correlation between the measurement of elevation angle and azimuth angle for any given array. Further we assume that measurement errors $\Delta\theta_i$ and $\Delta\varphi_i$, for $i = 1, 2, \cdots, N$, cause small changes to the elements of $\mathbf{A}$ and elements of $\mathbf{b}$ so that

$$\begin{cases} \Delta a_{(2i-1)k} = \dfrac{\partial a_{(2i-1)k}}{\partial \theta_i}\Delta\theta_i + \dfrac{\partial a_{(2i-1)k}}{\partial \varphi_i}\Delta\varphi_i, \\ \Delta a_{(2i)k} = \dfrac{\partial a_{(2i)k}}{\partial \theta_i}\Delta\theta_i + \dfrac{\partial a_{(2i)k}}{\partial \varphi_i}\Delta\varphi_i, \end{cases} \tag{5.44}$$
$$i = 1, 2, 3, 4,$$
$$k = 1,\ 2,\ 3,$$

and

$$\begin{cases} \Delta b_{(2i-1)} = \dfrac{\partial b_{(2i-1)}}{\partial \theta_i}\Delta\theta_i + \dfrac{\partial b_{(2i-1)}}{\partial \varphi_i}\Delta\varphi_i, \\ \Delta b_{(2i)} = \dfrac{\partial b_{(2i)}}{\partial \theta_i}\Delta\theta_i + \dfrac{\partial b_{(2i)}}{\partial \varphi_i}\Delta\varphi_i, \end{cases} \tag{5.45}$$
$$i = 1, 2, 3, 4.$$

The residuals for solving (5.39) are obtained as

$$\begin{cases} \varepsilon_{(2i-1)} = \sum\limits_{k=1}^{3} \Delta a_{(2i-1)k} \cdot \tilde{x}_k - \Delta b_{(2i-1)}, \\ \varepsilon_{(2i)} = \sum\limits_{k=1}^{3} \Delta a_{(2i)k} \cdot \tilde{x}_k - \Delta b_{(2i)}, \end{cases} \tag{5.46}$$
$$i = 1,\ 2,\ 3,\ 4,$$

where $\tilde{x}_k$, $k = 1, 2, 3$, in (5.46) represent the signal coordinates $\tilde{x}$, $\tilde{y}$, $\tilde{z}$ in (5.43).

The covariance matrix $\mathbf{\Omega}$ can be obtained by

$$\mathbf{\Omega} = E\left[\varepsilon\varepsilon^T\right], \tag{5.47}$$

where the elements of $\varepsilon$ are decided by (5.46).

Since the arrays are independent of each other, there is no correlation between the arrays,

$$\begin{cases} E\left[\left(\varepsilon_{2i-1}\right)\left(\varepsilon_{2j-1}\right)\right] = E\left[\left(\varepsilon_{2i-1}\right)\left(\varepsilon_{2j}\right)\right] = 0, \\ E\left[\left(\varepsilon_{2i}\right)\left(\varepsilon_{2j-1}\right)\right] = E\left[\left(\varepsilon_{2i}\right)\left(\varepsilon_{2j}\right)\right] = 0, \end{cases} \tag{5.48}$$
$$i \neq j,$$

while $\varepsilon_{(2i-1)}$ and $\varepsilon_{(2i)}$, $i = 1, 2, \cdots, N$, are correlated due to the fact that one needs two equations to decide one straight line in 3D. Equation (5.47) produces a band matrix. Denote $\omega_{ij}$ the element on $i^{th}$ row and $j^{th}$ column of $\mathbf{\Omega}$, the matrix is in the form of

$$\mathbf{\Omega} = \begin{bmatrix} \omega_{11} & \omega_{12} & & & & & \\ \omega_{21} & \omega_{22} & & & 0 & & \\ & & \ddots & & & & \\ & & & \ddots & & & \\ & 0 & & & \omega_{(2N-1)(2N-1)} & \omega_{(2N-1)(2N)} & \\ & & & & \omega_{(2N)(2N-1)} & \omega_{(2N)(2N)} & \end{bmatrix}_{2N \times 2N}, \tag{5.49}$$

where

$$
\begin{aligned}
\omega_{(2i-1)(2i-1)} &= E\left[\varepsilon_{(2i-1)}\varepsilon_{(2i-1)}\right] \\
&= \left[\sum_{k=1}^{3}\left(\frac{\partial a_{(2i-1)k}}{\partial \theta_i}\cdot\tilde{x}_k\right)-\frac{\partial b_{(2i-1)}}{\partial \theta_i}\right]^2 E\left[(\Delta\theta_i)^2\right] \\
&\quad +\left[\sum_{k=1}^{3}\left(\frac{\partial a_{(2i-1)k}}{\partial \varphi_i}\cdot\tilde{x}_k\right)-\frac{\partial b_{(2i-1)}}{\partial \varphi_i}\right]^2 E\left[(\Delta\varphi_i)^2\right], \\
\omega_{(2i-1)(2i)} &= E\left[\varepsilon_{(2i-1)}\varepsilon_{(2i)}\right] \\
&= \left[\sum_{k=1}^{3}\left(\frac{\partial a_{(2i-1)k}}{\partial \theta_i}\cdot\tilde{x}_k\right)-\frac{\partial b_{(2i-1)}}{\partial \theta_i}\right]\times \\
&\quad \left[\sum_{k=1}^{3}\left(\frac{\partial a_{(2i)k}}{\partial \theta_i}\cdot\tilde{x}_k\right)-\frac{\partial b_{(2i)}}{\partial \theta_i}\right] E\left[(\Delta\theta_i)^2\right] \\
&\quad +\left[\sum_{k=1}^{3}\left(\frac{\partial a_{(2i-1)k}}{\partial \varphi_i}\cdot\tilde{x}_k\right)-\frac{\partial b_{(2i-1)}}{\partial \varphi_i}\right]\times \\
&\quad \left[\sum_{k=1}^{3}\left(\frac{\partial a_{(2i)k}}{\partial \varphi_i}\cdot\tilde{x}_k\right)-\frac{\partial b_{(2i)}}{\partial \varphi_i}\right] E\left[(\Delta\varphi_i)^2\right], \\
\omega_{(2i)(2i-1)} &= E\left[\varepsilon_{(2i)}\varepsilon_{(2i-1)}\right] \\
&= \omega_{(2i-1)(2i)}, \\
\omega_{(2i)(2i)} &= E\left[\varepsilon_{(2i)}\varepsilon_{(2i)}\right] \\
&= \left[\sum_{k=1}^{3}\left(\frac{\partial a_{(2i)k}}{\partial \theta_i}\cdot\tilde{x}_k\right)-\frac{\partial b_{(2i)}}{\partial \theta_i}\right]^2 E\left[(\Delta\theta_i)^2\right] \\
&\quad +\left[\sum_{k=1}^{3}\left(\frac{\partial a_{(2i)k}}{\partial \varphi_i}\cdot\tilde{x}_k\right)-\frac{\partial b_{(2i)}}{\partial \varphi_i}\right]^2 E\left[(\Delta\varphi_i)^2\right].
\end{aligned}
\tag{5.50}
$$

Note that $E\left[|\Delta\theta_i|^2\right]$ and $E\left[|\Delta\varphi_i|^2\right]$ need to be pre-determined.

Substituting (5.41) and (5.42) into (5.50), one obtains the elements of sub-matrices

as follows:

$$\begin{aligned}
\omega_{11} &= \left[\cos(\theta_1)\sin(\varphi_1)\,\tilde{x} - \sin(\theta_1)\,\tilde{y} - \frac{W}{2}\cos(\theta_1)\sin(\varphi_1)\right]^2 E\left[(\Delta\theta_1)^2\right] \\
&\quad + \left[\sin(\theta_1)\cos(\varphi_1)\,\tilde{x} - \frac{W}{2}\sin(\theta_1)\cos(\varphi_1)\right]^2 E\left[(\Delta\varphi_1)^2\right], \\
\omega_{12} &= -\left[\sin(\theta_1)\cos(\varphi_1)\,\tilde{x} - \frac{W}{2}\sin(\theta_1)\cos(\varphi_1)\right] \times \\
&\quad \left[\sin(\varphi_1)\,\tilde{y} + \cos(\varphi_1)\,\tilde{z} - h\cos(\varphi_1)\right] E\left[(\Delta\varphi_1)^2\right], \\
\omega_{21} &= \omega_{12}, \\
\omega_{22} &= \left[\sin(\varphi_1)\,\tilde{y} + \cos(\varphi_1)\,\tilde{z} - h\cos(\varphi_1)\right]^2 E\left[(\Delta\varphi_1)^2\right].
\end{aligned} \tag{5.51}$$

$$\begin{aligned}
\omega_{33} &= \left[\sin(\theta_2)\,\tilde{x} + \cos(\theta_2)\sin(\varphi_2)\,\tilde{y} - \frac{L}{2}\cos(\theta_2)\sin(\varphi_2)\right]^2 E\left[(\Delta\theta_2)^2\right] \\
&\quad + \left[\sin(\theta_2)\cos(\varphi_2)\,\tilde{y} - \frac{L}{2}\sin(\theta_2)\cos(\varphi_2)\right]^2 E\left[(\Delta\varphi_2)^2\right], \\
\omega_{34} &= \left[\sin(\theta_2)\cos(\varphi_2)\,\tilde{y} - \frac{L}{2}\sin(\theta_2)\cos(\varphi_2)\right] \times \\
&\quad \left[\sin(\varphi_2)\,\tilde{x} - \cos(\varphi_2)\,\tilde{z} + h\cos(\varphi_2)\right] E\left[(\Delta\varphi_2)^2\right], \\
\omega_{43} &= \omega_{34}, \\
\omega_{44} &= \left[\sin(\varphi_2)\,\tilde{x} - \cos(\varphi_2)\,\tilde{z} + h\cos(\varphi_2)\right]^2 E\left[(\Delta\varphi_2)^2\right].
\end{aligned} \tag{5.52}$$

$$
\begin{aligned}
\omega_{55} &= \left[\cos(\theta_3)\sin(\varphi_3)\,\tilde{x} - \sin(\theta_3)\,\tilde{y} + \frac{W}{2}\cos(\theta_3)\sin(\varphi_3)\right]^2 E\left[(\Delta\theta_3)^2\right] \\
&\quad + \left[\sin(\theta_3)\cos(\varphi_3)\,\tilde{x} + \frac{W}{2}\sin(\theta_3)\cos(\varphi_3)\right]^2 E\left[(\Delta\varphi_3)^2\right], \\
\omega_{56} &= -\left[\sin(\theta_3)\cos(\varphi_3)\,\tilde{x} + \frac{W}{2}\sin(\theta_3)\cos(\varphi_3)\right] \times \\
&\quad \left[\sin(\varphi_3)\,\tilde{y} - \cos(\varphi_3)\,\tilde{z} + h\cos(\varphi_3)\right] E\left[(\Delta\varphi_3)^2\right], \\
\omega_{65} &= \omega_{56}, \\
\omega_{66} &= \left[\sin(\varphi_3)\,\tilde{y} - \cos(\varphi_3)\,\tilde{z} + h\cos(\varphi_3)\right]^2 E\left[(\Delta\varphi_3)^2\right].
\end{aligned}
\tag{5.53}
$$

$$
\begin{aligned}
\omega_{77} &= \left[\sin(\theta_4)\,\tilde{x} + \cos(\theta_4)\sin(\varphi_4)\,\tilde{y} + \frac{L}{2}\cos(\theta_4)\sin(\varphi_4)\right]^2 E\left[(\Delta\theta_4)^2\right] \\
&\quad + \left[\sin(\theta_4)\cos(\varphi_4)\,\tilde{y} + \frac{L}{2}\sin(\theta_4)\cos(\varphi_4)\right]^2 E\left[(\Delta\varphi_4)^2\right], \\
\omega_{78} &= \left[\sin(\theta_4)\cos(\varphi_4)\,\tilde{y} + \frac{L}{2}\sin(\theta_4)\cos(\varphi_4)\right] \times \\
&\quad \left[\sin(\varphi_4)\,\tilde{x} + \cos(\varphi_4)\,\tilde{z} - h\cos(\varphi_4)\right] E\left[(\Delta\varphi_4)^2\right], \\
\omega_{87} &= \omega_{78}, \\
\omega_{88} &= \left[\sin(\varphi_4)\,\tilde{x} + \cos(\varphi_4)\,\tilde{z} - h\cos(\varphi_4)\right]^2 E\left[(\Delta\varphi_4)^2\right].
\end{aligned}
\tag{5.54}
$$

Extending (5.21) to 3D results in

$$
\varepsilon^T \mathbf{\Omega}^{-1} \varepsilon = \left( \mathbf{A} \begin{bmatrix} \tilde{x} \\ \tilde{y} \\ \tilde{z} \end{bmatrix} - \mathbf{b} \right)^T \mathbf{\Omega}^{-1} \left( \mathbf{A} \begin{bmatrix} \tilde{x} \\ \tilde{y} \\ \tilde{z} \end{bmatrix} - \mathbf{b} \right). \tag{5.55}
$$

Thus, the WLSM solution of the target position in 3D case is given by

$$
\begin{bmatrix} \tilde{x} \\ \tilde{y} \\ \tilde{z} \end{bmatrix} = \left(\mathbf{A}^H \mathbf{\Omega}^{-1} \mathbf{A}\right)^{-1} \mathbf{A}^H \mathbf{\Omega}^{-1} \mathbf{b}. \tag{5.56}
$$

### 5.3.2 Simulation Using Uniform Circular Arrays in 3D

Simulations have been carried out using a standard swimming pool of $50m$ long, $25m$ wide, and $3m$ deep. Four UCAs are all placed $1.5m$ above the floor. One UCA is placed on each wall at the middle point along the wall, as shown in Fig. 5.6(a). The four UCAs are identical. Each element of the array is a circular one with a radius of $\lambda/4$ whose radiation pattern is given by (5.37).

To examine the performance of the proposed method, the root-mean-square estimates of 3D positions are obtained for Lane 8 (see Fig. 5.3(a)) under signal-to-noise ratio $-5dB$ and $5dB$, respectively. Two sets of UCAs with 8-elements and 12-elements, respectively, are used in the simulation to examine the effect of the number of elements in an UCA on the positioning accuracy. As expected, since a greater number of elements leads to a narrower beam and therefore higher DoA estimation accuracy, the positioning accuracy increases with the number of elements in the array. Both the LSM and the WLSM are used for positioning estimates, and a comparison of their RMSEs are shown in Fig. 5.7(a) and Fig. 5.7(b). It can be seen that the WLSM outperforms the conventional LSM significantly. Most improvement can be observed when the targets are closer to either end of the swimming pool.

## 5.4 Conclusion

The method of using multiple arrays for wireless positioning for 2D and 3D scenarios is studied. To mitigate the problem of DoA estimation inaccuracy when the DoA moves away from the array norm, a weighted least squares method (WLSM) is proposed with the weighting function derived from the generalized least squares method (GLSM). When the WLSM is applied for tracking swimmers in a swimming pool, it produces excellent results. Compared with the conventional least squares

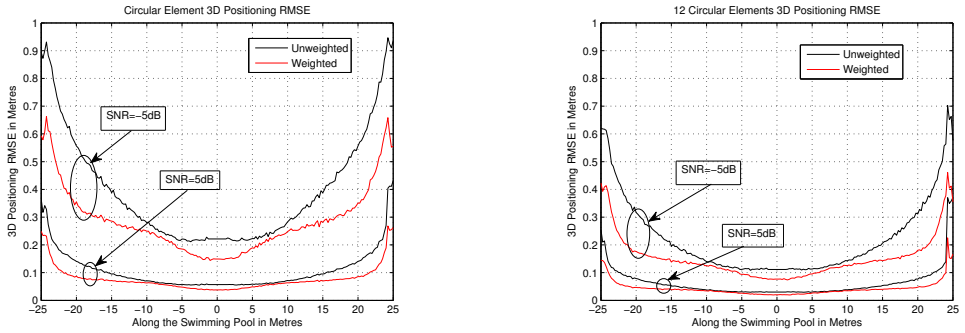


(a) Four 8-Element UCAs

(b) Four 12-Element UCAs

**Figure 5.7:** RMSE for 3D Positioning for Lane 8

method, the WLSM results in great improvement in positioning accuracy. The effectiveness of the method has been validated by simulations carried out in a standard swimming pool.

It should be noted that the method and results presented in the chapter are applicable to both wireless and acoustic positioning as no specific propagation channel information has been assumed.

# Chapter 6

# A Novel Ranging Based Array for Positioning

## 6.1 Introduction

Wireless positioning techniques can be classified into two main categories: ranging based and bearing or direction-of-arrival (DoA) based [1], [2]. The associated algorithms of the two techniques are presented in a fine review by Torrieri [117]. Typical techniques for DoA estimation employ a linear or circular antenna array. By directly or indirectly measuring the phase differences between antenna elements, the direction of the incident signal can be estimated [51], [92], [118]. A drawback of this technique is that it requires calibrations of different signal branches. Since the phase measurement is sensitive to the environment change such as temperature and aging, the calibration must be done on a regular basis. This could complicate the system and increase cost.

Wireless positioning systems using ranging estimations have been widely and deeply explored [119], [120], [121], [122]. The technique is to use ranging information,

which is obtained from the time-of-flight measurement, for instance, to estimate the target position using trilateration. The application is typically under the assumption that some fixed reference nodes are available in the area where positioning is conducted. This assumption may limit the applications of ranging based methods. In many situations, such as emergency rescue operation and mobile workforce management, it is impractical or even impossible to pre-install the reference nodes. Therefore, a positioning system without requiring fixed reference nodes would be desired.

This chapter presents a novel wireless positioning system which employs an array of sensors to estimate the position of a mobile target without using fixed reference nodes [123]. In contrast to the traditional array based method, every sensor is capable of doing ranging measurements individually by communicating with the target, but no phase measurement is required. These range measurements lead to a bearing estimate as well as a high accuracy ranging estimate via averaging. Given the proliferation of various standard wireless transceivers capable of doing ranging measurements, such a system can be built at a reasonably low cost.

The chapter is organised as follows. In Section 6.2, a wireless localisation system employing raging based arrays is described and an associated location estimator is presented. Section 6.4 derives the Cramér-Rao lower bound of the proposed location estimator. Section 6.4 presents a closed form expression of the standard deviation (STD) and it is proved that the estimator can reach its Cramér-Rao lower bound. Samples of STD calculations are compared with root-mean-square error (RMSE) of positioning simulation. Section 6.5 presents the derivation of CRLB when the array is placed at an arbitrary location, and Section 6.6 presents the closed-form of standard deviation for the array placed at an arbitrary location and proves that the estimator can reach its Cramér-Rao lower bound. Some numerical results are given in the same section to prove the theoretical results. Section 6.7 extends the theory of ranging

based sensor array to 3D. In Subsection 6.7.1, a 3D array model is introduced, and in Subsection 6.7.2, a closed-form standard deviation is derived, and in Subsection 6.7.3, numerical result is presented. Finally, Section 6.8 concludes the chapter.

## 6.2 System Description and Position Estimator

Conventional DoA based positioning systems typically employ phase measurements at the antenna branches and distance measurements to determine the location of a mobile target. To avoid ambiguity, the antenna inter-element spacing is normally chosen to be close to half wavelength. All the antenna branches need to be carefully calibrated in order to extract the DoA information from the received signal. Given the proliferation of low cost sensors capable of doing range measurement, we introduce the concept of using such sensors to form a positioning array. In contrast to conventional arrays, the inter-sensor distance is entirely the choice of the system designer, which can be as large as practically feasible to increase positioning accuracy. The bearing of the target node is determined by the differences of ranges measured at the individual sensors. The ranges estimated by each sensor are then employed to estimate the distance of the target node to the center of sensor array, thus leading to the target node position.

Without loss of generality, the size of the sensor array is considered to be in metres. Since the target node is typically far away from the sensor array and the distance far greater than the size of the sensor array, one can use the far field approximation to represent the ranges between the target node and the individual sensors. In other words, the signal impinging on the sensor array from the target node can be modeled as a plane wave. For convenience, we assume that all the sensors in the sensor array are uniformly distributed in a circle as shown in Fig. 6.1.

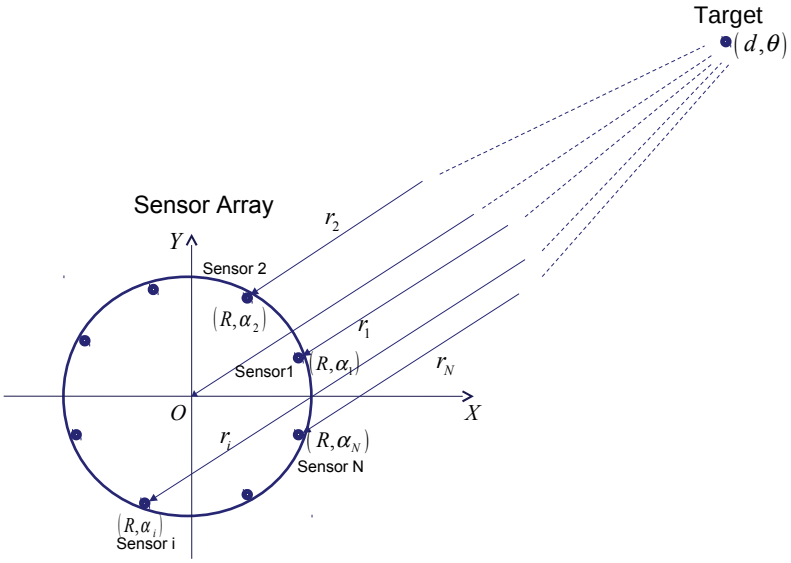


**Figure 6.1:** Far field estimation model

A polar coordinates system is set-up with its origin is at the centre of the sensor array, and the polar angle is measured from the $X$-axis counter-clockwise. We also denote $R$ as the radius of the circle, and the polar angle of the $i^{th}$ sensor is $\alpha_i$ . If the position of the target is represented as $(d, \theta)$ , the range between the $i^{th}$ sensor and the target is given by

$$\begin{aligned} r_i &= d - R\cos(\alpha_i - \theta) + \Delta r_i \\ &= d - R\cos(\alpha_i)\cos(\theta) - R\sin(\alpha_i)\sin(\theta) + \Delta r_i, \qquad (6.1) \\ i &= 1, \cdots, N. \end{aligned}$$

where $\Delta r_i$, $i = 1, \cdots, N$, are the deviations of ranges from their expected value respectively.

For a whole array, the ranges between the target and each individual sensor is

thus expressed in a matrix form as

$$\begin{bmatrix} r_1 \\ r_2 \\ \vdots \\ r_N \end{bmatrix} = \mathbf{A} \begin{bmatrix} d \\ \cos(\theta) \\ \sin(\theta) \end{bmatrix} + \begin{bmatrix} \Delta r_1 \\ \Delta r_2 \\ \vdots \\ \Delta r_N \end{bmatrix}, \tag{6.2}$$

where

$$\mathbf{A} = \begin{bmatrix} 1 & -R\cos(\alpha_1) & -R\sin(\alpha_1) \\ 1 & -R\cos(\alpha_2) & -R\sin(\alpha_2) \\ \vdots & \vdots & \vdots \\ 1 & -R\cos(\alpha_N) & -R\sin(\alpha_N) \end{bmatrix}_{N\times 3}. \tag{6.3}$$

is a matrix related with the radius of the array $R$ , and sinusoidal functions of the polar angles associated with each individual sensor.

Denote $\mathbf{r}$ as a vector form of ranges between each sensor and the target,

$$\mathbf{r} = \begin{bmatrix} r_1, & r_2, & \cdots, & r_N \end{bmatrix}^{\mathbf{T}}, \tag{6.4}$$

where $[\cdot]^T$ denotes the vector or matrix transposition. And denote $\Delta r$ as the vector form of range deviations from their expected value

$$\Delta\mathbf{r} = \begin{bmatrix} \Delta r_1, & \Delta r_2, & \cdots, & \Delta r_N \end{bmatrix}^{T}, \tag{6.5}$$

(6.2) can be re-written as

$$\mathbf{A} \begin{bmatrix} d \\ \cos(\theta) \\ \sin(\theta) \end{bmatrix} + \mathbf{\Delta r} = \mathbf{r}. \tag{6.6}$$

The least squares solution of (6.6) yields

$$\begin{bmatrix} d \\ c \\ s \end{bmatrix} = \left(\mathbf{A^T A}\right)^{-1} \mathbf{A^T r}. \tag{6.7}$$

Thus, the distance of the target is estimated as $d$ and the bearing of the target, $\theta$ , is estimated as

$$\theta = \tan^{-1}\left(\frac{s}{c}\right). \tag{6.8}$$

Equations (6.7) and (6.8) constitute a distance and bearing estimator.

## 6.3 Cramér-Rao Lower Bound for Ranging Based Sensor Array

In the model described in Section 6.2, the coordinates of target position in polar system, $d$ and $\theta$, are two parameters need to be estimated. The two estimators $\hat{d}$ and $\hat{\theta}$ are described by (6.7) and (6.8). Let *pdf* denote the probability density function of the array. With two parameters to be estimated, the Fisher information matrix is a $2 \times 2$ matrix [124], which is expressed as

$$\mathbf{I} = \begin{bmatrix} E\left\{\left[\frac{\partial}{\partial d}\ln(pdf)\right]^2\right\} & E\left\{\left[\frac{\partial}{\partial d}\ln(pdf)\right]\left[\frac{\partial}{\partial \theta}\ln(pdf)\right]\right\} \\ E\left\{\left[\frac{\partial}{\partial d}\ln(pdf)\right]\left[\frac{\partial}{\partial \theta}\ln(pdf)\right]\right\} & E\left\{\left[\frac{\partial}{\partial \theta}\ln(pdf)\right]^2\right\} \end{bmatrix}. \tag{6.9}$$

Let $pdf_i$ denote the probability density function of the $i^{th}$ sensor, $i = 1, \cdots, N$ . By the law of likelihood [124], the probability density function of the array, *pdf* , and the probability density function of individual sensor, $pdf_i$ , satisfy

$$pdf = \prod_{i=1}^{N} pdf_i. \tag{6.10}$$

Assume that the range measurements by each sensor, $r_i$, $i = 1, \cdots, N$, is corrupted by Gaussian noise with standard deviation $\sigma$. The probability density function for

each measurement is thus given by

$$\begin{aligned} pdf_i &= \frac{1}{\sqrt{2\pi}\sigma} \exp\left[-\frac{1}{2}\frac{(r_i-\mu_i)^2}{\sigma^2}\right], \\ i &= 1, \cdots, N. \end{aligned} \tag{6.11}$$

where $\mu_i$ is the expected value of the range between the target and the sensor $i$. In the model described in Section 6.2, the expected value of the range measured by sensor $i$ is expressed by

$$\begin{aligned} \mu_i &= d - R\cos(\alpha_i - \theta), \\ i &= 1, \cdots, N. \end{aligned} \tag{6.12}$$

where $\mu_i$ is a function of two parameters, the expected target distance $d$ and the expected target bearing $\theta$ .

To obtain the Fisher information matrix, we take the natural logarithm of 6.10 [124]:

$$\ln(pdf) = -N\ln\left(\sqrt{2\pi}\sigma\right) - \frac{1}{2}\sum_{i=1}^{N}\frac{(r_i-\mu_i)^2}{\sigma^2}. \tag{6.13}$$

Performing partial differentiation of (6.13) with respected to the two parameters results in the Fisher information matrix. The partial derivative of (6.13) with respect to distance $d$ is found to be

$$\begin{aligned} \frac{\partial}{\partial d}\ln(pdf) &= \sum_{i=1}^{N}\left\{\left[\frac{\partial}{\partial \mu_i}\ln(pdf_i)\right]\frac{\partial \mu_i}{\partial d}\right\} \\ &= \frac{1}{\sigma^2}\sum_{i=1}^{N}(r_i-\mu_i), \end{aligned} \tag{6.14}$$

and the partial derivative of (6.13) with respect to bearing $\theta$ is found to be

$$\begin{aligned} \frac{\partial}{\partial \theta}\ln(pdf) &= \sum_{i=1}^{N}\left\{\left[\frac{\partial}{\partial \mu_i}\ln(pdf_i)\right]\frac{\partial \mu_i}{\partial \theta}\right\} \\ &= -\frac{R}{\sigma^2}\sum_{i=1}^{N}(r_i-\mu_i)\sin(\alpha_i-\theta). \end{aligned} \tag{6.15}$$

From (6.14) and (6.15), one can obtain the elements of the Fisher information matrix

as follows. First,

$$I_{11} = E\left\{\left[\frac{\partial}{\partial d}\ln\left(pdf\right)\right]^2\right\} = \frac{1}{\sigma^4}E\left\{\left[\sum_{i=1}^{N}\left(r_i-\mu_i\right)\right]^2\right\}. \tag{6.16}$$

For independent sensors in the array, we assume that there is no correlation between the measurements, i.e.,

$$\begin{gathered} E\left[\left(r_i-\mu_i\right)\left(r_j-\mu_j\right)\right]=0, \\ i\neq j. \end{gathered} \tag{6.17}$$

This leads to

$$E\left\{\left[\sum_{i=1}^{N}\left(r_i-\mu_i\right)\right]^2\right\} = \sum_{i=1}^{N}E\left[\left(r_i-\mu_i\right)^2\right]. \tag{6.18}$$

Since

$$E\left[\left(r_i-\mu_i\right)^2\right]=\sigma^2, \tag{6.19}$$

applying (6.18) and (6.19) to (6.16) results in

$$I_{11}=\frac{N}{\sigma^2}. \tag{6.20}$$

Similarly,

$$\begin{aligned} I_{22} &= E\left\{\left[\frac{\partial}{\partial\theta}\ln\left(pdf\right)\right]^2\right\} \\ &= \left(\frac{-R}{\sigma^2}\right)^2 E\left\{\left[\sum_{i=1}^{N}\left(r_i-\mu_i\right)\sin\left(\alpha_i-\theta\right)\right]^2\right\}. \end{aligned} \tag{6.21}$$

Note that

$$\begin{aligned} & E\left\{\left[\left(r_i-\mu_i\right)\sin\left(\alpha_i-\theta\right)\right]\left[\left(r_j-\mu_j\right)\sin\left(\alpha_j-\theta\right)\right]\right\} \\ = \;& \sin\left(\alpha_i-\theta\right)\sin\left(\alpha_j-\theta\right)E\left\{\left[\left(r_i-\mu_i\right)\left(r_j-\mu_j\right)\right]\right\}. \end{aligned} \tag{6.22}$$

By virtue of (6.18), one obtains

$$\begin{gathered} E\left\{\left[\left(r_i-\mu_i\right)\sin\left(\alpha_i-\theta\right)\right]\left[\left(r_j-\mu_j\right)\sin\left(\alpha_j-\theta\right)\right]\right\}=0, \\ i\neq j. \end{gathered} \tag{6.23}$$

Substituting(6.23) in(6.21) gives

$$I_{22}=\left(\frac{R}{\sigma^2}\right)^2\sum_{i=1}^{N}E\left[\left(r_i-\mu_i\right)^2\right]\sin^2\left(\alpha_i-\theta\right). \tag{6.24}$$

Applying (6.19) to (6.24) leads to

$$I_{22} = \frac{R^2}{\sigma^2} \sum_{i=1}^{N} \sin^2 (\alpha_i - \theta) . \tag{6.25}$$

Further manipulation of (6.24) results in

$$I_{22} = \frac{NR^2}{2\sigma^2}. \tag{6.26}$$

We note,

$$\begin{aligned} I_{12} &= I_{21} \\ &= E\left\{ \left[ \frac{\partial}{\partial d} \ln (pdf) \right] \left[ \frac{\partial}{\partial \theta} \ln (pdf) \right] \right\}. \end{aligned} \tag{6.27}$$

Substituting (6.14) and (6.15) in (6.27) one has

$$\begin{aligned} I_{12} &= I_{21} \\ &= -\frac{R}{\sigma^4} E\left\{ \left[ \sum_{i=1}^{N} (r_i - \mu_i) \right] \left[ \sum_{i=1}^{N} (r_i - \mu_i) \sin (\alpha_i - \theta) \right] \right\}. \end{aligned} \tag{6.28}$$

Again, the zero correlation error between different measurements leads to

$$\begin{aligned} & E\left\{ \left[ \sum_{i=1}^{N} (r_i - \mu_i) \right] \left[ \sum_{i=1}^{N} (r_i - \mu_i) \sin (\alpha_i - \theta) \right] \right\} \\ &= \sum_{i=1}^{N} E\left[ (r_i - \mu_i)^2 \right] \sin (\alpha_i - \theta) \\ &= \sigma^2 \sum_{i=1}^{N} \sin (\alpha_i - \theta) \\ &= 0. \end{aligned} \tag{6.29}$$

Substituting (6.29) in (6.28), one obtains

$$I_{12} = I_{21} = 0. \tag{6.30}$$

Therefore, the Fisher information matrix of the array is obtained as

$$\mathbf{I} = \frac{N}{\sigma^2} \begin{bmatrix} 1 & 0 \\ 0 & \dfrac{R^2}{2} \end{bmatrix}. \tag{6.31}$$

It is seen that, for distance estimation, the array provides $N$ times the Fisher information of that of a single sensor. The Fisher information for bearing is not only determined by the number of the sensors, but also is proportional to the squared radius of the array. The greater the array size, the greater the Fisher information it provides. Comparing with using a single sensor, the advantage of using a sensor array is that the bearing information can be obtained. In the model, since the sensors are evenly distributed along the circumference of the array, the correlation of $d$ and $\theta$ happens to be zero with reference to the array centre, thus resulting in a diagonal Fisher information matrix.

The Cramér-Rao lower bound is given by the inversion of Fisher information matrix [125], denoted as $\mathbf{\Sigma}$. By inversing (6.31), one obtains

$$\mathbf{\Sigma} = \frac{\sigma^2}{N} \begin{bmatrix} 1 & 0 \\ 0 & \dfrac{2}{R^2} \end{bmatrix}. \tag{6.32}$$

Thus, the lower bound of the variance of distance estimates is found to be

$$Var\,(d) \geq \frac{1}{N}\sigma^2, \tag{6.33}$$

and the lower bound of the variance of bearing estimates is found to be

$$Var\,(\theta) \geq \frac{2}{NR^2}\sigma^2. \tag{6.34}$$

It is seen that the accuracy of the distance estimation can be increased by increasing $N$, the number of elements in the array, and the accuracy of the bearing estimation can be increased by increasing $N$ and $R$, with the latter being the radius of the array. However, the radius of the array is typically less than, say, two metres as the array is considered to be carried by a vehicle. Therefore, to certain extent, it is more practical to increase $N$. In practice, the inter-sensor spacing is limited to, say a half wavelength, by the coupling between sensors. One way of increasing N further

is to arrange the elements on multiple circles. Thus the Fisher information matrix, presented by equation (6.31) can be extended. When the $m^{th}$ circle has $N_m$ sensors and the radius $R_m$, and the total number of circles is $M$, by following the previous procedure, one obtains

$$\mathbf{I} = \frac{1}{\sigma^2} \begin{bmatrix} \sum_{m=1}^{M} N_m & 0 \\ 0 & \frac{\sum_{m=1}^{M} N_m {R_m}^2}{2} \end{bmatrix}. \tag{6.35}$$

Thus, the lower bound of the variance of distance estimates is given by

$$Var\,(d) \geq \frac{1}{\sum_{m=1}^{M} N_m}\sigma^2, \tag{6.36}$$

and the lower bound of the variance of bearing estimates is given by

$$Var\,(\theta) \geq \frac{2}{\sum_{m=1}^{M} N_m {R_m}^2}\sigma^2. \tag{6.37}$$

## 6.4 Variance and Standard Deviation of the Array

In this section, the variance of distance estimator, ${\sigma_d}^2$ , and the variance of bearing estimator, ${\sigma_\theta}^2$ , are derived from the positioning algorithm.

Assume $\Delta r_i$ , $i = 1, \cdots, N$ , are small, so are $\Delta d$, $\Delta c$ and $\Delta s$, they can be expressed in their differential forms.

Define the operator vector as

$$\frac{\partial}{\partial \mathbf{r}} = \left[ \begin{array}{cccc} \frac{\partial}{\partial r_1}, & \frac{\partial}{\partial r_2}, & \cdots, & \frac{\partial}{\partial r_N} \end{array} \right]^T, \tag{6.38}$$

The errors of $d$ , $c$ and $s$ are thus expressed as

$$\Delta d = \left(\frac{\partial d}{\partial \mathbf{r}}\right)^T \cdot (\Delta \mathbf{r}), \tag{6.39}$$

$$\Delta c = \left(\frac{\partial c}{\partial \mathbf{r}}\right)^T \cdot (\Delta \mathbf{r}), \tag{6.40}$$

and

$$\Delta s = \left(\frac{\partial s}{\partial \mathbf{r}}\right)^T \cdot (\Delta \mathbf{r}). \tag{6.41}$$

We also assume that the error of bearing estimation, $\Delta\theta$ , is small, so it can be expressed by the first order of partial differential (6.8) as

$$\Delta\theta = c_{EV} \cdot \Delta s - s_{EV} \cdot \Delta c, \tag{6.42}$$

where $\Delta c$ and $\Delta s$ are the deviations from the expected value of $c_{EV}$ and $s_{EV}$ , and $c_{EV}$ and $s_{EV}$ represent $\cos(\theta_{EV})$ and $\sin(\theta_{EV})$ respectively.

Defining

$$\mathbf{u} = c_{EV}\frac{\partial s}{\partial \mathbf{r}} - s_{EV}\frac{\partial c}{\partial \mathbf{r}}, \tag{6.43}$$

equation (6.42) can be simply re-written as

$$\Delta\theta = \mathbf{u}^T \cdot (\Delta \mathbf{r}). \tag{6.44}$$

Thus, by using (6.38), the variance of distance estimates, ${\sigma_d}^2$ , is obtained as

$${\sigma_d}^2 = E\left[(\Delta d)^2\right] = E\left\{\left[\left(\frac{\partial d}{\partial \mathbf{r}}\right)^T \cdot (\Delta \mathbf{r})\right]^2\right\}, \tag{6.45}$$

and by using (6.44), the variance of bearing estimates, ${\sigma_\theta}^2$ , can be obtained as

$${\sigma_\theta}^2 = E\left[(\Delta\theta)^2\right] = E\left\{\left[\mathbf{u}^T \cdot (\Delta \mathbf{r})\right]^2\right\}. \tag{6.46}$$

From (6.3), and by using Euler formula, one obtains (AppendixA, A.11)

$$\mathbf{A}^T\mathbf{A} = \begin{bmatrix} N & 0 & 0 \\ 0 & \frac{NR^2}{2} & 0 \\ 0 & 0 & \frac{NR^2}{2} \end{bmatrix}. \tag{6.47}$$

Noting that

$$\mathbf{A}^T\mathbf{r} = \begin{bmatrix} \sum_{i=1}^{N} r_i \\ -R\sum_{i=1}^{N} r_i \cos\alpha_i \\ -R\sum_{i=1}^{N} r_i \sin\alpha_i \end{bmatrix}, \tag{6.48}$$

one has

$$d = \frac{1}{N}\sum_{i=1}^{N} r_i, \tag{6.49}$$

$$c = -\frac{2}{NR}\sum_{i=1}^{N} r_i \cos(\alpha_i), \tag{6.50}$$

and

$$s = -\frac{2}{NR}\sum_{i=1}^{N} r_i \sin(\alpha_i). \tag{6.51}$$

Substituting (6.49) in (6.39) yields

$$\Delta d = \frac{1}{N}\sum_{i=1}^{N} (\Delta r_i), \tag{6.52}$$

thus

$$E\left[(\Delta d)^2\right] = \frac{1}{N^2} E\left\{\left[\sum_{i=1}^{N} (\Delta r_i)\right]^2\right\}. \tag{6.53}$$

Since the sensors in the array are independent of each other,

$$\begin{aligned} &E\left[(\Delta r_i)(\Delta r_j)\right] = 0, \\ &i \neq j, \end{aligned} \tag{6.54}$$

one obtains

$$\begin{aligned} & E\left\{\left[\sum_{i=1}^{N} (\Delta r_i)\right]^2\right\} \\ = & \sum_{i=1}^{N} \left\{E\left[(\Delta r_i)^2\right]\right\} \\ = & N\sigma^2. \end{aligned} \tag{6.55}$$

Therefore, one has

$$E\left[(\Delta d)^2\right] = \frac{1}{N}\sigma^2. \tag{6.56}$$

Substitute (6.56) in (6.45), the variance of distance estimation is obtained as

$$\sigma_d{}^2 = \frac{1}{N}\sigma^2. \tag{6.57}$$

Applying operation vector (6.38) to (6.50) and (6.51) one obtains

$$\frac{\partial c}{\partial \mathbf{r}} = -\frac{2}{NR}\left[\begin{array}{ccc} \cos(\alpha_1), & \cdots, & \cos(\alpha_N) \end{array}\right]^T, \tag{6.58}$$

and

$$\frac{\partial s}{\partial \mathbf{r}} = -\frac{2}{NR}\left[\begin{array}{ccc} \sin(\alpha_1), & \cdots, & \sin(\alpha_N) \end{array}\right]^T. \tag{6.59}$$

Substitute (6.58) and (6.59) in (6.44)

$$\Delta\theta = -\frac{2}{NR}\sum_{i=1}^{N}\{[c_{EV}\sin(\alpha_i) - s_{EV}\cos(\alpha_i)](\Delta r_i)\}. \tag{6.60}$$

Noting that item $[c_{EV}\sin(\alpha_i) - s_{EV}\cos(\alpha_i)]$ does not contain any variables, and also noting that the errors of range measurement are uncorrelated, which is expressed as (6.54), the variance of bearing is obtained to be

$$E\left[(\Delta\theta)^2\right] = \frac{4\sigma^2}{N^2R^2}\sum_{i=1}^{N}[c_{EV}\sin(\alpha_i) - s_{EV}\cos(\alpha_i)]^2. \tag{6.61}$$

Further simplification leads to (see Appendix B),

$$\sigma_\theta{}^2 = \frac{2}{NR^2}\sigma^2. \tag{6.62}$$

Comparing (6.57) with (6.33), and (6.62) with (6.34), finds that the variance of distance and the variance of bearing by proposed model reach their Cramér-Rao lower bound.

Denote $\Delta p$ as the positioning error. Since

$$(\Delta p)^2 = (\Delta d)^2 + d^2(\Delta\theta)^2, \tag{6.63}$$

one can obtain the positioning variance $\sigma_p^2$ by performing

$$E\left[(\Delta p)^2\right] = E\left[(\Delta d)^2\right] + d^2E\left[(\Delta\theta)^2\right]. \tag{6.64}$$

It leads to

$$\sigma_p{}^2 = \frac{\sigma^2}{N}\left(1 + \frac{2d^2}{R^2}\right), \tag{6.65}$$

where (6.57) and (6.62) have been used.

In order to understand the performance of the proposed location estimator, simulations have been carried out to obtain the root-mean-square errors (RMSE) of positioning. Further, to validate the theoretical analysis, the RMSE are compared with the standard deviation of positioning $\sigma_p$, which is obtained from (6.65).

In the simulations, we assume that the standard deviation of individual sensor measurement is $0.02m$ which can be achieved using ultra wideband signals, and the distance between the position of the target and the center of the sensor array is chosen as $50m$ and $100m$, respectively. The sensor array uses three different radius settings: $1m$, $1.5m$, and $2m$, and for each radius setting, two numbers of sensors are chosen, four and eight.

Fig. 6.2 shows the positioning errors for different array radii and different target distances from the array centre. The solid lines represent standard deviations, and the diamonds the RMSE. It is shown that simulation results agree with the theoretical STD ones.

One can reduce the positioning variance by increasing the number of sensors and the array size, and even by using multiple circles of sensors. When the $m^{th}$ circle is of the number of $N_m$ sensors and the radius $R_m$, and the total number of the circle is $M$, by following the previous procedure, the variance of positioning using multiple circles of sensors is found to be

$$\sigma_p{}^2 = \sigma^2 \left[\frac{1}{\sum_{m=1}^{M} N_m} + \frac{2d^2}{\sum_{m=1}^{M}\left(N_m {R_m}^2\right)}\right]. \tag{6.66}$$

It shows that, if space permits, the best way that distributes sensors is to place them

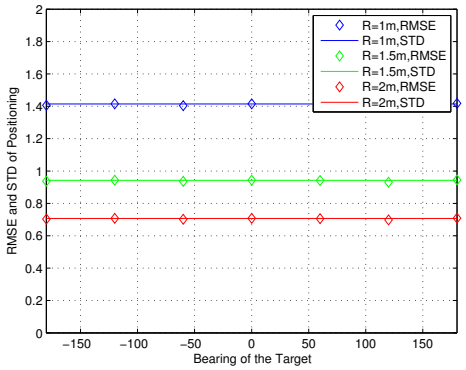


(a) Positioning error of a 4-sensor sensor array

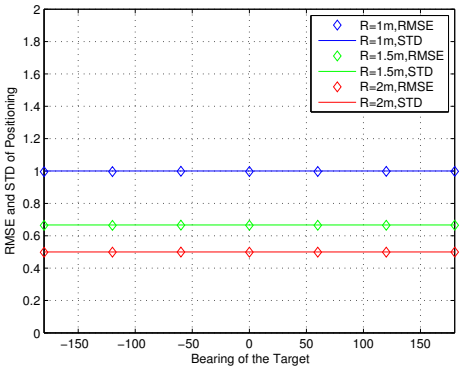


(b) Positioning error of an 8-sensor sensor array

**Figure 6.2:** Positioning error when the target is $100m$ away, and the STD of measurement is $0.02m$

on the outmost circumference of the array.

Fig. 6.3 shows the standard deviation of positioning as a function of the number of sensors, where Fig. 6.3(a) shows the relationships for three different sizes of the array radius when the target is $50m$ away from the center of the array, and Fig. 6.3(b) shows for the same sizes of the arrays when the target is $100m$ away. All the calculations are performed under the condition that, $\sigma$ , the STD of range measurement by each sensor, is $0.02m$. It is apparent that greater radius and larger number of sensors in the array lead to higher positioning accuracy.

Equations (6.57), (6.62) and (6.65) show that the positioning error caused by the ranging estimate, $\Delta d$, is relatively small. The overall positioning error is primarily determined by the squared distance, $d^2$, which serves as an amplification factor. A small error in the bearing estimate, $\Delta\theta$, would result in a large positioning error along the arc, named error arc, which is shown in Fig. 6.4 as $PQ$. Using Gaussian distribution, the length of the arc can be estimated to be $2 \times (3\sigma_\theta d)$.

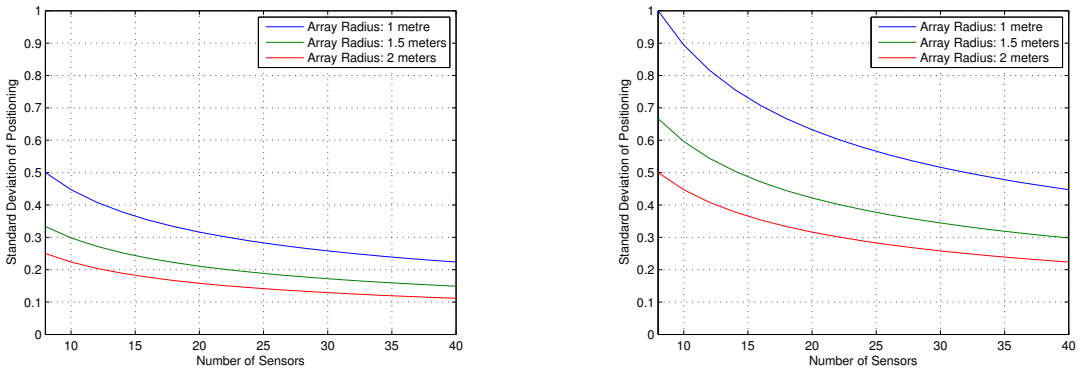


(a) Target $50m$ away from the array center

(b) Target $100m$ away from the array center

**Figure 6.3:** Standard deviation of positioning

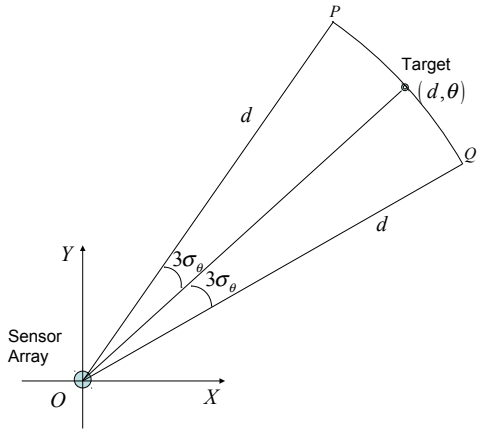


**Figure 6.4:** Positioning error analysis

## 6.5 Cramér-Rao Lower Bound for an Array at an Arbitrary Position

In the previous section, we have analysed the Fisher information matrix of an array with respect to its own center. In the following, we derive the Fisher information matrix of an array with respect to the origin of a co-ordinate system when the array is placed at an arbitrary position. It will be seen next chapter that this is for analysing the positioning performance of two co-operating arrays.

As shown in Fig. 6.5, an array same as that described in Section 6.2 is placed at $(a, \psi)$, and the target position is estimated at $(d_A, \theta_A)$ with respect to the center of the array $(a, \psi)$. In other words, the estimators are $\hat{d}_A$ and $\hat{\theta}_A$ with respect to the centre of array A.

The law of likelihood provides that the probability density function of array A equals the product of probability density function of its individual sensors,

$$pdf_A = \prod_{i=1}^{N} pdf_{Ai}. \tag{6.67}$$

From the model described in Section 6.2, the expected value of range between an individual sensor and the target is

$$\mu_{Ai}(d, \theta) = d_A(d, \theta) - R\cos(\alpha_i - \theta_A(d, \theta)). \tag{6.68}$$

The same assumption that the measurements are corrupted by Gaussian noise is made as in Section 6.3. The probability density function of individual sensors in the array, referred to as array A, is given by

$$pdf_{Ai} = \frac{1}{\sqrt{2\pi}\sigma} \exp\left[-\frac{1}{2}\frac{(r_{Ai} - \mu_{Ai})^2}{\sigma^2}\right]. \tag{6.69}$$

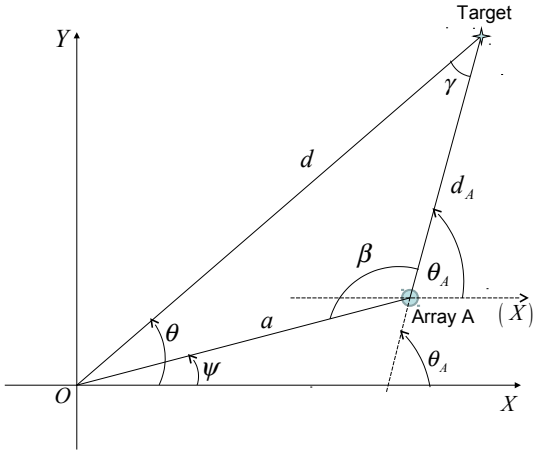


**Figure 6.5:** Array Placed at an Arbitrary Position

And the logarithm of probability density function of array A is given by

$$\ln\left(pdf_A\right) = -N\ln\left(\sqrt{2\pi}\sigma\right) - \frac{1}{2}\sum_{i=1}^{N}\frac{\left(r_{Ai}-\mu_{Ai}\right)^2}{\sigma^2}. \tag{6.70}$$

First we obtain the partial differentiation of natural logarithm of probability density function with respect to the two parameters, $d_A$ and $\theta_A$ as

$$\frac{\partial}{\partial d_A}\ln\left(pdf_A\right) = \frac{1}{\sigma^2}\sum_{i=1}^{N}\left(r_{Ai}-\mu_{Ai}\right), \tag{6.71}$$

and

$$\frac{\partial}{\partial \theta_A}\ln\left(pdf_A\right) = \frac{-R}{\sigma^2}\sum_{i=1}^{N}\left(r_{Ai}-\mu_{Ai}\right)\sin\left(\alpha_i-\theta_A\right). \tag{6.72}$$

The elements of Fisher information matrix are obtained as

$$E\left\{\left[\frac{\partial}{\partial d_A}\ln\left(pdf_A\right)\right]^2\right\} = \frac{N}{\sigma^2}, \tag{6.73}$$

$$E\left\{\left[\frac{\partial}{\partial \theta_A}\ln\left(pdf_A\right)\right]^2\right\} = \frac{NR^2}{2\sigma^2}, \tag{6.74}$$

and

$$E\left\{\left[\frac{\partial}{\partial d_A}\ln\left(pdf_A\right)\right]\left[\frac{\partial}{\partial \theta_A}\ln\left(pdf_A\right)\right]\right\}=0. \tag{6.75}$$

where uncorrelated measurement errors, the uniformed variance of measurement by individual array have been applied, also trigonometry identity and (A.7) have been employed.

To simplify the text, we use $I_{A11}$, $I_{A22}$, $I_{A12}$ and $I_{A21}$ denoting the elements of the Fisher information matrix,

$$\mathbf{I}_A=\begin{bmatrix} I_{A11} & I_{A12} \\ I_{A21} & I_{A22} \end{bmatrix}. \tag{6.76}$$

where

$$I_{A11}=E\left\{\left[\frac{\partial}{\partial d}\ln\left(pdf_A\right)\right]^2\right\}, \tag{6.77}$$

$$I_{A22}=E\left\{\left[\frac{\partial}{\partial \theta}\ln\left(pdf_A\right)\right]^2\right\}, \tag{6.78}$$

$$I_{A12}=E\left\{\left[\frac{\partial}{\partial d}\ln\left(pdf_A\right)\right]\left[\frac{\partial}{\partial \theta}\ln\left(pdf_A\right)\right]\right\}, \tag{6.79}$$

and

$$I_{A21}=E\left\{\left[\frac{\partial}{\partial \theta}\ln\left(pdf_A\right)\right]\left[\frac{\partial}{\partial d}\ln\left(pdf_A\right)\right]\right\}. \tag{6.80}$$

Note that the above are the elements of Fisher information matrix with respect to the center of array A. One needs to obtain the information with respect to the origin from where the position of the target is $(d,\theta)$ estimated. By using the transformation of

$$\frac{\partial}{\partial d}\ln\left(pdf_A\right)=\frac{\partial}{\partial d_A}\ln\left(pdf_A\right)\frac{\partial d_A}{\partial d}+\frac{\partial}{\partial \theta_A}\ln\left(pdf_A\right)\frac{\partial \theta_A}{\partial d}, \tag{6.81}$$

and

$$\frac{\partial}{\partial \theta}\ln\left(pdf_A\right)=\frac{\partial}{\partial d_A}\ln\left(pdf_A\right)\frac{\partial d_A}{\partial \theta}+\frac{\partial}{\partial \theta_A}\ln\left(pdf_A\right)\frac{\partial \theta_A}{\partial \theta}, \tag{6.82}$$

substituting (6.81) and (6.82) to (6.77), (6.78), (6.79) and (6.80) yields

$$I_{A11} = \frac{N}{\sigma^2}\left[\left(\frac{\partial d_A}{\partial d}\right)^2 + \frac{R^2}{2}\left(\frac{\partial \theta_A}{\partial d}\right)^2\right], \tag{6.83}$$

$$I_{A22} = \frac{N}{\sigma^2}\left[\left(\frac{\partial d_A}{\partial \theta}\right)^2 + \frac{R^2}{2}\left(\frac{\partial \theta_A}{\partial \theta}\right)^2\right], \tag{6.84}$$

and

$$\begin{aligned} I_{A12} &= I_{A21} \\ &= \frac{N}{\sigma^2}\left(\frac{\partial d_A}{\partial d}\frac{\partial d_A}{\partial \theta} + \frac{R^2}{2}\frac{\partial \theta_A}{\partial d}\frac{\partial \theta_A}{\partial \theta}\right). \end{aligned} \tag{6.85}$$

where during the manipulation of (6.83), (6.84) and (6.85), (6.73), (6.74) and (6.75) have been applied.

From the geometric relationship which is demonstrated in Appendix C, the polar coordinates transformation has been obtained as

$$\frac{\partial d_A}{\partial d} = \cos(\gamma) \qquad \text{(C.5)},$$

$$\frac{\partial d_A}{\partial \theta} = d\sin(\gamma) \qquad \text{(C.7)},$$

$$\frac{\partial \theta_A}{\partial d} = -\frac{\sin(\gamma)}{d_A} \qquad \text{(C.13)},$$

$$\frac{\partial \theta_A}{\partial \theta} = \frac{d}{d_A}\cos(\gamma) \qquad \text{(C.16)}.$$

Applying (C.5), (C.7), (C.13) and (C.16) to (6.83), (6.84) and (6.85), it leads the elements of Fisher information matrix to be

$$I_{A11} = \frac{N}{\sigma^2}\left[\frac{R^2}{2{d_A}^2}\sin^2(\gamma) + \cos^2(\gamma)\right], \tag{6.86}$$

$$I_{A22} = \frac{N}{\sigma^2}d^2\left[\sin^2(\gamma) + \frac{R^2}{2{d_A}^2}\cos^2(\gamma)\right], \tag{6.87}$$

and

$$\begin{aligned} I_{A12} &= I_{A21} \\ &= \frac{N}{\sigma^2} d \left(1 - \frac{R^2}{2{d_A}^2}\right) \sin(\gamma) \cos(\gamma). \end{aligned} \tag{6.88}$$

Equations (6.86), (6.87) and (6.88) give out the concise form of the elements of Fisher information matrix, but one of the variables is angle $\gamma$ which does not directly present the target position. We keep these equations for future use. To express the elements as the functions of target position, using trigonometry identities and sine rule that states

$$\frac{a}{\sin(\gamma)} = \frac{d_A}{\sin(\theta - \psi)}, \tag{6.89}$$

equations (6.86), (6.87) and (6.88) can be re-written as

$$I_{A11} = \frac{N}{\sigma^2} \left[1 - \frac{a^2}{{d_A}^2} \left(1 - \frac{R^2}{2{d_A}^2}\right) \sin^2(\theta - \psi)\right], \tag{6.90}$$

$$I_{A22} = \frac{N}{\sigma^2} d^2 \left[\frac{R^2}{2{d_A}^2} + \frac{a^2}{{d_A}^2} \left(1 - \frac{R^2}{2{d_A}^2}\right) \sin^2(\theta - \psi)\right], \tag{6.91}$$

and

$$\begin{aligned} I_{A12} &= I_{A21} \\ &= \frac{N}{\sigma^2} d \left(1 - \frac{R^2}{2{d_A}^2}\right) \frac{a}{d_A} \sin(\theta - \psi) \sqrt{1 - \frac{a^2}{{d_A}^2} \sin^2(\theta - \psi)}. \end{aligned} \tag{6.92}$$

When the array is placed at an arbitrary position, the elements of the Fisher information matrix are complicated as each of them is a function of the array position and the relative position of the target with reference to the array center, as well as the array parameters such as the number of the sensors and the radius of the array. In general, the matrix elements along the anti diagonal line, $I_{A12}$ and $I_{A21}$, are not zeros. This is due to the coordinates transfer which involves rotation, causing the estimates of $d$ and $\theta$ to become correlated. If $\theta = \psi$, or if $\theta = \pi + \psi$, while $a \neq 0$, $I_{A12} = I_{A21} = 0$, $\mathbf{I}_A$ is diagonal. This means that when the target, the array and the origin of the co-ordinates are along one line, there is no distance and bearing

correlation during the coordinate transfer. If $a = 0$, then $d_A = d$, thus leading to $\mathbf{I}_A = \mathbf{I}$, which is the situation when the array is placed at origin.

From the Fisher information matrix one can find the Cramér-Rao lower bound by inversing the matrix. The derivation of the determinant of the Fisher information matrix $\mathbf{I}_A$ is presented in Appendix D. The determinant is found to be

$$\det(\mathbf{I}_A) = \left(\frac{N}{\sigma^2}\right)^2 \frac{R^2 d^2}{2{d_A}^2}. \tag{6.93}$$

The inversion of Fisher information matrix $\mathbf{I}_A$ is denoted by the bold Greek letter $\mathbf{\Sigma}$ with subscript $A$

$$\mathbf{\Sigma}_A = (\mathbf{I}_A)^{-1}. \tag{6.94}$$

The elements of matrix $\mathbf{\Sigma}_A$ can be found by

$$\begin{bmatrix} \Sigma_{A11} & \Sigma_{A12} \\ \Sigma_{A21} & \Sigma_{A22} \end{bmatrix} = \frac{1}{\det(\mathbf{I}_A)} \begin{bmatrix} I_{A22} & -I_{A12} \\ -I_{A21} & I_{A11} \end{bmatrix}. \tag{6.95}$$

Applying (6.90), (6.91), (6.92) and (6.93) to (6.95), one finds

$$\Sigma_{A11} = \frac{\sigma^2}{N}\left[1 - \left(1 - \frac{2{d_A}^2}{R^2}\right)\frac{a^2}{{d_A}^2}\sin^2(\theta - \psi)\right], \tag{6.96}$$

$$\Sigma_{A22} = \frac{\sigma^2}{N}\frac{1}{d^2}\left[\frac{2{d_A}^2}{R^2} + \left(1 - \frac{2{d_A}^2}{R^2}\right)\frac{a^2}{{d_A}^2}\sin^2(\theta - \psi)\right], \tag{6.97}$$

and

$$\begin{aligned} \Sigma_{A12} &= \Sigma_{A21} \\ &= -\frac{1}{d}\left(1 - \frac{2{d_A}^2}{R^2}\right)\frac{a}{d_A}\sin(\theta - \psi)\sqrt{1 - \frac{a^2}{{d_A}^2}\sin^2(\theta - \psi)}. \end{aligned} \tag{6.98}$$

Equation (6.98) shows the covariances caused by coordinates transformation. When the target, the array and the origin are not in one line, the covariances, $\Sigma_{12}$ and $\Sigma_{21}$ are not zero due to the rotation operation. When $\theta = \psi$, or $\theta = \pi + \psi$ , there is no rotation involved in the coordinates transfer, so $\Sigma_{A12} = \Sigma_{A21} = 0$.

## 6.6 Variance and Standard Deviation for an Array at an Arbitrary Position

As shown in Fig. 6.5, we assume that the array is placed at $(a, \psi)$, and a target is estimated at $(d_A, \theta_A)$ with respect to the location of the array.

It is assumed that the estimation errors for both distance $d_A$ and bearing $\theta_A$ are small, so they can be expressed by differentials when transformed to system coordinates $d$ and $\theta$. In Appendix E, the error $\Delta d$ and $\Delta\theta$ are found to be

$$\Delta d = \cos(\gamma)\,\Delta d_A - d_A \sin(\gamma)\,\Delta\theta_A \qquad \text{(E.4)},$$

$$\Delta\theta = \frac{\sin(\gamma)}{d}\Delta d_A + \frac{d_A\cos(\gamma)}{d}\Delta\theta_A \qquad \text{(E.7)}.$$

Since $d_A$ and $\theta_A$ are independent variables,

$$E\left[(\Delta d_A)\,(\Delta\theta_A)\right] = 0. \tag{6.99}$$

Substituting (6.6) to (E.4) and (E.7), one obtains

$$E\left[(\Delta d)^2\right] = \cos^2(\gamma)\,E\left[(\Delta d_A)^2\right] + {d_A}^2\sin^2(\gamma)\,E\left[(\Delta\theta_A)^2\right], \tag{6.100}$$

and

$$E\left[(\Delta\theta)^2\right] = \frac{\sin^2(\gamma)}{d^2}E\left[(\Delta d_A)^2\right] + \frac{{d_A}^2\cos^2(\gamma)}{d^2}E\left[(\Delta\theta_A)^2\right]. \tag{6.101}$$

With reference to the array center, one has

$$E\left[(\Delta d_A)^2\right] = \frac{\sigma^2}{N}, \tag{6.102}$$

and

$$E\left[(\Delta\theta_A)^2\right] = \frac{2\sigma^2}{NR^2}. \tag{6.103}$$

Substituting (6.102) and (6.103) to (6.100) and (6.101), and denoting ${\sigma_{Ar}}^2$ as $E\left[(\Delta d)^2\right]$ , and ${\sigma_{Ab}}^2$ as $E\left[(\Delta\theta)^2\right]$ , one has

$${\sigma_{Ar}}^2 = \frac{\sigma^2}{N}\left[\cos^2(\gamma) + \frac{2{d_A}^2}{R^2}\sin^2(\gamma)\right], \tag{6.104}$$

and

$${\sigma_{Ab}}^2 = \frac{\sigma^2}{N}\frac{1}{d^2}\left[\sin^2(\gamma) + \frac{2{d_A}^2}{R^2}\cos^2(\gamma)\right]. \tag{6.105}$$

Applying trigonometry identities and sine rule expressed by (6.89), one gets

$${\sigma_{Ad}}^2 = \frac{\sigma^2}{N}\left[1 - \left(1 - \frac{2{d_A}^2}{R^2}\right)\frac{a^2}{{d_A}^2}\sin^2(\theta - \psi)\right], \tag{6.106}$$

and

$${\sigma_{Ab}}^2 = \frac{\sigma^2}{N}\frac{1}{d^2}\left[\frac{2{d_A}^2}{R^2} + \left(1 - \frac{2{d_A}^2}{R^2}\right)\frac{a^2}{{d_A}^2}\sin^2(\theta - \psi)\right]. \tag{6.107}$$

By comparing (6.106) with (6.96), and (6.107) with (6.97), one concludes that both variance of distance and variance of bearing reach their Cramér-Rao lower bound.

Positioning variance ${\sigma_{Ap}}^2$ can be found by performing

$${\sigma_{Ap}}^2 = {\sigma_{Ad}}^2 + d^2{\sigma_{Ab}}^2 = \frac{\sigma^2}{N}\left(1 + \frac{2{d_A}^2}{R^2}\right). \tag{6.108}$$

It is observed that (6.108) is effectively the same as (6.65). It should be noted, however, that when $d_A$ is fixed, the STD we observe from the origin of the coordinates will vary with the bearing. Simulations have been used to evaluate the performance of the distance and bearing estimator given by (6.108). Fig. 6.6 shows the standard deviation, the solid lines, and root-mean-square error (RMSE), the diamond shapes, for an array is placed at $150m$ and $30^\circ$ of bearing, the number of the sensor in the array is four, and the standard deviation of single sensor is $0.1m$. As shown in the legend, the arrays of different sizes have been used in three different sizes. The trend of RMSE results agree with those of standard deviation.

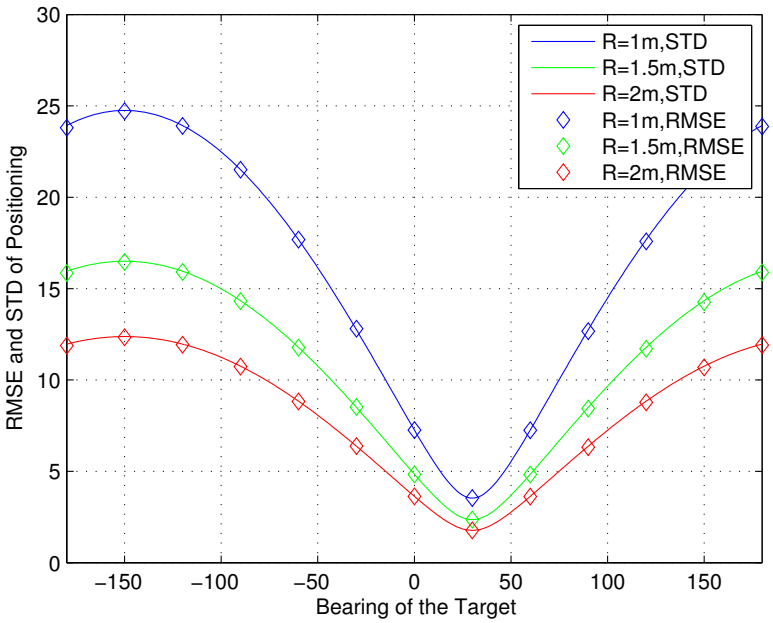


**Figure 6.6:** STD and RMSE when array A is placed at $150m$ and $30°$

As shown in (6.108), no matter where the array is placed, the variance of positioning is always proportional to the squared distance of the target to the array, as $\frac{2{d_A}^2}{R^2} \gg 1$ . This suggests that a single array only provides limited accuracy due to the error arc. To improve the positioning accuracy, a means that can be used to determine a position on the error arc ought to be employed.

## 6.7 Ranging Based Sensor Arrays for 3D Positioning

### 6.7.1 System Model for 3D

The concept of ranging based positioning arrays can be extended into three dimensions. For 3D positioning, the array should be able to make the measurements in

distance, elevation angle and azimuth angle. In the following, a cubic array is sued, which is equipped with twelve sensors and each of them is placed in the middle point of the cubic frame. To make it simple, we assume that each side of the cube is of length $2b$, as shown in Fig. 6.7.

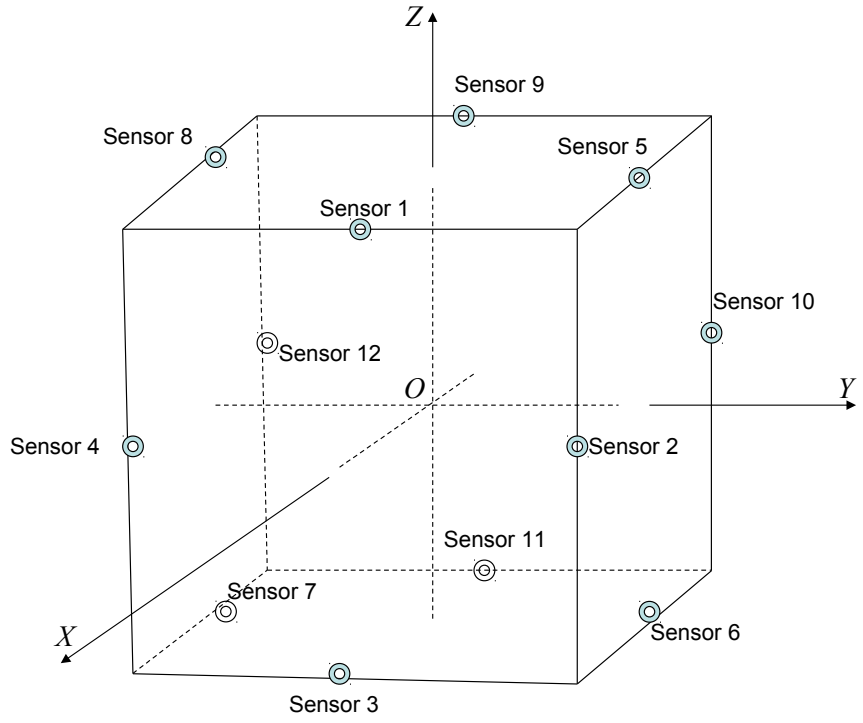


**Figure 6.7:** A cubic array with sensors on each side

We choose the center of the cubic frame as the origin of the coordinates. The coordinates of the sensors are listed in the Table 6.1:

Suppose that a target is at distance $d$ , elevation angle $\theta$, and azimuth angle $\varphi$. We assume the target is far from the array so when the signal reaches the array, the wave front is a plane. We choose the plane that parallels to the wave front and passes the origin as the reference plane. We choose the normal direction of the reference

**Table 6.1:** Coordinates of sensors in a cubic array

| Sensor | $S1$ | $S2$ | $S3$ | $S4$ | $S5$ | $S6$ | $S7$ | $S8$ | $S9$ | $S10$ | $S11$ | $S12$ |
|---|---|---|---|---|---|---|---|---|---|---|---|---|
| $X$-coordinate | b | b | b | b | 0 | 0 | 0 | 0 | -b | -b | -b | -b |
| $Y$-coordinate | 0 | b | 0 | -b | b | b | -b | -b | 0 | b | 0 | -b |
| $Z$-coordinate | b | 0 | -b | 0 | b | -b | -b | b | b | 0 | -b | 0 |

plane $\mathbf{n}$ opposite to the wave vector direction, thus $\theta$ is the elevation angle of $\mathbf{n}$ and $\varphi$ the azimuth angle of $\mathbf{n}$. Denote $t_i(\theta, \varphi)$ as the distance from sensor $i$, $i = 1, 2, \cdots, N$ to the reference plane, it is obvious that $t_i$, $i = 1, 2, \cdots, N$, are the functions of $\theta$ and $\varphi$, as shown in Fig. 6.8.

Denote $r_i$, $i = 1, 2, \cdots, N$, as the target range measured by sensor $i$. The target distance $d$, the ranges of the target measured by each sensor and the distances of each sensor to the reference plane, $t_i$, $i = 1, 2, \cdots, N$, have the relationship

$$\begin{aligned} d - t_i(\theta, \varphi) &= r_i, \\ i &= 1, 2, \cdots, 12. \end{aligned} \tag{6.109}$$

The equation for a plane that passes the origin is given by

$$x\cos\alpha + y\cos\beta + z\cos\gamma = 0, \tag{6.110}$$

where $\alpha$, $\beta$, and $\gamma$ are the direction angles of the normal direction of the plane, as shown in Fig. 6.9. The relationship between the direction angles and elevation angle, $\theta$, and azimuth angle, $\varphi$, is given by

$$\begin{cases} \cos\alpha = \cos\theta\cos\varphi, \\ \cos\beta = \cos\theta\sin\varphi, \\ \gamma = \dfrac{\pi}{2} - \theta. \end{cases} \tag{6.111}$$

Therefore, the equation of the reference plane can be re-written as

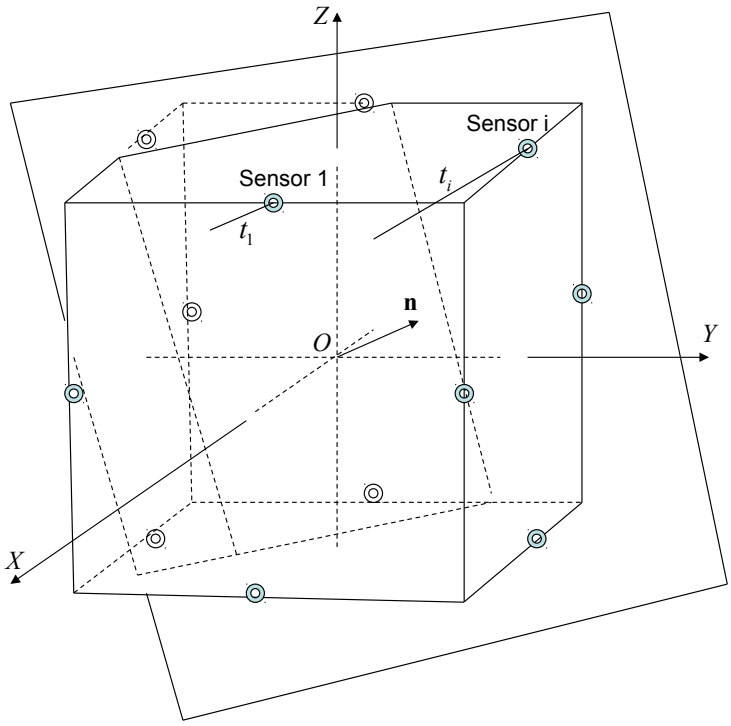


**Figure 6.8:** Range difference between the sensors

$$x\cos\theta\cos\varphi + y\cos\theta\sin\varphi + z\sin\theta = 0. \tag{6.112}$$

The distance from the $i^{th}$ sensor, whose coordinates are $(x_i, y_i, z_i)$, to the reference plane is

$$t_i = x_i\cos\theta\cos\varphi + y_i\cos\theta\sin\varphi + z_i\sin\theta. \tag{6.113}$$

Denote

$$\mathbf{B} = \begin{bmatrix} 1 & 1 & 1 & 1 & 1 & 1 & 1 & 1 & 1 & 1 & 1 & 1 \\ -b & -b & -b & -b & 0 & 0 & 0 & 0 & b & b & b & b \\ 0 & -b & 0 & b & -b & -b & b & b & 0 & -b & 0 & b \\ -b & 0 & b & 0 & -b & b & b & -b & -b & 0 & b & 0 \end{bmatrix}^T, \tag{6.114}$$

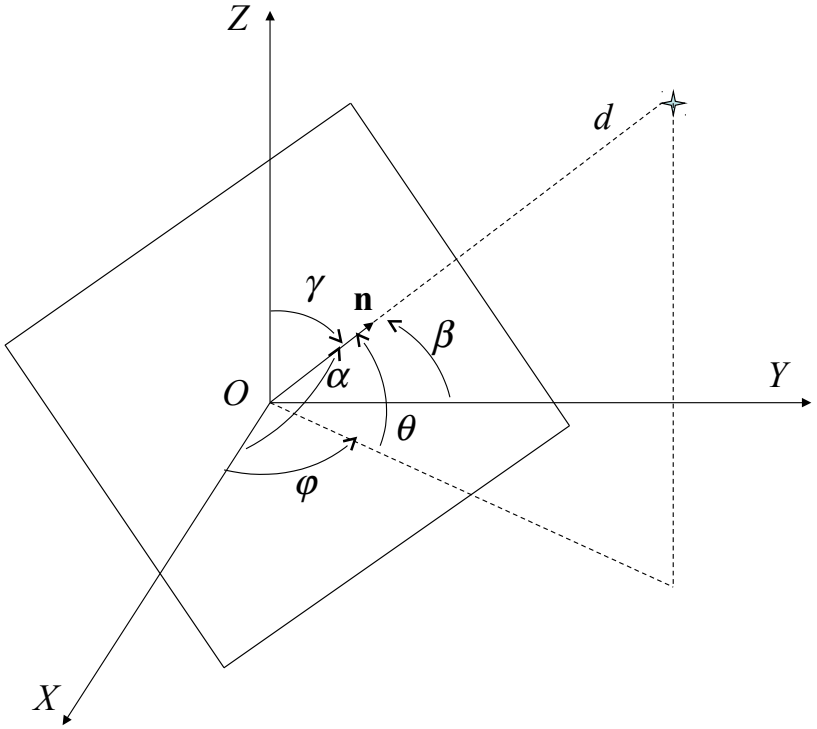


**Figure 6.9:** The reference plane and its parameters

and

$$\mathbf{r} = \left[ \begin{array}{cccc} r_1, & r_2, & \cdots, & r_{12} \end{array} \right]^T. \tag{6.115}$$

one obtains the matrix form of the linear equation

$$\mathbf{B} \left[ \begin{array}{c} d \\ \cos\theta\cos\varphi \\ \cos\theta\sin\varphi \\ \sin\theta \end{array} \right] = \mathbf{r}. \tag{6.116}$$

The least squares solution of (6.116) is given by

$$\begin{bmatrix} d \\ u \\ v \\ w \end{bmatrix} = \left(\mathbf{B}^T\mathbf{B}\right)^{-1}\mathbf{B}^T\mathbf{r}, \tag{6.117}$$

where

$$\begin{aligned} u &= \cos\theta\cos\varphi, \\ v &= \cos\theta\sin\varphi, \\ w &= \sin\theta. \end{aligned} \tag{6.118}$$

The elevation angle $\theta$ can be decided by

$$\theta = \tan^{-1}\frac{w}{\sqrt{u^2+v^2}}, \tag{6.119}$$

and the azimuth angle ban be decided by

$$\varphi = \tan^{-1}\frac{v}{u}. \tag{6.120}$$

### 6.7.2 Standard Deviation of the Cubic Array

Assume that the errors in range measurements made by the sensors, $r_i$ , $i = 1, 2, \cdots, 12$ , are small, so are the errors in the solutions of (6.117) , $d$, $u$ , $v$ , and $w$ . Furthermore, we assume that the errors in position parameters , $\theta$ , and $\varphi$ , are small so that the errors of position parameters can be expressed as the first order of partial differentials. Differentiating (6.119) , one obtains the error of elevation angle, $\Delta\theta$ , to the first order of partial differentials of its parameters $u$, $v$ and $w$. When $\theta \neq \frac{\pi}{2}$ , one has

$$\Delta\theta = \cos\theta\Delta w - \sin\theta\cos\varphi\Delta u - \sin\theta\sin\varphi\Delta v. \tag{6.121}$$

Differentiating (6.120) to obtain $\Delta\varphi$, and applying (6.118), Assuming $\varphi \neq \frac{\pi}{2}$ or $\varphi \neq \frac{3\pi}{2}$ , one can have the expression

$$\Delta\varphi = \frac{\cos\varphi\Delta v - \sin\varphi\Delta u}{\cos\theta}. \tag{6.122}$$

Next, we investigate the effect of measurements to $d$, $u$, $v$, and $w$. Employing (6.114), one gets

$$\mathbf{B}^T\mathbf{B} = \begin{bmatrix} 12 & 0 & 0 & 0 \\ 0 & 8b^2 & 0 & 0 \\ 0 & 0 & 8b^2 & 0 \\ 0 & 0 & 0 & 8b^2 \end{bmatrix}, \tag{6.123}$$

Substitute (6.114) to (6.117), one obtains

$$\begin{aligned} d &= \frac{1}{12}\sum_{i=1}^{12} r_i, \\ u &= \frac{1}{8b}\left(-\sum_{i=1}^{4} r_i + \sum_{i=9}^{12} r_i\right), \\ v &= \frac{1}{8b}\left(-r_2 + r_4 - r_5 - r_6 + r_7 + r_8 - r_{10} + r_{12}\right), \\ w &= \frac{1}{8b}\left(-r_1 + r_3 - r_5 + r_6 + r_7 - r_8 - r_9 + r_{11}\right). \end{aligned} \tag{6.124}$$

Take the first order of derivative of (6.124), one has the deviation of the target distance

$$\Delta d = \frac{1}{12}\sum_{i=1}^{12} \Delta r_i, \tag{6.125}$$

and the deviations of elements $u$, $v$ and $w$

$$\begin{aligned} \Delta u &= \frac{1}{8b}\left(-\sum_{i=1}^{4} \Delta r_i + \sum_{i=9}^{12} \Delta r_i\right), \\ \Delta v &= \frac{1}{8b}\left(-\Delta r_2 + \Delta r_4 - \Delta r_5 - \Delta r_6 + \Delta r_7 + \Delta r_8 - \Delta r_{10} + \Delta r_{12}\right), \\ \Delta w &= \frac{1}{8b}\left(-\Delta r_1 + \Delta r_3 - \Delta r_5 + \Delta r_6 + \Delta r_7 - \Delta r_8 - \Delta r_9 + \Delta r_{11}\right). \end{aligned} \tag{6.126}$$

Since $u$ , $v$ , and $w$ are independent elements in (6.117),

$$E\left[(\Delta u)(\Delta w)\right] = E\left[(\Delta v)(\Delta w)\right] = E\left[(\Delta u)(\Delta v)\right] = 0, \tag{6.127}$$

resulting

$$E\left[(\Delta u)^2\right] = E\left[(\Delta v)^2\right] = E\left[(\Delta w)^2\right] = \frac{\sigma^2}{8b^2}. \tag{6.128}$$

Denote ${\sigma_\theta}^2$ as the variance of elevation angle estimate, and ${\sigma_\varphi}^2$ the variance of azimuth angle estimate. Substituting (6.128) to (6.121) and (6.122), one gets

$${\sigma_\theta}^2 = \frac{\sigma^2}{8b^2} \ . \tag{6.129}$$

and

$${\sigma_\varphi}^2 = \frac{1}{\cos^2\theta}\frac{\sigma^2}{8b^2}. \tag{6.130}$$

In the spherical coordinates, a positioning error $\Delta p$ is expressed as

$$\Delta p = \sqrt{(\Delta d)^2 + d^2(\Delta\theta)^2 + d^2\cos^2\theta(\Delta\varphi)^2}, \tag{6.131}$$

Finally, denote ${\sigma_p}^2$ as the 3D positioning variance $E\left[(\Delta p)^2\right]$, one gets

$${\sigma_p}^2 = \frac{\sigma^2}{12}\left(1 + d^2\frac{3}{b^2}\right). \tag{6.132}$$

Since one can write

$$\frac{\sigma^2}{12}\left(1 + d^2\frac{3}{b^2}\right) = \frac{\sigma^2}{12}\left[1 + d^2\frac{2}{8b^2 + 4\left(\sqrt{2}b\right)^2}\right]. \tag{6.133}$$

Equation (6.133) indicates that the same positioning variance can be produced by a spherical array with 12 sensors, of which 8 sensors are fixed at radius of $b$ and 4 of them are fixed at radius of $\sqrt{2}b$.

### 6.7.3 Calculation of STD and Simulation of RMSE

From (6.132) one can see that the standard deviation of the positioning is a function of target distance once the array size is chosen. The calculation of standard

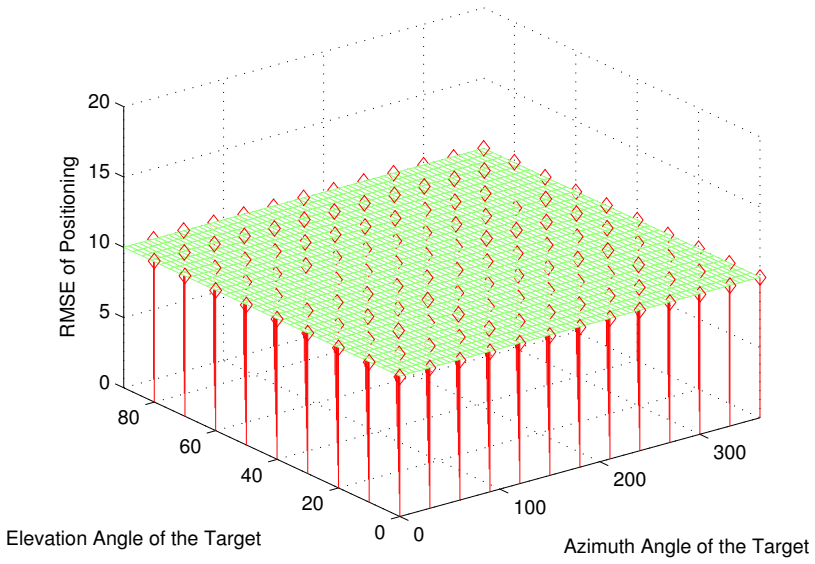


**Figure 6.10:** Comparison of RMSE from measurement with STD from analysis

deviation when the target distance is $200m$ and the side of the array is $2m$ is shown as the green surface in Fig. 6.10. The simulation result of positioning RMSE is shown as the red diamond shape in Fig. 6.10. The simulation is conducted for a target whose distance is $200m$, and moves with its angle of elevation changing $0°$ to $90°$, and its angle of azimuth changing from $0°$ to $360°$. The iteration is 1000. The simulation results validate the theoretical ones.

## 6.8 Conclusion

A novel localisation method employing ranging based arrays is proposed. It consists of a number of sensors each being able to conduct ranging measurements individually. It can be constructed by using commercial off the shelf wireless ranging devices at a low cost. Owing to its modular structure, it is easy to maintain as individual sensors can be simply replaced. It is proved that the proposed location estimator

can reach its Cramér-Rao lower bound. The proposed array is suited for applications such as fleet management, sport training, security and military operations.

# Chapter 7

# Co-operative Ranging Based Sensor Arrays

## 7.1 Introduction

In the previous chapter, it is shown that an array equipped with ranging based sensors is able to locate a target by estimating the range and bearing of the target, hence providing the information of the target location. Unfortunately, all bearing or DoA based methods suffer from a main limitation: the positioning error caused by the DoA estimation error increases with the increasing distance from the array used for DoA estimation. To solve the problem, this chapter introduces the use of co-operation between adjacent sensor arrays [126]. It is demonstrated that the ranging measurement between the target node and the second sensor array makes it possible to increase the overall positioning accuracy.

This chapter is organised as follows. Following the introduction in Section 7.2, the Cramér-Rao lower bound and standard deviation for the co-operative arrays, which are placed at the origin and an arbitrary position, respectively, are derived in

Section 7.2. Section 7.3 introduces the use of co-operation between sensor arrays, and describes the theoretical foundation for Cramér-Rao lower bound (CRLB) and the standard deviation. Section 7.4 analysis the method to approach CRLB. Section 7.5 studies the 3D co-operative array positioning. In Subsection 7.5.1, 3D ranging based sensor array is introduced; Subsection 7.5.2 the STD for 3D positioning is derived; and in Subsection 7.5.3, simulations results to verify the theory. Finally, conclusions are given in Section 7.6.

## 7.2 Cramér-Rao Lower Bound for Co-operative Arrays

Suppose that two arrays are employed to estimate the position of a target. One array is placed at the center of the coordinates, called array C, and the other is placed at an arbitrary position $(a, \psi)$, called array A.

Suppose the two arrays have the same radius $R$, and each of them has the same number of sensor $N$. The measurements by each sensor are corrupted by Gaussian noise, and the measurements are made by the respective sensors independently. All the data are transferred to a fusion center to process.

By the law of likelihood, the Fisher information of the system is the sum of the individuals' [124],

$$\mathbf{I}_{CA} = \mathbf{I}_C + \mathbf{I}_A. \tag{7.1}$$

We use $\mathbf{\Sigma}_{CA}$ denoting the inversion matrix of $\mathbf{I}_{CA}$. The elements of $\mathbf{\Sigma}_{CA}$ can be obtained by performing

$$\begin{bmatrix} \Sigma_{CA11} & \Sigma_{CA12} \\ \Sigma_{CA21} & \Sigma_{CA22} \end{bmatrix} = \frac{1}{\det(\mathbf{I}_{CA})} \begin{bmatrix} I_{CA22} & -I_{CA12} \\ -I_{CA21} & I_{CA11} \end{bmatrix}. \tag{7.2}$$

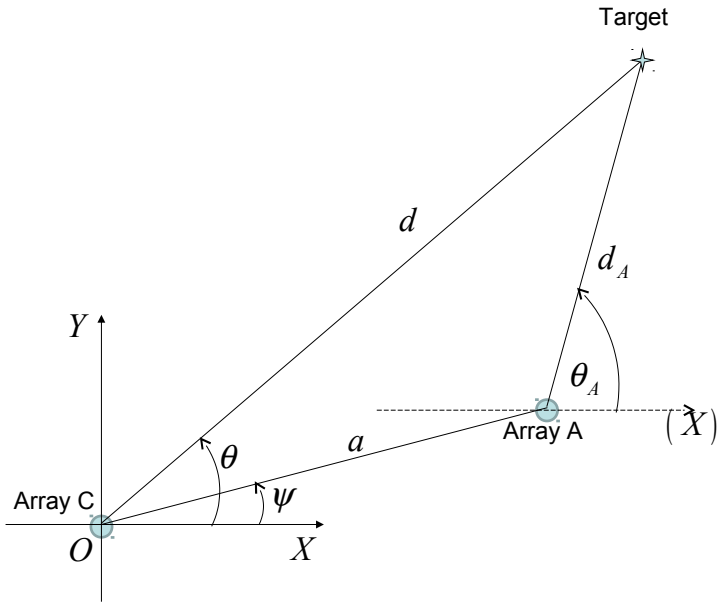


**Figure 7.1:** Two arrays

where the determinant of (7.1) is (see Appendix F for the derivation).

$$\begin{aligned} & \det\left(\mathbf{I}_{CA}\right) \\ = \; & \frac{N^2}{\sigma^4}\left[R^2\left(1+\frac{d^2}{{d_A}^2}\right)+\left(d^2-\frac{R^2}{2}\right)\left(1-\frac{R^2}{2{d_A}^2}\right)\frac{a^2}{{d_A}^2}\sin^2\left(\theta-\psi\right)\right] \end{aligned} \tag{F.9}.$$

They are found to be

$$\begin{aligned} & \Sigma_{CA11} \\ = \; & \frac{\sigma^2}{N}\frac{\frac{R^2}{2}\left(1+\frac{d^2}{{d_A}^2}\right)+d^2\left(1-\frac{R^2}{2{d_A}^2}\right)\frac{a^2}{{d_A}^2}\sin^2\left(\theta-\psi\right)}{R^2\left(1+\frac{d^2}{{d_A}^2}\right)+\left(d^2-\frac{R^2}{2}\right)\left(1-\frac{R^2}{2{d_A}^2}\right)\frac{a^2}{{d_A}^2}\sin^2\left(\theta-\psi\right)}, \end{aligned} \tag{7.3}$$

$$\begin{aligned}
&\Sigma_{CA22} \\
&= \frac{\sigma^2}{N}\frac{2-\left(1-\dfrac{R^2}{2{d_A}^2}\right)\dfrac{a^2}{{d_A}^2}\sin^2(\theta-\psi)}{R^2\left(1+\dfrac{d^2}{{d_A}^2}\right)+\left(d^2-\dfrac{R^2}{2}\right)\left(1-\dfrac{R^2}{2{d_A}^2}\right)\dfrac{a^2}{{d_A}^2}\sin^2(\theta-\psi)},
\end{aligned} \tag{7.4}$$

and

$$\begin{aligned}
\Sigma_{CA12} &= \Sigma_{CA21} \\
&= -\frac{\sigma^2}{N}\frac{d\left(1-\dfrac{R^2}{2{d_A}^2}\right)\dfrac{a}{d_A}\sin(\theta-\psi)\sqrt{1-\dfrac{a^2}{{d_A}^2}\sin^2(\theta-\psi)}}{R^2\left(1+\dfrac{d^2}{{d_A}^2}\right)+\left(d^2-\dfrac{R^2}{2}\right)\left(1-\dfrac{R^2}{2{d_A}^2}\right)\dfrac{a^2}{{d_A}^2}\sin^2(\theta-\psi)}.
\end{aligned} \tag{7.5}$$

Since $R \ll d$ and $R \ll d_A$, one has

$$1-\frac{R^2}{2{d_A}^2} \approx 1, \tag{7.6}$$

$$d^2-\frac{R^2}{2} \approx d^2, \tag{7.7}$$

which leads to

$$\Sigma_{CA11} \approx \frac{\sigma^2}{N}\frac{\dfrac{R^2}{2}\left(1+\dfrac{d^2}{{d_A}^2}\right)+\dfrac{d^2a^2}{{d_A}^2}\sin^2(\theta-\psi)}{R^2\left(1+\dfrac{d^2}{{d_A}^2}\right)+\dfrac{d^2a^2}{{d_A}^2}\sin^2(\theta-\psi)}, \tag{7.8}$$

and

$$\Sigma_{CA22} \approx \frac{\sigma^2}{N}\frac{2-\dfrac{a^2}{{d_A}^2}\sin^2(\theta-\psi)}{R^2\left(1+\dfrac{d^2}{{d_A}^2}\right)+d^2\dfrac{a^2\sin^2(\theta-\psi)}{{d_A}^2}}. \tag{7.9}$$

Since $d$, $d_A$ and $a$ are expected to be of the same magnitude and they are two order of magnitude greater than $R$, when $\sin^2(\theta-\psi)$ is not too small, one has

$$R^2\left(1+\frac{d^2}{{d_A}^2}\right) \ll \frac{d^2a^2}{{d_A}^2}\sin^2(\theta-\psi), \tag{7.10}$$

which leads to

$$\Sigma_{CA11} \approx \frac{\sigma^2}{N}, \tag{7.11}$$

and

$$\Sigma_{CA22} \approx \frac{\sigma^2}{N} \frac{2{d_A}^2 - a^2 \sin^2(\theta - \psi)}{d^2 a^2 \sin^2(\theta - \psi)}. \tag{7.12}$$

## 7.3 Standard Deviation by Fusion of Two Arrays

If the two arrays are used independently to conduct the range and bearing estimates, the standard deviation of a two array system can be simply obtained by averaging the two variances. Array C is the one placed at the origin, and its variance of positioning, ${\sigma_{Cp}}^2$ , which is given in Section 6.4, is $\frac{\sigma^2}{N}\left(1 + \frac{2d^2}{R^2}\right)$. The variance of array A is given by (6.108) in Section 6.6. The fusion [119] of the two arrays produces the following average variances

$$(\sigma_{CAp})^2 = \frac{1}{2}\left({\sigma_{Cp}}^2 + {\sigma_{Ap}}^2\right), \tag{7.13}$$

and therefore the standard deviation by fusion is found to be

$$\sigma_{CAp} = \frac{\sigma}{\sqrt{N}} \sqrt{1 + \frac{d^2}{R^2} + \frac{{d_A}^2}{R^2}}. \tag{7.14}$$

Fig. 7.2 shows the comparison between the Cramér-Rao lower bounds (CRLB) of a two array system, and the standard deviation achieved by using two arrays independently as well as simulated root-mean-square error when the two arrays are employed independently. It shows that using the two arrays independently lead to errors well above the CRLB

## 7.4 Co-operation between Sensor Arrays

In the previous section, it was shown that using two independent arrays is not an effective approach to improving the positioning accuracy of ranging based positioning arrays. To make full use of the two arrays, the two arrays must co-operate in the

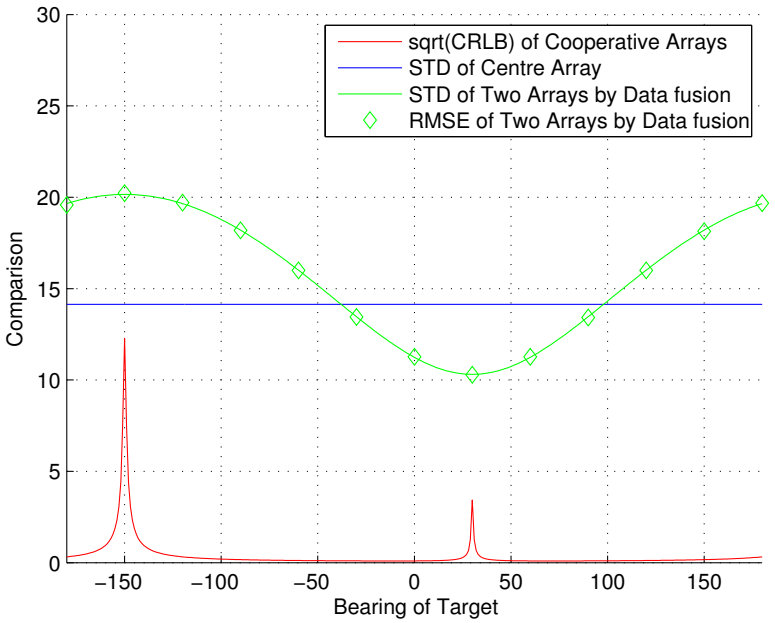


**Figure 7.2:** Comparison with data fusion

positioning process. Since a sensor array is a supernode which can afford certain degree of sophistication, we assume that they are equipped with additional sensors to obtain its position with high accuracy. The positions of the two arrays and the target are linked by the cosine rule

$$d_A{}^2 = d^2 + a^2 - 2da\cos(\theta - \psi). \tag{7.15}$$

The differential of (7.15) is given by

$$d_A \Delta d_A = d\Delta d - a\cos(\theta - \psi)\Delta d + da\sin(\theta - \psi)\Delta\theta, \tag{7.16}$$

which leads

$$\Delta\theta = \frac{[a\cos(\theta - \psi) - d]\Delta d + d_A \Delta d_A}{ra\sin(\theta - \psi)}. \tag{7.17}$$

Since the measurements made by two separate arrays are uncorrelated, one has

$$E\left[(\Delta d)^2\right] = E\left[(\Delta d_A)^2\right] = \frac{\sigma^2}{N}, \tag{7.18}$$

and

$$E\left[(\Delta d)\left(\Delta d_A\right)\right] = 0. \tag{7.19}$$

The variance of bearing determined by these two arrays is found to be

$$\begin{aligned} {\sigma_\theta}^2 &= E\left[(\Delta\theta)^2\right] \\ &= \frac{\sigma^2}{N}\frac{\left[d - a\cos\left(\theta-\psi\right)\right]^2 + {d_A}^2}{d^2a^2\sin^2\left(\theta-\psi\right)}. \end{aligned} \tag{7.20}$$

The sides of the triangle satisfy (see Fig. C.1)

$$\left[a\cos\left(\theta-\psi\right) - d\right]^2 = {d_A}^2 - a^2\sin^2\left(\theta-\psi\right). \tag{7.21}$$

Substituting (7.21) to (7.20) yields

$${\sigma_\theta}^2 = \frac{\sigma^2}{N}\frac{2{d_A}^2 - a^2\sin^2\left(\theta-\psi\right)}{d^2a^2\sin^2\left(\theta-\psi\right)}. \tag{7.22}$$

Compare (7.22) with (7.12), it can be observed that now ${\sigma_\theta}^2$ reaches the Cramér-Rao lower bound. By virtue of co-operation between the two arrays, the variance of positioning, ${\sigma_p}^2 = {\sigma_d}^2 + d^2{\sigma_\theta}^2$, becomes

$${\sigma_p}^2 = \frac{\sigma^2}{N}\frac{2{d_A}^2}{a^2\sin^2\left(\theta-\psi\right)}. \tag{7.23}$$

Therefore, the standard deviation of the positioning is obtained as

$$\sigma_p = \sigma\sqrt{\frac{2}{N}}\frac{d_A}{a\left|\sin\left(\theta-\psi\right)\right|}. \tag{7.24}$$

Comparing (7.24) with that of a single array standard deviation ${\sigma_{Cp}}^2 = \frac{\sigma^2}{N}\left(1 + \frac{2d^2}{R^2}\right)$, it is observed that, for a single array, the positioning error is proportional to the ratio of the target distance over the array radius, whereas that for two co-operative arrays, it is proportional to the ratio of the distance of the target from the second array and the distance between the two arrays. Since the two arrays can be placed far away from each other, the positioning accuracy for two co-operative arrays is much greater.

To further support the conclusion, simulation results are shown in Fig. 7.3. It should be noted that in (7.24), $\sigma_p$ becomes very large when the bearing of the target node approaches that of the second sensor array $\psi$, or $\psi + \pi$. In this circumstance, the accuracy of the proposed scheme degrades significantly. This is a typical problem of geometric dilution of precision (GDoP) [127], [106], [128]. It can be resolved if one can use a different pair of arrays for co-operation.

Fig. 7.3 shows the RMSE (diamond shapes) of simulation when two arrays co-operatively work together, with the comparison of square root of CRLB (red solid line) and theoretical analysis of STD (blue dashed line). In this example, the second array is known to the primary array at $150m$ and 30°. The target is at $200m$, and moves from $-180°$ to 180°. The simulation result validates the derived STD. Furthermore, it proves that the standard deviation of positioning by the co-operation of two arrays reaches the Cramém-Rao lower bound.

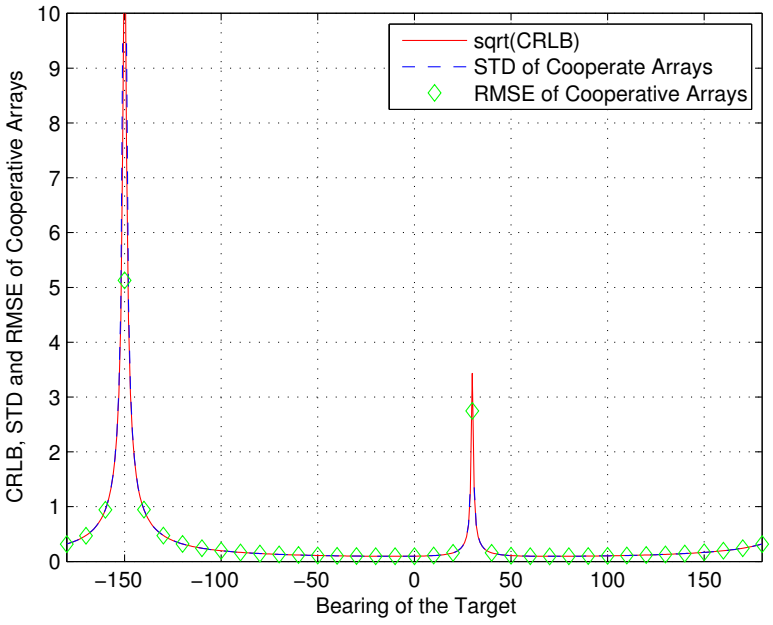


**Figure 7.3:** Co-operative of two arrays

The simulation result verifies the theoretical analysis of CRLB and STD. It is seen that using two co-operative arrays to determine a position on the uncertainty arc provides highly improved positioning accuracy. The contribution of each array is to provide an arc of positioning uncertainty. The higher the sensor number is, the shorter the arc appears.

It is interesting to compare the above scheme to that of using two single sensors for positioning. In the latter case, each sensor contributes a circle, the radius of which is the measured distance between the target and the sensor. The intersection of the two circles typically produces two possible target locations.

## 7.5 Co-operative Positioning in 3D

### 7.5.1 Co-operative Positioning in 3D

In this section, we extend the concept of co-operative arrays for wireless positioning to three-dimensional cases. Assume each array is composed of 12 sensors that are located in the middle of the 12 sides a cubical frame, so that one can make the following measurements: range $d$ , elevation angle $\theta$ , and azimuth angle $\varphi$ .

To improve the positioning accuracy, two additional arrays are introduced to co-operate with the array located at the origin of the coordinate. Suppose that array A is known to the main array with $a_A$ as the range, $\psi_A$ as the elevation angle, and $\zeta_A$ as the azimuth angle, shown as Fig. 7.4.

Denote $l$ as the projection of $d_A$ on $XOY$ plane. Consider that $d\cos(\theta)$ represents the projection of $d$ onto $XOY$ plane , and $a_A\cos(\psi_A)$ the projection of $a_A$ onto $XOY$ plane, the cosine rule states

$$l^2 = (d\cos\theta)^2 + (a_A\cos\psi_A)^2 - 2da_A\cos\theta\cos\psi_A\cos(\varphi-\zeta_A)\,. \qquad (7.25)$$

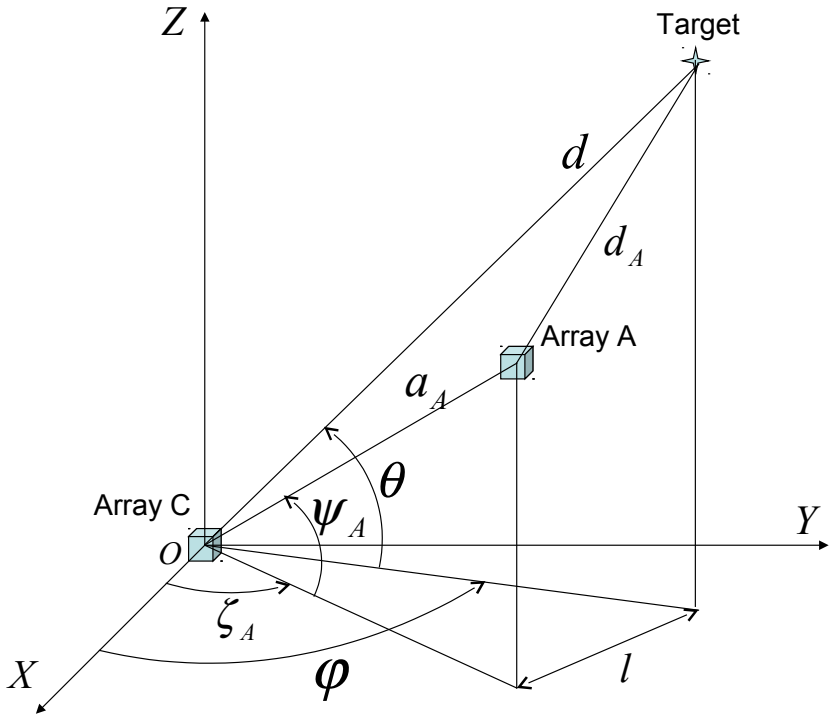


**Figure 7.4:** Coordinates of array A and a target in 3D

The height difference between the target and array A is $(d\sin\theta - a_A\sin\psi_A)$. Applying the heights difference to Pythagoras' Theorem results in

$$\sin\theta\sin\psi_A + \cos\theta\cos\psi_A\cos(\varphi - \zeta_A) = \frac{d^2 + {a_A}^2 - {d_A}^2}{2da_A}. \tag{7.26}$$

We introduce the third array, array B. Array B is known to the main array by $a_B$, $\psi_B$, $\zeta_B$ , and $\zeta_B > \zeta_A$. Assume that the distance between array B and the target is $d_B$, shown as Fig. 7.5, one has

$$\sin\theta\sin\psi_B + \cos\theta\cos\psi_B\cos(\varphi - \zeta_B) = \frac{d^2 + {a_B}^2 - {d_B}^2}{2da_B}. \tag{7.27}$$

$\theta$ and $\varphi$ can be found by solving non-linear equations (7.26) and (7.27).

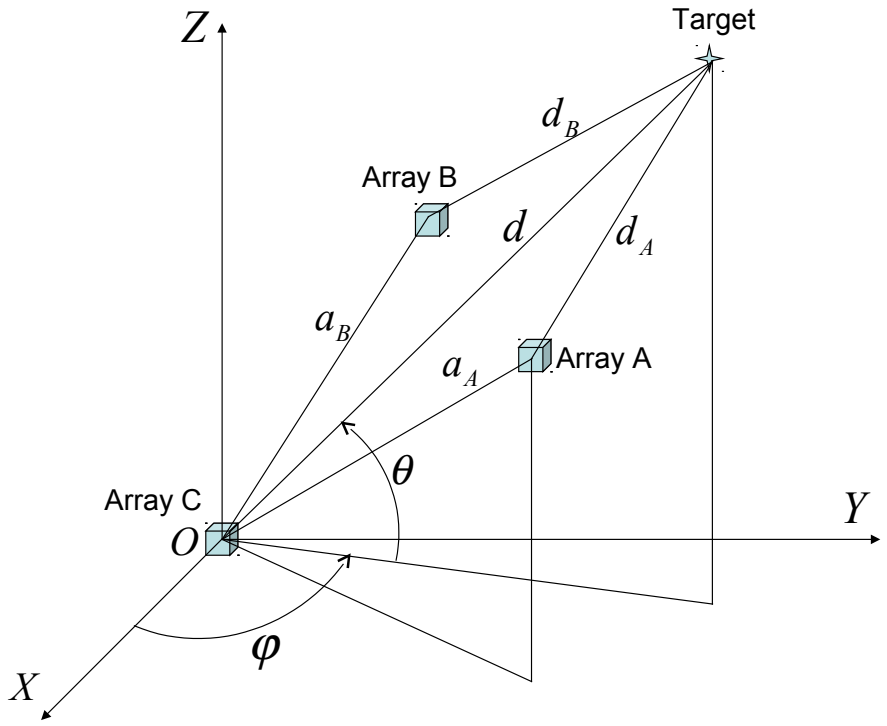


**Figure 7.5:** The coordinates of three co-operative arrays and a target in 3D.

### 7.5.2 Statistical Analysis of 3D Co-operative Arrays

Denote $\Delta d_A$ and $\Delta d_B$ as the measurement error of $d_A$ and $d_B$ respectively, and assuming they are small with corresponding to $\Delta r_i$, $i = 1, \cdots, N$.

Differentiating (7.26), and denoting

$$\Theta_A = \cos\theta \sin\psi_A - \sin\theta \cos\psi_A \cos(\varphi - \zeta_A), \tag{7.28}$$

$$\Phi_A = \cos\theta \cos\psi_A \sin(\varphi - \zeta_A), \tag{7.29}$$

and

$$\rho_A = \frac{d^2 - {a_A}^2 + d_A^2}{2da_A}, \tag{7.30}$$

lead to

$$\Theta_A \Delta\theta - \Phi_A \Delta\varphi = \frac{\rho_A}{d}\Delta d - \frac{d_A}{da_A}\Delta d_A. \tag{7.31}$$

Differentiating (7.27) and denoting

$$\Theta_B = \cos\theta \sin\psi_B - \sin\theta \cos\psi_B \cos\left(\varphi - \zeta_B\right), \tag{7.32}$$

$$\Phi_B = \cos\theta \cos\psi_B \sin\left(\varphi - \zeta_B\right), \tag{7.33}$$

and

$$\rho_B = \frac{d^2 - {a_B}^2 + d_B^2}{2da_B}, \tag{7.34}$$

lead to

$$\Theta_B \Delta\theta - \Phi_B \Delta\varphi = \frac{\rho_B}{d}\Delta d - \frac{d_B}{da_B}\Delta d_B. \tag{7.35}$$

Solving equations (7.31) and (7.35) for $\Delta\theta$ and $\Delta\varphi$ yields

$$\Delta\theta = \frac{\left(\Phi_B\rho_A - \Phi_A\rho_B\right)\Delta d + \Phi_A\frac{d_B}{a_B}\Delta d_B - \Phi_B\frac{d_A}{a_A}\Delta d_A}{d\left(\Theta_A\Phi_B - \Theta_B\Phi_A\right)}, \tag{7.36}$$

and

$$\Delta\varphi = \frac{\left(\Theta_B\rho_A - \Theta_A\rho_B\right)\Delta d - \Theta_B\frac{d_A}{a_A}\Delta d_A + \Theta_A\frac{d_B}{a_B}\Delta d_B}{d\left(\Theta_A\Phi_B - \Theta_B\Phi_A\right)}. \tag{7.37}$$

Noting that the arrays are independent of each other and are identical

$$E\left[\left(\Delta d\right)\left(\Delta d_A\right)\right] = E\left[\left(\Delta d\right)\left(\Delta d_B\right)\right] = E\left[\left(\Delta d_A\right)\left(\Delta d_B\right)\right] = 0, \tag{7.38}$$

and

$$E\left[\left(\Delta d\right)^2\right] = E\left[\left(\Delta d_A\right)^2\right] = E\left[\left(\Delta d_B\right)^2\right] = \frac{\sigma^2}{N}. \tag{7.39}$$

Thus

$${\sigma_\theta}^2 = \frac{\left(\Phi_B\rho_A - \Phi_A\rho_B\right)^2 + \left(\Phi_A\frac{d_B}{a_B}\right)^2 + \left(\Phi_B\frac{d_A}{a_A}\right)^2}{d^2\left(\Theta_A\Phi_B - \Theta_B\Phi_A\right)^2}\frac{\sigma^2}{N}, \tag{7.40}$$

and

$${\sigma_\varphi}^2 = \frac{\left(\Theta_B\rho_A - \Theta_A\rho_B\right)^2 + \left(\Theta_B\frac{d_A}{a_A}\right)^2 + \left(\Theta_A\frac{d_B}{a_B}\right)^2}{d^2\left(\Theta_A\Phi_B - \Theta_B\Phi_A\right)^2}\frac{\sigma^2}{N}. \tag{7.41}$$

### 7.5.3 Arrays on the Same Plane

When all the arrays are in the same plane, $\psi_A = 0$ , and $\psi_B = 0$ , (7.26) and (7.27) are simplified as

$$\cos\theta\cos\left(\varphi - \zeta_A\right) = \frac{d^2 + {a_A}^2 - {d_A}^2}{2da_A}, \tag{7.42}$$

and

$$\cos\theta\cos\left(\varphi - \zeta_B\right) = \frac{d^2 + {a_B}^2 - {d_B}^2}{2da_B}. \tag{7.43}$$

When $\cos\theta \neq 0$ , which are valid for all the positions except the point that is on the top of the central array, one obtains the closed for solution for elevation angle $\theta$ and azimuth angle $\varphi$ as

$$\theta = \cos^{-1}\frac{d^2 + {a_A}^2 - {d_A}^2}{2da_A\cos\left(\varphi - \zeta_A\right)}, \tag{7.44}$$

and

$$\varphi = \tan^{-1}\frac{p\cos\zeta_B - \cos\zeta_A}{\sin\zeta_A - p\sin\zeta_B}, \tag{7.45}$$

where

$$p = \frac{a_B}{a_A}\frac{d^2 + {a_A}^2 - {d_A}^2}{d^2 + {a_B}^2 - {d_B}^2}. \tag{7.46}$$

The variance of the elevation angle expressed as

$${\sigma_\theta}^2 = \frac{\eta^2 + \sin^2\left(\varphi - \zeta_A\right)\left(\frac{d_B}{a_B}\right)^2 + \sin^2\left(\varphi - \zeta_B\right)\left(\frac{d_A}{a_A}\right)^2}{d^2\sin^2\theta\sin^2\left(\zeta_A - \zeta_B\right)}\frac{\sigma^2}{N}, \tag{7.47}$$

and the variance of the azimuth angle expressed as

$${\sigma_\varphi}^2 = \frac{\kappa^2 + \cos^2\left(\varphi - \zeta_B\right)\left(\frac{d_A}{a_A}\right)^2 + \cos^2\left(\varphi - \zeta_A\right)\left(\frac{d_B}{a_B}\right)^2}{d^2\cos^2\theta\sin^2\left(\zeta_A - \zeta_B\right)}\frac{\sigma^2}{N}, \tag{7.48}$$

where

$$\eta = \sin\left(\varphi - \zeta_B\right)\rho_A - \sin\left(\varphi - \zeta_A\right)\rho_B, \tag{7.49}$$

and

$$\kappa = \cos(\varphi - \zeta_A)\,\rho_B - \cos(\varphi - \zeta_B)\,\rho_A. \tag{7.50}$$

The positioning variance can be expressed as

$$\sigma_p{}^2 = \sigma_d{}^2 + d^2\sigma_\theta{}^2 + d^2\cos^2(\theta)\,\sigma_\varphi{}^2, \tag{7.51}$$

which leads to

$$\begin{aligned} & \sigma_p{}^2 \\ = \; & \frac{\sigma^2}{N} + \frac{\sigma^2}{N}\frac{\eta^2 + \kappa^2\sin^2\theta}{\sin^2\theta\sin^2(\zeta_A - \zeta_B)} \\ & + \frac{\sigma^2}{N}\frac{\sin^2(\varphi - \zeta_B) + \sin^2\theta\cos^2(\varphi - \zeta_B)}{\sin^2\theta\sin^2(\zeta_A - \zeta_B)}\left(\frac{d_A}{a_A}\right)^2 \\ & + \frac{\sigma^2}{N}\frac{\sin^2(\varphi - \zeta_A) + \sin^2\theta\cos^2(\varphi - \zeta_A)}{\sin^2\theta\sin^2(\zeta_A - \zeta_B)}\left(\frac{d_B}{a_B}\right)^2. \end{aligned} \tag{7.52}$$

Simulation for 3D positioning is performed in the condition that the three cubic arrays being in the same plane, array A is at $100m$ with azimuth angle, $\varphi_A$ of 30°, and array B is at $150m$ and the azimuth angle, $\varphi_B$ of 120°. The true target range is $200m$, and the elevation angle of the target, $\theta$, changes from 0° to 90°, the azimuth angle of the target, $\varphi$, changes from 0° to 360°. The standard deviation (STD) of positioning as a function of elevation angle and azimuth angle, express by (7.52), is illustrated in Fig. 7.6 as the surface. It appears that when the target is close to the plane where the arrays are placed, i.e., the elevation angle is close to 0°, the STD of positioning increases shapely. There is a dip when the azimuth angle of the target is at 30°, where the target is at the closest position to array A in the simulation, and a valley when the azimuth angle of the target is at 120°, where the target is at the closest position to array B. There are two peaks where the azimuth angle of the target is either 210° or 300°, which are the the angles of either $\varphi_A + 180°$, where the target is at furthest point from array A, or $\varphi_B + 180°$, where the target is at the furthest point

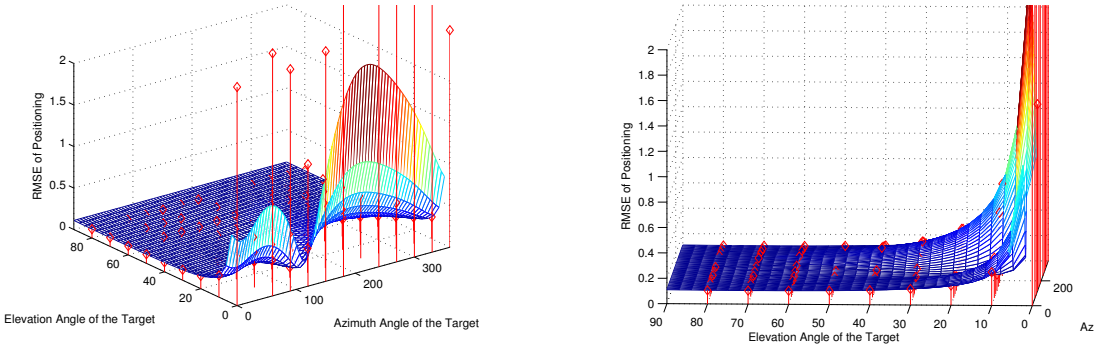


(a) RMSE and STD of co-operative arrays in 3D. The red diamonds represent the RMSE, and the surface represents the STD.

(b) RMSE (red diamond) and STD (the surface) of co-operative arrays in 3D side view

**Figure 7.6:** RMSE and STD of co-operative arrays in 3D.

from array B. The simulation result of root-mean-square error (RMSE) are shown in Fig. 7.6 as the red diamonds when the error distribution is chosen as the Gaussian distribution. The simulation result agrees with the STD expressed by (7.52) very well except when the elevation angle is close to 0°.

## 7.6 Conclusion

In this chapter, we have proposed a co-operative positioning method employing sensor arrays. It involves two arrays and three arrays for 2D and 3D scenarios, respectively. The Cramér-Rao lower bounds (CRLB) of the positioning accuracy when employing co-operative arrays have been derived for both cases. Simulation results demonstrate that the co-operative positioning method achieves the CRLB. Compared with using single array and non-co-operative arrays, the positioning accuracy is significantly improved.

# Chapter 8

# Conclusions and Future Work

In the past decade, the Global Positioning System (GPS) has played a pivotal role in various location based services (LBS) including place-finding, fleet management, emergency rescue and defense, thus contributing to the growth of a multi billion dollar industry. It is generally believed that the next decade will witness the penetration of location based services into GPS-denial environments such as dense urban centers, in-buildings and warehouse and supermarket logistics management. The defense industry has also been contemplating the scenario when GPS satellites are destroyed by enemy forces. All of these factors have created strong interest in non-GPS based wireless positioning networks which can either stand alone or be part of a seamless positioning system.

Ground based positioning networks have also been in existence for decades, but the state of the art still falls far short of the accuracy and robustness required for many location based services. This thesis has attempted to address a number of problems in GPS-denial wireless positioning. These include the optimisation of sensor node placement for tracking mobile nodes in a given area with the highest accuracy/lowest number of nodes; the development of the weighted least squares method (WLSM)

to increase the accuracy of triangulation based positing system using multiple sensor arrays; the invention of a novel ranging based sensor array and the development of the associated statistical theory; the introduction of the scheme of employing co-operative sensor arrays and the underlying theory. These new algorithms, methods and systems should help system designers and practitioners to design high accuracy positioning networks with lower cost. It is also aimed to stimulate new ideas/concepts in the research of GPS-denial wireless positioning networks.

For certain applications, there is a demand to increase the positioning accuracy to a few millimetres. These include the tracking of swimmers in a swimming pool. Our study shows that, although its is theoretically possible by designing an optimum positioning network, the ranging accuracy required is probably beyond what is feasible with radio and acoustic systems. This is more complicated by the fact that radio signals do not penetrate water very well and acoustic systems tend to be bulky and very costly.

We have just commenced the investigation of using optical systems for high accuracy and short range positioning. This has been inspired by the availability of low cost LEDs and lasers and the renewed interest in wireless optical communications [129], [130], [131], [132]. It is expected that such optical positioning networks will play a complementary role for certain applications where there is line-of-sight between the target and some networks sensors.

# Appendix A

# Trigonometric Properties of a Ranging Based Sensor Array

This appendix details the trigonometry properties of a ranging based sensor array proposed in Section 6.2. These properties play essential roles in Section 6.3.

As the model described in Section 6.2, all the sensors in the array are evenly distributed on the circumference so the center angle of the $i^{th}$ sensor is expressed as

$$\alpha_i = (i-1)\frac{2\pi}{N} + \alpha_0, \tag{A.1}$$

where $N$ is the number of the sensor, and $\alpha_0$ is an arbitrary angle. $\sum_{i=1}^{N} e^{j\alpha_i}$ is the sum of geometric series with the initial $e^{j\alpha_0}$ and common ratio of $e^{j\frac{2\pi}{N}}$. It results in

$$\sum_{i=1}^{N} e^{j\alpha_i} = e^{j\alpha_0}\frac{1-e^{jN\frac{2\pi}{N}}}{1-e^{j\frac{2\pi}{N}}} = 0. \tag{A.2}$$

Thus

$$\sum_{i=1}^{N} \cos(\alpha_i) = 0, \tag{A.3}$$

and

$$\sum_{i=1}^{N} \sin(\alpha_i) = 0. \tag{A.4}$$

In the same way, one obtains

$$\sum_{i=1}^{N} \cos(k\alpha_i) = 0, \tag{A.5}$$

and

$$\sum_{i=1}^{N} \sin(k\alpha_i) = 0, \tag{A.6}$$

where $k$ is an arbitrary integer.

Employing trigonometry identity $\sin^2(\alpha_i) = \dfrac{1-\cos(2\alpha_i)}{2}$ and (A.5), one gets

$$\sum_{i=1}^{N} \sin^2(\alpha_i) = \frac{N}{2}. \tag{A.7}$$

Employing trigonometry identity $\cos^2(\alpha_i) = \dfrac{1+\cos(2\alpha_i)}{2}$ and (A.5), one gets

$$\sum_{i=1}^{N} \cos^2(\alpha_i) = \frac{N}{2}. \tag{A.8}$$

And employing trigonometry identity $2\sin(\alpha_i)\cos(\alpha_i) = \sin(2\alpha_i)$ and (A.6), one gets

$$\sum_{i=1}^{N} \sin(\alpha_i)\cos(\alpha_i) = 0. \tag{A.9}$$

From the definition of matrix $\mathbf{A}$ by (6.3) one obtains

$$\mathbf{A}^T\mathbf{A} = \begin{bmatrix} N & -R\sum_{i=1}^{N}\cos(\alpha_i) & -R\sum_{i=1}^{N}\sin(\alpha_i) \\ -R\sum_{i=1}^{N}\cos(\alpha_i) & R^2\sum_{i=1}^{N}\cos^2(\alpha_i) & R^2\sum_{i=1}^{N}\sin(\alpha_i)\cos(\alpha_i) \\ -R\sum_{i=1}^{N}\sin(\alpha_i) & R^2\sum_{i=1}^{N}\sin(\alpha_i)\cos(\alpha_i) & R^2\sum_{i=1}^{N}\sin^2(\alpha_i) \end{bmatrix}, \tag{A.10}$$

where the superscript $T$ denotes the matrix or vector transpose operation.

Applying (A.3), (A.4), (A.7), (A.8), and (A.9) to (A.10) yields

$$\mathbf{A}^T\mathbf{A} = \begin{bmatrix} N & 0 & 0 \\ 0 & \dfrac{NR^2}{2} & 0 \\ 0 & 0 & \dfrac{NR^2}{2} \end{bmatrix}. \tag{A.11}$$

# Appendix B

# Derivation of Variance of Bearing for Ranging Based Sensor Array

This appendix details derivation of bearing variance expressed by (6.62) in Section 6.4.

From the variance of bearing expressed by (6.61) in Section 6.4, expanding the item in the squared bracket one has

$$\begin{aligned} & \sum_{i=1}^{N} \left\{ \left[ c_{EV} \sin(\alpha_i) - s_{EV} \cos(\alpha_i) \right]^2 \right\} \\ = \; & {c_{EV}}^2 \sum_{i=1}^{N} \sin^2(\alpha_i) + {s_{EV}}^2 \sum_{i=1}^{N} \cos^2(\alpha_i) - 2 c_{EV} s_{EV} \sum_{i=1}^{N} \sin(\alpha_i) \cos(\alpha_i). \end{aligned} \tag{B.1}$$

Employing (A.7) and (A.8) leads to

$${c_{EV}}^2 \sum_{i=1}^{N} \sin^2(\alpha_i) + {s_{EV}}^2 \sum_{i=1}^{N} \cos^2(\alpha_i) = \frac{N}{2}. \tag{B.2}$$

Employing (A.9) leads to

$$2 c_{EV} s_{EV} \sum_{i=1}^{N} \sin(\alpha_i) \cos(\alpha_i) = 0. \tag{B.3}$$

The contribution of the item in the squared bracket is $\frac{N}{2}$. Substituting this result to

(6.61) results in

$$E\left[(\Delta\theta)^2\right] = \frac{2}{NR^2}\sigma^2. \tag{B.4}$$

# Appendix C

# Parameter Transform

This appendix details the derivation of parameter transform, $\frac{\partial d_A}{\partial d}$ , $\frac{\partial d_A}{\partial \theta}$ , $\frac{\partial \theta_A}{\partial d}$ , and $\frac{\partial \theta_A}{\partial \theta}$ which are used in Section 6.5. The result is presented in four equations (C.5), (C.7), (C.13) and (C.16).

The target, the array and the origin position are as shown in Fig. C.1.

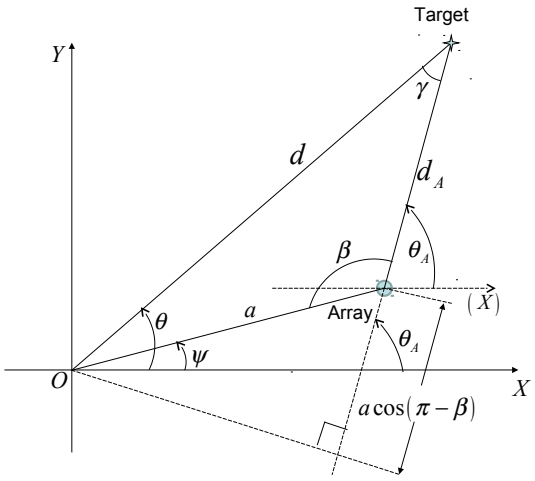


**Figure C.1:** Geometric relationship of an array at an arbitrary position

The cosine rule states

$$d_A{}^2 = d^2 + a^2 - 2ad\cos(\theta - \psi). \tag{C.1}$$

Differentiating (C.1) with respect to $d$ leads to

$$d_A \frac{\partial d_A}{\partial d} = d - a\cos(\theta - \psi), \tag{C.2}$$

and differentiating (C.1) with respect to $\theta$ leads to

$$d_A \frac{\partial d_A}{\partial \theta} = ad\sin(\theta - \psi). \tag{C.3}$$

Geometrical relationship provides

$$d = a\cos(\theta - \psi) + d_A\cos(\gamma), \tag{C.4}$$

where $\gamma$ is the interior angle made by sides $d$ and $d_A$. Substituting (C.4) to (C.2) leads to

$$\frac{\partial d_A}{\partial d} = \cos(\gamma). \tag{C.5}$$

The sine rule states

$$\frac{\sin(\gamma)}{a} = \frac{\sin(\theta - \psi)}{d_A}. \tag{C.6}$$

Substituting (C.6) to (C.3) leads to

$$\frac{\partial d_A}{\partial \theta} = d\sin(\gamma). \tag{C.7}$$

Geometrical relationship provides

$$d_A + a\cos(\pi - \beta) = d\cos(\gamma), \tag{C.8}$$

and

$$\beta = \pi - \theta_A + \psi. \tag{C.9}$$

Differentiating (C.8) with respect to $d$ and applying (C.5) lead to

$$\frac{\partial \theta_A}{\partial d} = \frac{\partial \gamma}{\partial d}, \tag{C.10}$$

where the partial differentiation of (C.9) with respect to $d$ and the sine rule that states

$$\frac{\sin(\beta)}{d} = \frac{\sin(\gamma)}{a} \tag{C.11}$$

have been applied to obtain (C.10).

Differentiating (C.6) with respect to $d$ provides

$$\frac{\partial \gamma}{\partial d} = -\frac{\sin(\gamma)}{d_A}, \tag{C.12}$$

where (C.6) has been employed to simplify (C.12). Substituting (C.12) to (C.10), and applying (C.6) lead to

$$\frac{\partial \theta_A}{\partial d} = -\frac{\sin(\gamma)}{d_A}. \tag{C.13}$$

Differentiating (C.8) with respect to $\theta$ and applying (C.7) lead to

$$1 - \frac{\partial \theta_A}{\partial \theta} = -\frac{\partial \gamma}{\partial \theta}, \tag{C.14}$$

where partial differentiation of (C.9) with respect to $\theta$ has been applied to obtain (C.14), and (C.11) has been employed to simplify (C.14).

Differentiating (C.11)with respect to $\theta$ leads to

$$d\cos(\gamma)\frac{\partial \gamma}{\partial \theta} = -a\cos(\beta)\frac{\partial \theta_A}{\partial \theta}. \tag{C.15}$$

Substituting (C.15) to (C.14), and applying (C.8) lead to

$$\frac{\partial \theta_A}{\partial \theta} = \frac{d}{d_A}\cos(\gamma). \tag{C.16}$$

# Appendix D

# The Determinant of Fisher Information Matrix for Array Placed at Arbitrary Position

This appendix details the derivation for the determinant of Fisher information matrix in Section 6.5. The $2 \times 2$ matrix and its elements are obtained in Section 6.5. There two sets of formulae to express the elements. Equations (6.86), (6.87) and (6.88) express the matrix elements in the concise form, although they do not show the obvious functions as bearing. Equations (6.90), (6.91) and (6.92) show the elements as functions of range and bearing of the target, but the forms are lengthy. In the following demonstration, the former set of equations are used. The result shows that the determinant is not a function of target bearing.

From Chapter 6, Section 6.5, the Fisher information matrix for positioning when the array is place at $(a, \psi)$ is expressed as

$$\mathbf{I}_A = \begin{bmatrix} I_{A11} & I_{A12} \\ I_{A21} & I_{A22} \end{bmatrix} \qquad (6.76),$$

where

$$I_{A11} = \frac{N}{\sigma^2}\left[\frac{R^2}{2{d_A}^2}\sin^2(\gamma) + \cos^2(\gamma)\right] \qquad (6.86),$$

$$I_{A12} = \frac{N}{\sigma^2} d\left(1 - \frac{R^2}{2{d_A}^2}\right)\sin(\gamma)\cos(\gamma) \qquad (6.88),$$

$$I_{A21} = \frac{N}{\sigma^2} d\left(1 - \frac{R^2}{2{d_A}^2}\right)\sin(\gamma)\cos(\gamma) \qquad (6.88),$$

$$I_{A22} = \frac{N}{\sigma^2} d^2\left[\sin^2(\gamma) + \frac{R^2}{2{d_A}^2}\cos^2(\gamma)\right] \qquad (6.87).$$

$$\begin{aligned} & I_{A11}I_{A22} \\ = \; & \frac{1}{2}\left(\frac{N}{\sigma^2}\right)^2 d^2\frac{R^2}{{d_A}^2}\left\{\left[\sin^2(\gamma)\right]^2 + \left[\cos^2(\gamma)\right]^2\right\} \\ & + \left(\frac{N}{\sigma^2}\right)^2 d^2\left[1 + \left(\frac{R^2}{2{d_A}^2}\right)^2\right]\sin^2(\gamma)\cos^2(\gamma). \end{aligned} \qquad (D.1)$$

Adding $\left[\left(\frac{N}{\sigma^2}\right)^2 d^2\frac{R^2}{{d_A}^2}\sin^2(\gamma)\cos^2(\gamma)\right]$ to the first item leads the item to be $\left(\frac{N}{\sigma^2}\right)^2\frac{R^2d^2}{2{d_A}^2}$, and subtracting $\left[\left(\frac{N}{\sigma^2}\right)^2 d^2\frac{R^2}{{d_A}^2}\sin^2(\gamma)\cos^2(\gamma)\right]$ from the second item leads the item to be $\left(\frac{N}{\sigma^2}\right)^2 d^2\left(1 - \frac{R^2}{2{d_A}^2}\right)^2\sin^2(\gamma)\cos^2(\gamma)$. The product of main diagonal items is

$$\begin{aligned} & I_{A11}I_{A22} \\ = \; & \left(\frac{N}{\sigma^2}\right)^2\frac{R^2d^2}{2{d_A}^2} + \left(\frac{N}{\sigma^2}\right)^2 d^2\left(1 - \frac{R^2}{2{d_A}^2}\right)^2\sin^2(\gamma)\cos^2(\gamma). \end{aligned} \qquad (D.2)$$

And the product of anti-diagonal items is

$$I_{A12}I_{A21} = \left(\frac{N}{\sigma^2}\right)^2 d^2\left(1 - \frac{R^2}{2{d_A}^2}\right)^2\sin^2(\gamma)\cos^2(\gamma). \qquad (D.3)$$

Therefore

$$\det\left(\mathbf{I}_A\right) = \left(\frac{N}{\sigma^2}\right)^2 \frac{R^2 d^2}{2{d_A}^2}. \tag{D.4}$$

# Appendix E

# Error of Variables

This appendix details relationship between variable errors in Section 6.6. There are two sets of variables, $(d, \theta)$ and $(d_A, \theta_A)$, shown as Fig. 6.5. The latter set is estimated by the array which is placed at $(a, \psi)$. The aim of this appendix is to present the relationship between the error of a target position and the error made by array estimation.

For the relationship between distance and bearing, cosine rule is the way to express. Take the side $d$ and its opposite angle $\beta$, the cosine rule states

$$d^2 = {d_A}^2 + a^2 - 2 d_A a \cos\left[\beta\left(\theta_A\right)\right], \tag{E.1}$$

noting that

$$\beta = \pi - \theta_A + \psi. \tag{E.2}$$

The deviation of $d$ is thus expressed as

$$\Delta d = \left[\frac{d_A}{d} - \frac{a}{d}\cos\left(\beta\right)\right]\Delta d_A - \frac{d_A a}{d}\sin\left(\beta\right)\Delta\theta_A. \tag{E.3}$$

Employing (C.8) and (C.11) leads to

$$\Delta d = \cos\left(\gamma\right)\Delta d_A - d_A \sin\left(\gamma\right)\Delta\theta_A. \tag{E.4}$$

Geometrical relationship has

$$d_A \cos(\gamma) + a \cos(\theta - \psi) = d. \tag{E.5}$$

The sine rule states

$$\frac{\sin(\gamma)}{a} = \frac{\sin(\theta - \psi)}{d_A}. \tag{E.6}$$

Differentiating (E.5) and (E.6), and having eliminated $\Delta\gamma$, it leads to

$$\Delta\theta = \frac{\sin(\gamma)}{d}\Delta d_A + \frac{d_A \cos(\gamma)}{d}\Delta\theta_A. \tag{E.7}$$

# Appendix F

# The Determinant of Fisher Information Matrix for Co-operative Arrays

This appendix derives the determinant of Fisher information matrix for two co-operative arrays in Section 7.2. In this appendix, the same subscriptions as in 7 are used, i.e.,subscript C denotes the array located at the center of the system, i.e. the origin, subscript A denotes the array located at an arbitrary location but known to the system as located at $(a, \psi)$, and subscript CA denotes the two co-operative arrays.

From the definition of determinant one has

$$\det\left(\mathbf{I}_{CA}\right) = I_{CA11}I_{CA22} - I_{CA12}I_{CA21}. \tag{F.1}$$

Applying (7.1) to (F.1) yields

$$\begin{aligned} & \det\left(\mathbf{I}_{CA}\right) \\ = \; & \left(I_{C11} + I_{A11}\right)\left(I_{C22} + I_{A22}\right) - \left(I_{C12} + I_{A12}\right)\left(I_{C21} + I_{A21}\right). \end{aligned} \tag{F.2}$$

Noting that (6.31) in 6.3 states

$$I_{C12} = I_{C21} = 0. \tag{F.3}$$

Equation (F.2) can be written as

$$\begin{aligned} & \det\left(\mathbf{I}_{CA}\right) \\ = \; & \det\left(\mathbf{I}_{C}\right) + \det\left(\mathbf{I}_{A}\right) + I_{C11}I_{A22} + I_{A11}I_{C22}. \end{aligned} \tag{F.4}$$

Substituting (6.31) from Section 6.3 and (6.93) from Section 6.5 leads to

$$\begin{aligned} & \det\left(\mathbf{I}_{C}\right) + \det\left(\mathbf{I}_{A}\right) \\ = \; & \frac{N^2R^2}{2\sigma^4} + \frac{N^2R^2}{2\sigma^4}\frac{d^2}{{d_A}^2} \\ = \; & \frac{N^2}{\sigma^4}\frac{R^2}{2}\left(1 + \frac{d^2}{{d_A}^2}\right). \end{aligned} \tag{F.5}$$

The rest items in (F.4) are

$$\begin{aligned} & I_{C11}I_{A22} + I_{A11}I_{C22} \\ = \; & \left(\frac{N}{\sigma^2}\right)^2\frac{R^2}{2}\left(1 + \frac{d^2}{{d_A}^2}\right) \\ & + \left(\frac{N}{\sigma^2}\right)^2\left(d^2 - \frac{R^2}{2}\right)\left(1 - \frac{R^2}{2{d_A}^2}\right)\sin^2\left(\gamma\right). \end{aligned} \tag{F.6}$$

Substituting (F.5) and (F.6) to (F.4) results in

$$\det\left(\mathbf{I}_{CA}\right) = \frac{N^2}{\sigma^4}\left[R^2\left(1 + \frac{d^2}{{d_A}^2}\right) + \left(d^2 - \frac{R^2}{2}\right)\left(1 - \frac{R^2}{2{d_A}^2}\right)\sin^2\left(\gamma\right)\right]. \tag{F.7}$$

The sine rule states

$$\frac{a}{\sin\left(\gamma\right)} = \frac{d_A}{\sin\left(\theta - \psi\right)}. \tag{F.8}$$

Substituting (F.8) in (F.7) leads to

$$\begin{aligned} & \det\left(\mathbf{I}_{CA}\right) \\ = \; & \frac{N^2}{\sigma^4}\left[R^2\left(1 + \frac{d^2}{{d_A}^2}\right) + \left(d^2 - \frac{R^2}{2}\right)\left(1 - \frac{R^2}{2{d_A}^2}\right)\frac{a^2}{{d_A}^2}\sin^2\left(\theta - \psi\right)\right]. \end{aligned} \tag{F.9}$$

# References


[1] A. Bensky, *Wireless Positioning Technologies and Applications*. Artech House Inc., 2008.

[2] E. D. Kaplan and C. J. Hegarty, *Understanding GPS: Principles and Applications*, 2nd ed. Artech House Inc., 2005.

[3] J. T. Nielson, G. W. Swearingen, and A. Witsmeer, "GPS aided inertial navigation," *IEEE Aerospace and Electronic Systems Magazine*, vol. 1, no. 3, pp. 20 – 26, 1986.

[4] J. Huang and H. S. Tan, "A low-order DGPS-Based vehicle positioning system under urban environment," *IEEE/ASME Transactions on Mechatronics*, vol. 11, no. 5, pp. 567 – 575, 2006.

[5] M. Kazemi, M. Ardebilipour, and N. Noori, "Improved weighted RSS positioning algorithm for cognitive radio," *IEEE 10th International Conference on Signal Processing (ICSP)*, pp. 1502 – 1506, 2010.

[6] P. Heidenreich, A. Zoubir, and M. Rubsamen, "Joint 2-D DOA estimation and phase calibration for uniform rectangular arrays," *IEEE Transactions on Signal Processing*, vol. 60, no. 9, pp. 4683 – 4693, 2012.

[7] Y. Nagata, T. Fujioka, and M. Abe, "Two-dimensional DOA estimation of sound sources based on weighted wiener gain exploiting two-directional microphones," *IEEE Transactions on Audio, Speech, and Language Processing*, vol. 15, no. 2, pp. 416 – 429, 2007.

[8] A. Noureldin, T. Karamat, M. Eberts, and A. El-Shafie, "Performance enhancement of MEMS-Based INS/GPS integration for Low-Cost navigation applications," *IEEE Transactions on Vehicular Technology*, vol. 58, no. 3, pp. 1077 – 1096, 2009.

[9] H. Liu, H. Darabi, P. Banerjee, and J. Liu, "Survey of wireless indoor positioning techniques and systems," *IEEE Transactions on Systems, Man, and Cybernetics, Part C: Applications and Reviews*, vol. 37, no. 6, pp. 1067 – 1080, 2007.

[10] A. D'Amico, L. Taponecco, and U. Mengali, "Ultra-wideband toa estimation in the presence of clock frequency offset," *IEEE Transactions on Wireless Communications*, vol. 12, no. 4, pp. 1606 – 1616, 2013.

[11] W. Lee and V. Patanavijit, "Performance evaluation of TOA estimation for Ultra-wideband system under AWGN and IEEE 802.13a Channel Model," *Seventh International Conference on Signal-Image Technology and Internet-Based Systems (SITIS)*, pp. 237 – 244, 2011.

[12] M. Dashti, M. Ghoraishi, K. Haneda, and J. I. Takada, "Sources of ToA estimation error in LoS scenario," *IEEE International Conference on Ultra-Wideband (ICUWB)*, vol. 2, pp. 1 – 4, 2010.

[13] F. Zhao, W. Yao, C. Logothetis, and Y. Song, "Super-resolution TOA estimation in OFDM systems for indoor environments," *IEEE International Conference on Networking, Sensing and Control, 2007*, pp. 723 – 728, 2007.

[14] H. Xu, C. C. Chong, I. Guvenc, F. Watanabe, and L. Yang, "High-resolution TOA estimation with multi-band OFDM UWB signals," *IEEE International Conference on Communications*, pp. 4191 – 4196, 2008.

[15] H. Ding, W. Liu, X. Huang, and L. Zheng, "First path detection using rank test in IR UWB ranging with energy detection receiver under harsh environments," *IEEE Communications Letters*, vol. 17, no. 4, pp. 761 – 764, 2013.

[16] D. Chong, S. Kim, E. Lee, S. Y. Kim, and S. Yoon, "A new UWB synchronization scheme using multipath components jointly," *IEEE 10th International Conference on Advanced Communication Technology (ICACT)*, vol. 3, pp. 1719 – 1724, 2008.

[17] D. Liu, M. C. Lee, C. M. Pun, and H. Liu, "Analysis of wireless localization in Nonline-of-Sight conditions," *IEEE Transactions on Vehicular Technology*, vol. 62, no. 4, pp. 1484 – 1492, 2013.

[18] B. Denis and N. Daniele, "NLOS ranging error mitigation in a distributed positioning algorithm for indoor UWB ad-hoc networks," *International Workshop on Wireless Ad-Hoc Networks*, pp. 356 – 360, 31 May-3 June 2004.

[19] J. Tao and R. Buehrer, "Collaborative position location with NLOS mitigation," *IEEE 21st International Symposium on Personal, Indoor and Mobile Radio Communications Workshops (PIMRC Workshops)*, pp. 267 – 271, 26-30 Sept. 2010.

[20] J. Huerta and J. Vidal, "LOS-NLOS situation tracking for positioning systems," *IEEE 7th Workshop on Signal Processing Advances in Wireless Communications (SPAWC '06)*, pp. 1 – 5, 2-5 July 2006.

[21] G. Ding, Z. Tan, L. Zhang, Z. Zhang, and J. Zhang, "Hybrid TOA/AOA cooperative localization in Non-Line-of-Sight environments," *IEEE 75th Vehicular Technology Conference*, pp. 1 – 5, 6-9 May 2012.

[22] S. W. Chen and S. Y. Tan, "Cooperative non-line-of-sight localization technique for indoor wireless network," *8th International Conference on Information, Communications and Signal Processing*, pp. 1 – 5, December 2011.

[23] C. H. Lim, C. M. S. See, A. Zoubir, and J. P. Lie, "Robust geo-location in mixed LOS and NLOS environment," *IEEE/SP 15th Workshop on Statistical Signal Processing (SSP '09)*, pp. 189 – 192, 31 Aug. - 3 Sept. 2009.

[24] F. Benedetto, G. Giunta, A. Toscano, and L. Vegni, "Dynamic LOS/NLOS statistical discrimination of wireless mobile channels," *IEEE 65th Vehicular Technology Conference (VTC2007-Spring)*, pp. 3071 – 3075, 22-25 April 2007.

[25] Y. Li and H. Ma, "Time delay estimation basing on narrow-band signal in multipath environments," *Proceedings of the 2008 Congress on Image and Signal Processing*, vol. 5, pp. 547–551, 2008.

[26] C. Ma, R. Klukas, and G. Lachapelle, "A Nonline-of-Sight error-mitigation method for TOA measurements," *IEEE Transactions on Vehicular Technology*, vol. 56, no. 2, pp. 641 – 651, 2007.

[27] R. Ouyang and A. K. S. Wong, "An enhanced ToA-Based wireless location estimation algorithm for dense NLOS environments," *IEEE Wireless Communications and Networking Conference (WCNC 2009)*, pp. 1 – 6, 2009.

[28] A. Hossain, H. N. Van, Y. Jin, and W. S. Soh, "Indoor localization using multiple wireless technologies," *IEEE Internatonal Conference on Mobile Adhoc and Sensor Systems (MASS)*, pp. 1 – 8, 2007.

[29] S. Gezici, Z. Tian, G. Giannakis, H. Kobayashi, A. Molisch, H. Poor, and Z. Sahinoglu, "Localization via ultra-wideband radios: a look at positioning aspects for future sensor networks," *IEEE Signal Processing Magazine*, vol. 22, no. 4, pp. 70 – 84, 2005.

[30] S. Venkatesh and R. Buehrer, "Multiple-access design for ad hoc UWB position-location networks," *IEEE Wireless Communications and Networking Conference (WCNC)*, vol. 4, pp. 1866 – 1873, 2006.

[31] G. Hussein, I. Eldokany, A. Mohamed, and O. Oraby, "Efficient transceiver architecture to mitigate the effect of MAI in optical CDMA," *International Conference on Computer Engineering and Systems (ICCES 2010)*, pp. 85 – 92, 2010.

[32] S. B. Hong, J. S. Baek, and J. S. Seo, "Efficient two-stage frequency-domain equalisation for mitigating mai in cdma systems," *Electronics Letters*, vol. 44, no. 8, pp. 538 – 539, 2008.

[33] J. Mitra and L. Lampe, "Comparison of detectors for multiple-access interference mitigation in TH-IR UWB," *IEEE International Conference on Ultra-Wideband (ICUWB 2008)*, vol. 1, pp. 153 – 156, 2008.

[34] Z. Zhao and G. Wang, "A novel training sequence design algorithm for OFDM system," *International Conference on Computer Science and Service System (CSSS)*, pp. 2900 – 2903, 2011.

[35] E. Falletti, L. L. Presti, and F. Sellone, "SAM LOST smart antennas-based movable localization system," *IEEE Transactions on Vehicular Technology*, vol. 55, no. 1, pp. 25 – 42, 2006.

[36] S. Mazuelas, F. Lago, D. Gonzalez, A. Bahillo, J. Blas, P. Fernandez, R. Lorenzo, and E. Abril, "Dynamic estimation of optimum path loss model in a rss positioning system," *Position, Location and Navigation Symposium, 2008 IEEE/ION*, pp. 679 – 684, 2008.

[37] G. Attanayake and Y. Rong, "RSS-based indoor positioning accuracy improvement using antenna array in WLAN environments," *International Conference on Indoor Positioning and Indoor Navigation (IPIN)*, pp. 1 – 6, 2012.

[38] S. Chitte, S. Dasgupta, and Z. Ding, "Distance estimation from received signal strength under Log-Normal shadowing: Bias and Variance," *IEEE Signal Processing Letters*, vol. 16, no. 3, pp. 216 – 218, March 2009.

[39] S. H. Fang, T. N. Lin, and K. C. Lee, "A novel algorithm for multipath fingerprinting in indoor WLAN environments," *IEEE Transactions on Wireless Communications*, vol. 7, no. 9, pp. 3579 – 3588, 2008.

[40] A. Wadhwa, U. Madhow, J. Hespanha, and B. Sadler, "Following an RF trail to its source," *49th Annual Allerton Conference on Communication, Control, and Computing (Allerton)*, pp. 580 – 587, 2011.

[41] M. Grabner, V. Kvicera, P. Pechac, and O. Jicha, "Measured and simulated fluctuations of received power on 11 GHz terrestrial path using vertical profiles of atmospheric refractivity," *Proceedings of the 5th European Conference on Antennas and Propagation (EUCAP)*, pp. 182 – 185, 2011.

[42] S. Wang and R.Inkol, "A near-optimal least squares solution to received signal strength difference based geolocation," *IEEE International Conference on Acoustics, Speech and Signal Processing (ICASSP)*, pp. 2600 – 2603, 2011.

[43] X. Hu, L. Cheng, and G. Zhang, "A Zigbee-based localization algorithm for indoor environments," *Computer Science and Network Technology (ICCSNT), 2011 International Conference on*, vol. 3, pp. 1776 – 1781, 2011.

[44] N. Salman, Y. J. Guo, and A. H. Kemp, "Analysis of linear least square solution for rss based localization," *IEEE ISCIT2012*, Gold Coast, Australia 2012.

[45] J. Xiao, K. Wu, Y. Yi, and L. Ni, "FIFS: Fine-grained indoor fingerprinting system," *21st International Conference on Computer Communications and Networks (ICCCN)*, pp. 1 – 7, 2012.

[46] M. Laaraiedh, S. Avrillon, and B. Uguen, "Hybrid data fusion techniques for localization in uwb networks," *6th Workshop on Positioning, Navigation and Communication (WPNC 2009)*, pp. 51 – 57, 2009.

[47] J. H. Cui, J. Kong, M. Gerla, and S. Zhou, "The challenges of building scalable mobile underwater wireless sensor networks for aquatic applications," *IEEE Network*, vol. 20, no. 3, pp. 12–18, May-June 2006.

[48] J. Catipovic, D. Brady, and S. Etchemendy, "Development of underwater acoustic modems and networks," *Oceanography*, vol. 6, pp. 112–119, Mar 1993.

[49] B. D. V. Veen and K. M. Buckley, "Beamforming: A versatile approach to spatial filtering," *IEEE ASSP MAGAZINE*, vol. 5, no. 2, pp. 4–24, April 1988.

[50] T. Pham and B. M. Sadler, "Adaptive wideband aeroacoustic array processing," *8th IEEE Signal Processing Workshop on Statistical Signal and Array Processing*, pp. 295 – 298, 1996.

[51] H. Krim and M. Viberg, "Two decades of array signal processing research," *IEEE Signal Processing Magazine*, vol. 13, no. 4, pp. 67–94, July 1996.

[52] E. M. Sozer, M. Stojanovic, and J. G. Proakis, "Underwater acoustic networks," *IEEE Journal of Oceanic Engineering*, vol. 25, no. 1, pp. 72–83, January 2000.

[53] P. Xiong, M. Medley, and S. Batalama, "Spatial and temporal processing for global navigation satellite systems: the GPS receiver paradigm," *IEEE Transactions on Aerospace and Electronic Systems*, vol. 39, no. 4, pp. 1471 – 1484, 2003.

[54] G. B. Frank and M. D. Yakos, "Next generation digital GPS receiver," *IEEE Aerospace and Electronic Systems Magazine*, vol. 5, no. 7, pp. 10 – 15, 1990.

[55] M. Braasch and A. van Dierendonck, "GPS receiver architectures and measurements," *Proceedings of the IEEE*, vol. 87, no. 1, pp. 48 – 64, 1999.

[56] G. Zhao, D. Wang, M. Fattouche, and M. Jin, "Novel wireless positioning system for OFDM-Based cellular networks," *IEEE Systems Journal*, vol. 6, no. 3, pp. 444 – 454, 2012.

[57] J. Yao, A. Balaei, M. Hassan, N. Alam, and A. Dempster, "Improving cooperative positioning for vehicular networks," *IEEE Transactions on Vehicular Technology*, vol. 60, no. 6, pp. 2810 – 2823, 2011.

[58] H. Li and F. Nashashibi, "Cooperative multi-vehicle localization using split covariance intersection filter," *IEEE Intelligent Transportation Systems Magazine*, vol. 5, no. 2, pp. 33 – 44, 2013.

[59] M. Schlingelhof, D. Betaille, P. Bonnifait, and K. Demaseure, "Advanced positioning technologies for co-operative systems," *IET Intelligent Transport Systems*, vol. 2, no. 2, pp. 81 – 91, 2008.

[60] X. Tan and J. Li, "Cooperative positioning in underwater sensor networks," *IEEE Transactions on Signal Processing*, vol. 58, no. 11, pp. 5860 – 5871, 2010.

[61] N. Miwa, S. Tagashira, H. Matsuda, T. Tsutsui, Y. Arakawa, and A. Fukuda, "A multilateration-based localization scheme for Adhoc wireless positioning networks used in information-oriented construction," *IEEE 27th International Conference on Advanced Information Networking and Applications (AINA)*, pp. 690 – 695, 2013.

[62] H. B. Lee, "Accuracy of range-range and range-sum multilateration systems," *IEEE Transactions on Aerospace and Electronic Systems*, vol. AES-11, no. 6, pp. 1346 – 1361, 1975.

[63] F. Beutler and U. Hanebeck, "A two-step approach for offset and position estimation from pseudo-ranges applied to multilateration tracking," *13th Conference on Information Fusion (FUSION)*, pp. 1 – 8, 2010.

[64] S. Capkun and J. P. Hubaux, "Secure positioning in wireless networks," *IEEE Journal on Selected Areas in Communications*, vol. 24, no. 2, pp. 221 – 232, 2006.

[65] H. Lee, "A novel procedure for assessing the accuracy of hyperbolic multilateration systems," *IEEE Transactions on Aerospace and Electronic Systems*, vol. AES-11, no. 1, pp. 2 – 15, 1975.

[66] Y. Wakuda, S. Asano, N. Koshizuka, and K. Sakamura, "Ubiquitous sensor-based pedestrian dead-reckoning for LBS applications," *International Symposium on Micro-NanoMechatronics and Human Science (MHS)*, pp. 374 – 379, 2012.

[67] Y. J. Guo, *Advances in Mobile Radio Access Networks*. Artech House Inc., 2004.

[68] M. A. Spirito, "On the accuracy of cellular mobile station location estimation," *IEEE Transactions on Vehicular Technology*, vol. 50, no. 3, pp. 674 – 685, 2001.

[69] T. Kos, M. Grgic, and G. Sisul, "Mobile user positioning in GSM/UMTS cellular networks," *48th International Symposium focused on Multimedia Signal Processing and Communications (ELMAR-2006)*, 2006.

[70] E. Hepsaydir, "Mobile positioning in CDMA cellular networks," *IEEE VTS 50th Vehicular Technology Conference (VTC 1999 - Fall)*, vol. 2, pp. 795 – 799, 1999.

[71] R. Cardinali, L. D. Nardis, M.-G. D. Benedetto, and P. Lombardo, "UWB ranging accuracy in high- and low-data-rate applications," *IEEE Transactions on Mircowave Theory and Techniques*, vol. 54, no. 4, pp. 1865 – 1875, APRIL 2006.

[72] J. Heidemann, W. Ye, J. Wills, A. Syed, and Y. Li, "Research challenges and applications for underwater sensor networking," *IEEE Wireless Communica-*

*tions and Networking Conference (WCNC)*, vol. 1), pp. 228 – 235, 3-6 April 2006.

[73] J. Partan, J. Kurose, and B. N. Levine, "A survey of practical issues in underwater networks," *WUWNet'06, Los Angeles,California, USA*, September 2006.

[74] D. E. Lucani, M. Médard, and M. Stojanovic, "Underwater acoustic networks: Channel models and network coding based Lower Bound to transmission power for multicast," *Journal of Selected Areas in Communications*, vol. 1, no. 11, November 2008.

[75] Z. Zhou, J. H. Cui, and A. Bagtzoglou, "Scalable localization with mobility prediction for underwater sensor networks," *Proceedings IEEE INFOCOM*, 2008.

[76] W. Cheng, A. Y. Teymorian, L. Ma, and X. Cheng, "Underwater localization in sparse 3D acoustic sensor networks," *Proceedings IEEE INFOCOM*, 2008.

[77] H. Luo, Z. Guo, W. Dong, F. Hong, and Y. Zhao, "LDB: Localization with directional beacons for sparse 3D underwater acoustic sensor networks," *Journal of Networks*, vol. 5, no. 1, January 2010.

[78] I. F. Akyildiz, D. Pompili, and T. Melodia, "State-of-the-art in protocol research for underwater acoustic sensor networks," *Proceedings of the 1st ACM international workshop on Underwater Networks, New York, USA*, pp. 7–16, 2006.

[79] A. F. HarrisIII, M. Stojanovic, and M. Zorzi, "When underwater acoustic nodes should sleep with one eye open idle-time power management in underwater senosr networks," *Proceedings of the First ACM International Workshop on Underwater Networks*, pp. 105–108, 2006.

[80] H. Chen, K. Sezaki, P. Deng, and H. C. So, "An improved DV-Hop localization algorithm for wireless sensor networks," *3rd IEEE Conference on Industrial Electronics and Applications*, 2008.

[81] A. Savvides, C. Han, and M. Strivastava, "Dynamic fine-grained localization in Ad Hoc Networks of sensors," *Proceedings of the 7th annual international conference on Mobile computing and networking*, pp. 166–179, 2001.

[82] Y. Kwon, K. Mechitov, S. Sundresh, W. Kim, and G. Agha, "Resilient localization for sensor networks in outdoor environments," *Proceedings of 25th IEEE International Conference on Distributed Computing Systems*, 2005.

[83] J. M. Hovem, "Underwater acoustics: propagation devices and systems," *Journal of Electroceramics*, vol. 19, pp. 339–347, 2007.

[84] O. Tekdas and V. Isler, "Sensor placement for triangulation-based localization," *IEEE Transactions on Automation Science and Engineering*, vol. 7, no. 3, pp. 681–685, July 2010.

[85] A. Kelly, "Precision dilution in triangulation based mobile robot position estimation," *Intelligent Autonomous Systems*, Amsterdam, The Netherlands, Holland 2003.

[86] V. Isler, "Placement and distributed deployment of sensor teams for triangulation based localization," *Proceedings of the 2006 IEEE International Conference on Robotics and Automation, Orlando, Florida*, May 2006.

[87] J. Cortés, S. Martínez, T. Karatas, and F. Bullo, "Coverage control for mobile sensing networks," *IEEE Transactions on Robotics and Automation*, vol. 20, no. 2, pp. 243–255, April 2004.

[88] V. Isler and R. Bajcsy, "The sensor selection problem for bounded uncertainty sensing models," *IEEE Transaction on Automation Science and Engineering*, vol. 3, no. 4, pp. 372 – 381, Oct. 2006.

[89] L. Justham, S. Slawson, A. Westand, P. Conway, M. Caine, and R. Harrison, *Enabling Technologies for Robust Performance Monitoring, The Engineering of Sport 7*. Springer Paris, 2008.

[90] K. C. Xu, Y. J. Guo, and E. Dutkiewicz, "Swimmer tracking with underwater acoustic networks," *IEEE ISCIT2010*, Tokyo, Japan 2010.

[91] I. Sharp, K. Yu, and Y. J. Guo, "GDOP for positioning system design," *IEEE Transactions on Vehicular Technology*, vol. 58, no. 7, pp. 3371–3382, September 2009.

[92] K. Yu, I. Sharp, and Y. J. Guo, *Ground-Based Wireless Positioning*. IEEE Press, John Wiley and Sons Ltd, 2009.

[93] J. O. Smith and J. S. Abel, "Closed-form least-squares source location estimation from range-difference measurements," *IEEE Transactions on Acoustic, Speech, and Signal Processing*, vol. 35, no. 12, pp. 1661–1669, December 1987.

[94] M. T. Isik and O. B. Akan, "A three dimensional localization algorithm for underwater acoustic sensor networks," *IEEE Transactions on Wireless Communications*, vol. 8, no. 9, pp. 4457–4463, September 2009.

[95] J. Chaffee and J. Abel, "GDOP and the Cramér-Rao Bound," *IEEE Position Location and Navigation Symposium*, pp. 663–668, 1994.

[96] G. Frenkel, "Geometric dilution of position (GDOP) in position determination through radio signals," *Proceedings of the IEEE*, vol. 61, no. 4, pp. 496 – 497, 1973.

[97] N.Levanon, "Lowest GDOP in 2-D scenarios," *IEE Proceedings Radar, Sonar and Navigation*, vol. 147, no. 3, pp. 149 – 155, 2000.

[98] X. Lv, K. Liu, and P. Hu, "Geometry influence on GDOP in TOA and AOA positioning systems," *Second International Conference on Networks Security Wireless Communications and Trusted Computing (NSWCTC), 2010*, vol. 2, pp. 58 – 61, 2010.

[99] D. Boeringer and D. Werner, "Particle swarm optimization versus genetic algorithms for phased array synthesis," *IEEE Transactions on Antennas and Propagation*, vol. 52, no. 3, pp. 771 – 779, 2004.

[100] G. Ciuprina, D. Ioan, and I. Munteanu, "Use of intelligent-particle swarm optimization in electromagnetics," *IEEE Transactions on Magnetics*, vol. 38, no. 2 , Part: 1, pp. 1037 – 1040, 2002.

[101] F. van den Bergh and A. Engelbrecht, "A cooperative approach to particle swarm optimization," *IEEE Transactions on Evolutionary Computation*, vol. 8, no. 3, pp. 225 – 239, 2004.

[102] J. Robinson and Y. Rahmat-Samii, "Particle swarm optimization in electromagnetics," *IEEE Transactions on Antennas and Propagation*, vol. 52, no. 2, pp. 397 – 407, 2004.

[103] M. Clerc and J. Kennedy, "The particle swarm - explosion, stability, and convergence in a multidimensional complex space," *IEEE Transactions on Evolutionary Computation*, vol. 6, no. 1, pp. 58 – 73, 2002.

[104] J. Kennedy and R. Eberhart, "Particle swarm optimization," *IEEE International Conference on Neural Networks*, vol. 4, pp. 1942 – 1948, Nov / Dec 1995.

[105] Y. Valle, G. Venayagamoorthy, S. Mohagheghi, J.C.Hernandez, and R. Harley, "Particle swarm optimization: Basic concepts, variants and applications in power systems," *IEEE Transactions on Evolutionary Computation*, vol. 12, no. 2, pp. 171 – 195, April 2008.

[106] A. J. Weiss, "Direct position determination of narrowband radio frequency transmitters," *IEEE Signal Processing Letters*, vol. 11, no. 5, pp. 513–516, May 2004.

[107] M. Hawkes and A. Nehorai, "Acoustic vector-sensor beamforming and capon direction estimation," *IEEE Transactions on Signal Processing*, vol. 46, no. 9, pp. 2291–2304, September 1998.

[108] R. E. Collin, *Antennas and Radiowave Propagation.* McGraw-Hill, 1985.

[109] H. Goldsein, "Multilevel mixed linear model analysis using iterative generalized least squares," *Biometrika*, vol. 73, no. 1, pp. 43–56, April 1986.

[110] G. J. McLachlan, *Discriminant Analysis and Statistical Pattern Recognition.* Wiley Interscience, 1992.

[111] K. C. Xu, Y. J. Guo, X. Huang, and E. Dutkiewicz, "A weighted least squares method for wireless positioning using multiple linear antenna arrays," *IEEE International Symposium on Antennas and Propagation and USNC/URSI National Radio Science Meeting*, Spokane, WA 2011.

[112] K. C. Xu, Y. J. Guo, X. Huang, and E. Dutkiewicz, "DoA based positioning employing uniform circular arrays," *IEEE ISCIT2011*, Hangzhou, China 2011.

[113] K. C. Xu, Y. J. Guo, X. Huang, and E. Dutkiewicz, "3D wireless positioning using uniform circular arrays," *IEEE International Symposium on Antennas and Propagation and USNC/URSI National Radio Science Meeting*, Spokane, WA 2011.

[114] R. J. Urich, *Principles of Underwater Sound*. McGraw-Hill, Inc., 1983.

[115] L. E. Kinsler, A. R. Frey, A. B. Coppens, and J. V. Sanders, *Fundamentals of Acoustic*, 4th ed. John Wiley and Sons, Inc., 1999.

[116] J. D. Kraus, *Antennas*, 2nd ed. McGraw-Hill, Inc., 1988.

[117] D. J. Torrieri, "Statistical theory of passive location systems," *IEEE Transactions on Aerospace and Electronic Systems*, vol. AES-20, no. 2, pp. 183–198, March 1984.

[118] Y. Fu and Z. Tian, "Cramér-Rao bounds for hybrid TOA/DOA-based location estimation in sensor networks," *IEEE Signal Processing Letters*, vol. 16, no. 8, pp. 655–658, August 2009.

[119] R. J. Kozick and B. M. Sadler, "Source localization with distributed sensor arrays and partial coherence," *IEEE Transactions on Signal Processing*, vol. 52, no. 3, pp. 601–616, March 2004.

[120] B. Liao and S. C. Chan, "Direction finding with partly calibrated uniform linear arrays," *IEEE Transactions on Antennas and Propagation*, vol. 60, no. 2, pp. 922–929, February 2012.

[121] Z. F. Ye and C. liu, "2-D DOA estimation in the presence of mutual coupling," *IEEE Transactions on Antennas and Propagation*, vol. 56, no. 10, pp. 3150–3158, Oct. 2008.

[122] A. Kisliansky and J. Tabrikian, "Direction of arrival estimation in the presence of noise coupling in antenna arrays," *IEEE Transactions on Antennas and Propagation*, vol. 55, no. 7, pp. 1940–1947, July 2007.

[123] K. C. Xu, Y. J. Guo, X. Huang, and E. Dutkiewicz, "A hybrid wireless positioning system," *IEEE International Symposium on Antennas and Propagation and USNC/URSI National Radio Science Meeting*, Chicago, U.S.A. 2012.

[124] B. R. Frieden, *Physics from Fisher Information: A Unification.* Cambridge University Press, 1998.

[125] H. Cramér, *Mathematical Methods of Statistics.* Princeton, NJ: Princeton Univ. Press, 1946.

[126] K. C. Xu, Y. J. Guo, X. Huang, and E. Dutkiewicz, "Ranging based positioning employing co-operative arrays," *IEEE ISCIT2012*, Gold Coast, Australia 2012.

[127] T. Sathyan, D. Humphrey, and M. Hedley, "WASP: A system and algorithms for accurate radio localization using low-cost hardware," *IEEE Transactions on Society, Man and Cybernetics, Part C*, vol. 41, no. 2, pp. 211–222, March 2011.

[128] M. Navarro and M. Nájar, "TOA and DOA estimation for positioning and tracking in IR-UWB," *Proc. IEEE International Conference on Ultra-Wideband*, pp. 574–579, September 2007.

[129] S. Hann, J. H. Kim, S. Y. Jung, and C. S. Park, "White LED ceiling lights positioning systems for optical wireless indoor applications," *36th European Conference and Exhibition on Optical Communication (ECOC)*, pp. 1 – 3, 2010.

[130] M. Rahman, M. Haque, and K. D. Kim, "High precision indoor positioning using lighting LED and image sensor," *14th International Conference on Computer and Information Technology (ICCIT)*, pp. 309 – 314, 2011.

[131] S. Y. Jung, S. Hann, and C. S. Park, "TDOA-based optical wireless indoor localization using LED ceiling lamps," *IEEE Transactions on Consumer Electronics*, vol. 57, no. 4, pp. 1592 – 1597, 2011.

[132] Y. Zhang and F. Shao, "Study of active ultrasonic localization in LED street light controller," *Second International Conference on Mechanic Automation and Control Engineering (MACE) 2011*, pp. 694 – 696, 2011.